



ΠΑΝΕΠΙΣΤΗΜΙΟ ΙΩΑΝΝΙΝΩΝ
ΤΜΗΜΑ ΜΑΘΗΜΑΤΙΚΩΝ



Γρηγόριος Χρηματόπουλος

ΜΑΓΝΗΤΟΪΔΡΟΔΥΝΑΜΙΚΗ ΡΟΗ ΡΕΥΣΤΟΥ ΣΕ ΚΑΝΑΛΙ,
ΥΠΟΛΟΓΙΣΤΙΚΕΣ ΠΡΟΣΕΓΓΙΣΕΙΣ ΜΕΣΩ ΤΗΣ ΜΕΘΟΔΟΥ
ΤΩΝ ΠΕΠΕΡΑΣΜΕΝΩΝ ΟΓΚΩΝ

ΜΕΤΑΠΤΥΧΙΑΚΗ ΔΙΑΤΡΙΒΗ

Ιωάννινα, 2023



UNIVERSITY OF IOANNINA
Department of Mathematics



Grigorios Chrimatopoulos

MAGNETOHYDRODYNAMIC FLUID FLOW IN A
CHANNEL, COMPUTATIONAL APPROACHES USING
THE FINITE VOLUME METHOD

Master's Thesis

Ioannina, 2023

To my family.

Η παρούσα Μεταπτυχιακή Διατριβή εκπονήθηκε στο πλαίσιο των σπουδών για την απόκτηση του Μεταπτυχιακού Διπλώματος Ειδίκευσης στα Εφαρμοσμένα Μαθηματικά και την Πληροφορική που απομένει το Τμήμα Μαθηματικών του Πανεπιστημίου Ιωαννίνων.

Εγκρίθηκε την 30/06/2023 από την εξεταστική επιτροπή:

Όνοματεπώνυμο	Βαθμίδα
Μιχαήλ Ξένος	Αναπληρωτής Καθηγητής
Θεόδωρος Χωρίκης	Καθηγητής
Ευστράτιος Τζιρτζιλιάκης	Καθηγητής

ΥΠΕΥΘΥΝΗ ΔΗΛΩΣΗ

“Δηλώνω υπεύθυνα ότι η παρούσα διατριβή εκπονήθηκε κάτω από τους διεθνείς ηθικούς και ακαδημαϊκούς κανόνες δεοντολογίας και προστασίας της πνευματικής ιδιοκτησίας. Σύμφωνα με τους κανόνες αυτούς, δεν έχω προβεί σε ιδιοποίηση ξένου επιστημονικού έργου και έχω πλήρως αναφέρει τις πηγές που χρησιμοποίησα στην εργασία αυτή.”

Γρηγόριος Χρηματόπουλος

ΕΥΧΑΡΙΣΤΙΕΣ

Η παρούσα διατριβή εκπονήθηκε στα πλαίσια των υποχρεώσεων μου για την απόκτηση του Μεταπτυχιακού Διπλώματος Ειδίκευσης “Εφαρμοσμένων Μαθηματικών και Πληροφορικής” του τμήματος Μαθηματικών, Πανεπιστημίου Ιωαννίνων, με επιβλέποντα τον Αναπληρωτή Καθηγητή κ. Μιχαήλ Ξένο και μέλη της Τριμελούς Εξεταστικής Επιτροπής, κ. Θεόδωρο Χωρίκη και κ. Ευστράτιο Τζιρτζιλάκη.

Ευχαριστώ θερμά, τον κ. Μιχαήλ Ξένο, Αναπληρωτή Καθηγητή του τμήματος Μαθηματικών του Πανεπιστημίου Ιωαννίνων, που με προθυμία δέχτηκε να αναλάβει την επίβλεψη της παρούσας μεταπτυχιακής διατριβής. Τον ευχαριστώ για την επιστημονική βοήθεια, την καθοδήγηση, την υποστήριξη, τον χρόνο και τις πολύτιμες συμβουλές που μου προσέφερε καθόλη τη διάρκεια της εκπόνησης της διατριβής. Τέλος, θα ήθελα να τον ευχαριστήσω θερμά για την εμπιστοσύνη που έδειξε στη δουλειά μου.

Επίσης, ευχαριστώ τους, κ. Θεόδωρο Χωρίκη, Καθηγητή του τμήματος Μαθηματικών του Πανεπιστημίου Ιωαννίνων και κ. Ευστράτιο Τζιρτζιλάκη, Καθηγητή του Τμήματος Μηχανολόγων Μηχανικών του Πανεπιστημίου Πελοποννήσου, για την συμμετοχή τους στην Τριμελή Εξεταστική Επιτροπή και για τις πολύτιμες παρατηρήσεις και υποδείξεις τους στην διατριβή μου με σκοπό την βελτίωσή της.

Τέλος, θα ήθελα να ευχαριστήσω την οικογένειά μου. Ευχαριστώ τους γονείς μου, Θεόδωρο Χρηματόπουλο και Ευτυχία Νούση, τον αδερφό μου, Χριστόφορο Χρηματόπουλο και την γιαγιά μου, Ερμιόνη Νούση για την άπλετη αγάπη και πλήρη στήριξη που έλαβα σε κάθε στιγμή και απόφαση της ζωής μου.

Ιωάννινα 2023,
Γρηγόριος Χρηματόπουλος

ΠΕΡΙΛΗΨΗ

Πολλά ρευστομηχανικά προβλήματα περιγράφουν τις μεταβολές της ροής υπό την επίδραση καθολικών ή μαζικών ηλεκτρομαγνητικών δυνάμεων. Η παρούσα μεταπτυχιακή διατριβή εξετάζει την συμπεριφορά της ροής ενός ηλεκτρικά αγώγιμου και Νευτώνιου ρευστού χρησιμοποιώντας αρχές της Μαγνητοϋδροδυναμικής και της Φερροϋδροδυναμικής. Οι εξισώσεις που μοντελοποιούν τις ροές αυτές είναι συζευμένα συστήματα διαφορικών εξισώσεων με μερικές παραγώγους, μη γραμμικές, δεύτερης τάξης και προκύπτουν από νόμους του Ηλεκτρομαγνητισμού όπως των Ampere, Faraday και Ohm. Η διακριτοποίηση επιτυγχάνεται μέσω της μεθόδου των Πεπερασμένων Όγκων, η οποία οδηγεί σε πεπλεγμένα συστήματα μη γραμμικών αλγεβρικών εξισώσεων. Ο αλγόριθμος που έχει γραφτεί για αυτή την διατριβή συγκρίνεται αρχικά σε προβλήματα με αναλυτική λύση όπως η ροή Poiseuille και η ροή Hartmann. Οι αμελητέες διαφορές μεταξύ των αναλυτικών και αριθμητικών λύσεων, επιβεβαιώνουν τα αποτελέσματα του αλγόριθμου. Οι περιπτώσεις της Μαγνητοϋδροδυναμικής καθώς και της Φερροϋδροδυναμικής, λόγω της ισχυρής μη γραμμικότητας, δεν έχουν αναλυτικές λύσεις και τα αποτελέσματα θα συγκριθούν με αυτά από ήδη δημοσιευμένες εργασίες, όπου τα αποτελέσματα είναι της ίδιας τάξης μεγέθους.

ABSTRACT

Many problems in Fluid Mechanics describe the change in the flow under the effect of electromagnetic forces. The present thesis studies the behaviour of an electric conducting, Newtonian fluid flow applying the Magnetohydrodynamics (MHD) and Ferrohydrodynamics (FHD) principles. The equations that formulate such flows are the Navier-Stokes equations with the Conservation of Mass and Energy PDEs and compose non linear systems of Differential equations, second order and are derived from Electromagnetic principles such as Ampere's, Faraday's and Ohm's laws. The discretization is achieved using the Finite Volumes Method, from which, implicit non linear system of algebraic equations is obtained. The results using the numerical algorithm written for this thesis are compared, to those of problems with analytical solution such as the Poiseuille and Hartmann flow. The relative small differences between the analytical and numerical solutions verify the results of the algorithm. The cases of Magnetohydrodynamics as well as the case of Ferrohydrodynamic flow, due to the dominant non linear terms, do not have analytical solutions. The results are compared to those of already published numerical studies, where the results are qualitatively the same.

CONTENTS

Περίληψη	i
Abstract	ii
1 Introduction	5
1.1 History and Applications of Magnetofluid Dynamics (MFD) . . .	7
2 Mathematical formulation	9
2.1 The Induction equation	9
2.2 The Conservation of Mass and Navier-Stokes equations	13
2.3 The Energy equation	14
3 The Finite Volume Method, Newton's method and the Trust Region Method	15
3.1 The Finite Volume Method	15
3.2 Newton's Method (advantages of the method)	19
3.2.1 Newton's Method	19
3.2.2 The trust-region method	20
3.2.3 The dogleg method	22
3.2.4 Quadratic Convergence of Newton's Method	23
3.3 Root Mean Square	26
3.4 Grid Independence	26
4 Poiseuille Flow	27

4.1	Introduction to the Poiseuille Flow	27
4.1.1	Analytical Solution of the Poiseuille Flow	28
4.2	The Finite Volume Method on the Poiseuille Flow	31
4.2.1	Numerical results of the Poiseuille flow	35
5	Hartmann Flow	39
5.1	Lorentz Force influence on fluid flow	39
5.2	Introduction to the Hartmann Flow	40
5.2.1	Boundary Conditions for the Hartmann flow	42
5.3	The Hartmann Flow	43
5.3.1	Analytical solution of the Hartmann Flow	44
5.4	The Finite Volume Method for The Hartmann Flow	48
5.4.1	Residual equations and numerical results of the descriti- zation for the Hartmann Flow	48
6	Magnetohydrodynamics	55
6.1	Introduction to the MHD Flow	55
6.2	The Finite Volume Method on the MHD Flow	57
6.2.1	Residual equations, numerical results of the descritiza- tion for the MHD Flow	57
7	Ferrohydrodynamics	65
7.1	Introduction to the FHD flow	65
7.2	The Finite Volume Method on FHD Flow	68
7.2.1	Residual equations and numerical results of the descriti- zation for the FHD Flow	68
8	Discussion and conclusion	73
9	Appendix	77
9.1	Descritization in Matlab	77

9.2	Structure and performance of the code	80
9.3	Non dimensional numbers calculations	81
9.4	Speed up and Residuals of the algorithm	82
9.5	List of symbols	84
	Bibliography	85

CHAPTER 1

INTRODUCTION

For decades, various scientists try to give solutions to problems in the field of Fluid Mechanics. The main concern of the scientific community is the lack of analytical solutions to the majority of the problems.

The difficulty of this field lies in the characteristics of the mathematical equations that describe the problem. In most cases, meaning real life problems these systems of equations are high order (usually 2nd order), non linear systems of Partial Differential equations (PDEs).

These characteristics create a near impossible, to solve analytically, problem. In the chapters below we introduce several assumptions to simplify these systems and in some cases analytical solutions exist whereas, in some others there are no analytical ones.

These systems of equations can be very complicated as we dive deeper in more interesting applications. Such examples are the study of a fluid flow with Magnetohydrodynamic (MHD) and Ferrohydrodynamic (FHD) principles. These principles will be introduced later.

It is commonly used, in Computational Fluid Dynamics (CFD), to discretize the governing system of PDEs to obtain, a new system of non linear Algebraic equations, using a method called Finite Volumes Method (FVM). The new system is larger in size than the governing one but can be solved numerically.

The FVM uses a partition in each axes which creates subdomains. Each side of these shapes is called face, where the flux of the fluid is calculated through these faces, resulting in the algebraic equations. For the calculation of the flux, central differences will be used, as we will introduce in a chapter bellow. This partition is called the computational mesh.

The concept of this study is to examine the behaviour of such flows using an algorithm that solves, with direct numerical methods, the algebraic equations.

Chapter 1

At first we will derive the non dimensional equations and the laws for the general cases which will be discretized with the FVM.

Poiseuille flow: The first case studied in this thesis is the Poiseuille flow which describes the flow of a fluid in a two dimensional channel. Using the solution of the fluid velocity, the fluid temperature can be calculated. An analytical solution exists, hence this will be a very good test problem for the validation of the method, since we can compare the analytical solution with the numerical one.

Hartmann flow: The second case studied is the Hartmann flow which describes the flow of a conducting fluid in a two dimensional channel, where an external inducted magnetic field is vertically applied to the channel. The Hartmann flow also describes the change of the magnetic field inside the channel due to the conducting fluid. An analytical solution can be found in this case, introducing another test problem, where we can compare, again, the analytical solution with the numerical one.

The Poiseuille and Hartmann flow are simplifications where assumptions had to be made.

MHD and FHD flows: After the validation of the method, we can examine more complicated problems. Such an example is the study of a conducting fluid flowing through a channel while an external, uniform, inducted magnetic field, constant in magnitude is applied with an angle. Similar to the Poiseuille flow, the numerical solution of the fluid velocity will be used to calculate the temperature and the change of it due to the induced magnetic field. This problem is based on MHD principles. Another example, is the study of a fluid that flows through a channel while an external magnetic pole, close to the channel, generates a non uniform magnetic field, with constant in magnitude but varying in directionality. This problem is based on FHD principles.

For the last two problems, there are no analytical solutions and the comparison as the first two problems is not possible. A numerical solution, however, can be obtained with the validated FVM and that solution will be compared with solutions derived in previously published studies.

1.1 History and Applications of Magnetofluid Dynamics (MFD)

Magnetofluid Dynamics is the general category where the Magnetohydrodynamics is a subtopic of it. The MFD deals with an electrically conducting fluid, whereas the MHD is specifically concerned with electrically conducting liquids.

The first MFD effects were first demonstrated from Faraday's and Ritchie's experiments. In 1832, Faraday studied mercury flow inside glass tubes with magnetic poles placed around the tubes. He discovered an induced voltage across the tube due to the motion of the mercury across the magnetic field. This voltage was perpendicular to the fluid flow as well as the magnetic field. The induced voltage generated a current which interacted with the magnetic field resulting in the retard of the fluid motion. The electric current generated its own magnetic field which obeyed Ampere's right hand rule, resulting in the distortion of the field of the magnet. Faraday suggested, based on the experiments, that electrical power could be obtained in a load circuit using the interaction between the flow of an electrically conducting fluid and a magnetic field [3].

Some practical applications are those of Smith's and Slepian's inventions of an instrument for the measurement of a ship's velocity as well as Williams' MFD flow meter which was based in the principle that the induced voltage is commensurate to the flow rate. In 1920 Young, Gerrard and Jevons were the first to study tidal motions with an induced-voltage device, a technique that is widely used in oceanography. Fundamental work in this area was done by Hartmann and Lazarus, where they also studied the channel flow of mercury.

Other experiments such as Ahlstrom's, demonstrated that disturbances generated by an aerodynamic body could also create disturbances in the magnetic field and the fluid, to produce both upstream and downstream wakes. Most of the practical work has been done since 1950. At that era the interest was in high-temperature gases, nuclear engineering as well as space technology. Since 1960 the concept of MFD power generator has been an object of global research and development [3].

The flow meter: When a conducting fluid flows through a channel with insulating walls and a magnetic field is applied, a potential gradient (proportional to the flow) is generated and can be measured by sensors inside the walls. Using these, the flow rate can be measured without, for example, contaminating the fluid. This technique is used to measure the blood flow [18].

Direct conservation of energy: Electricity is usually produced from the chemical energy of fuel such as coal or oil. The fuel is burnt and the heat generated is used to create high pressure steam which turns a turbine connected to a dynamo. Suppose that the gases are burnt at high temperatures in a flame far from the walls, to prevent as much loss of strength as possible from the walls due to high temperature. By applying a perpendicular to the flow, magnetic field, the kinetic energy inside the hot ionized gas can be directly converted into electric energy. A potential gradient, in a direction perpendicular to the flow is then generated. The electric currents can be collected by electrodes embedded in the gas [18].

Separation of the red blood cells from the whole blood: Certain cancer treatments require clean separation of the white cells from the whole blood for chemical treatment. The red blood cells, when oxygenated have the characteristics of a diamagnetic material. Using this characteristic, a device that uses a magnetic field for a more efficient separation method, developed in [5]. The blood is collected in a device which is surrounded by a magnetic field. The higher the magnitude of the magnetic field, the higher the drop of the magnitude of the velocity resulting in a very slow process. A solution is the increase of the susceptibility of the red blood cells using encapsulated magnetic microspheres that are bound to the red blood cells. This create a ferrofluid, where the low in magnitude magnetic field can achieve the same results in the separation, in a less time consuming process.

Energy harvesting: Electromagnetic energy harvesting has become a very interesting method, compared to other methods, due to the resource being easily found in artificial environments. A device that uses this method is studied in [29], which is based on Faraday's law of induction, meaning relative motions under a magnetic field causes a change of magnetic flux. As a result a voltage and an electrical current is generated in a surrounding coil. The device uses a ferrofluid which is inside a channel with a coil wrapped around it and magnets outside the coil. A syringe is used to inject a uniform flow of air inside the ferrofluid, which creates in air droplet. The magnetic field in the ferrofluid is affected by the creation and the motion of the droplet which leads to the induction of the electric voltage and current.

CHAPTER 2

MATHEMATICAL FORMULATION

2.1 The Induction equation

Magnetic fields can be found in nature where a ferromagnetic material such as lodestone (natural magnets) can be used as a magnet to attract iron. A magnetic field, however, can be formed from the flow of electric current in a conductor, for example an axisymmetric field is created around a wire when electrical current flows through it. We call that magnetic field \vec{H} [12]. This analysis is applied on a domain $A \subseteq \mathbb{R}^3$, with a closed surface C . All introduced functions are considered smooth, C^∞ . For the integral calculations below Stokes' Theorem was used [1].

Ampere's Law. The integral of the magnetic field \vec{H} , on a closed surface C is equal to the flux of the electric current \vec{J} which flows through an area A inside the surface C , in mathematical formulation:

$$\int_C \vec{H} \cdot d\vec{r} = \int_A (\vec{\nabla} \times \vec{H}) \cdot \vec{n} dA = \int_A \vec{J} \cdot \vec{n} dA, \quad (2.1)$$

where \vec{n} is the unit vector perpendicular to the area, A . Since equation (2.1) holds true for every closed surface C of area A we can conclude that:

$$\vec{\nabla} \times \vec{H} = \vec{J}. \quad (2.2)$$

Equation (2.2) is called Ampere's Law in differential form. This law is valid for slowly varying electromagnetic processes in which the occurring velocities and related time scales are much smaller compared to the speed of light. The divergence of Ampere's Law is identically:

$$\vec{\nabla} \cdot (\vec{\nabla} \times \vec{H}) = 0 \Rightarrow \vec{\nabla} \cdot \vec{J} = 0, \quad (2.3)$$

which equation (2.3) is called the Conservation of electric current, \vec{J} .

Faraday's Law. A voltage is induced in a wire loop which is penetrated

by a varying magnetic field. The variation of the magnetic flux, through the loop of the wire, may occur in different ways. The loop conductor may move through a spatially varying magnetic field. It can also change its orientation with regard to the field, or the magnetic field may be time depended. In mathematical formulation we have the following:

$$\phi_1 - \phi_2 = \int_C \bar{E} \cdot d\bar{r} = -\frac{\partial}{\partial t} \left(\mu \int_A \bar{H} \cdot \bar{n} dA \right). \quad (2.4)$$

Due to the induced voltage, at the ends of the wire loop there is electrical potential difference, $\phi_1 - \phi_2$. \bar{E} is the electric field and μ is the magnetic permeability of the material ($\mu \approx \mu_0$). The negative sign can be explained by the fact that the induced voltage will always force current flows counteracting the magnetic flux variation. This phenomenon is called Lenz's rule. Faraday's Law can be written as:

$$\int_C \bar{E} \cdot d\bar{r} = \int_A (\bar{\nabla} \times \bar{E}) \cdot \bar{n} dA = \int_A -\frac{\partial}{\partial t} (\mu \bar{H}) \cdot \bar{n} dA. \quad (2.5)$$

Since equation (2.5) holds true for every closed surface C and area A , we can conclude that:

$$\bar{\nabla} \times \bar{E} = -\frac{\partial}{\partial t} (\mu \bar{H}). \quad (2.6)$$

The equation (2.6) is called differential form of Faraday's Law. We define a new magnetic parameter, the magnetic induction \bar{B} by the linear constitutive equation:

$$\bar{B} = \mu \bar{H} \quad (2.7)$$

providing a new equation by substituting in Equation (2.6):

$$\bar{\nabla} \times \bar{E} = -\frac{\partial}{\partial t} \bar{B} \quad (2.8)$$

The divergence of Faraday's Law is identically given as:

$$\bar{\nabla} \cdot (\bar{\nabla} \times \bar{E}) = \bar{\nabla} \cdot \left(-\frac{\partial}{\partial t} \bar{B} \right) = -\frac{\partial}{\partial t} (\bar{\nabla} \cdot \bar{B}) = 0 \Rightarrow \bar{\nabla} \cdot \bar{B} = \text{constant}.$$

The integration constant should be zero, because at an initial time we assume that the current vanishes and there are no permanent magnets, therefore zero, giving the following:

$$\bar{\nabla} \cdot \bar{B} = 0. \quad (2.9)$$

Using equation (2.7) in equation (2.2) we have:

$$\bar{\nabla} \times \bar{B} = \mu \bar{J}. \quad (2.10)$$

The basic equations of electromagnetic induction are the **Maxwell's equations** which are [18]:

$$\bar{\nabla} \times \bar{B} = \mu \bar{J}, \quad \bar{\nabla} \times \bar{E} = -\frac{\partial}{\partial t} \bar{B}, \quad \bar{\nabla} \cdot \bar{B} = 0. \quad (2.11)$$

An important factor in the study of Magnetohydrodynamics is the so called Lorentz force. A given magnetic field acts on a slender conductor with electric current flow for example a wire of length L , by the force:

$$\bar{F} = L \bar{I} \times \bar{B}, \quad (2.12)$$

where \bar{I} is the current in the conductor and \bar{B} is the magnetic induction. The current \bar{I} is given by the flux of the electric current density \bar{J} through an area dA as: $\bar{I} = \bar{J} dA$. Using that we can write the Lorentz force:

$$\bar{F} = L \bar{I} \times \bar{B} = L (\bar{J} dA) \times \bar{B} = L dA \bar{J} \times \bar{B} \quad (2.13)$$

and since $L dA$ provides us the volume, we divide with that quantity and we get the Lorentz force per volume:

$$\bar{f} = \bar{J} \times \bar{B}. \quad (2.14)$$

Since, in this study the conductor is the fluid that flows through a channel, we introduce the Ohm's Law for moving fluids.

Ohm's Law. Any electric field in conductors generates an electric current of density \bar{J} . If a conductor is moving with a velocity \bar{q} , an observer moving with the conductor, realizes a potential difference between two end points on the conductor, which is generated by the electrical field \bar{E} . The motion induced field gives rise to an electric current. In mathematical prescription we have:

$$\bar{J} = \sigma (\bar{E} + \bar{q} \times \bar{B}), \quad (2.15)$$

where σ is the electrical conductivity of the fluid and \bar{q} is the vector of velocity of the conductor (fluid). Equation (2.15) holds true only under simplifying conditions such as:

1. The magnitude of velocity should be way smaller than the speed of light which is true in the case of the two dimensional channel.
2. The velocity of the charge carriers, such as electrons or ions, should be smaller than the conductor's (fluid) velocity, implying a velocity driven flow.

3. There is no resistance for the charge carriers and there are no thermoelectric sources which is also true as we will assume that the induced magnetic field is externally applied to the flow.

We now apply the curl operator to the Equation (2.15) and we get:

$$\bar{\nabla} \times \bar{J} = \bar{\nabla} \times (\sigma \bar{E}) + \bar{\nabla} \times (\sigma (\bar{q} \times \bar{B})), \quad (2.16)$$

for this study, we assume that the conductivity of the fluid is constant. We substitute the Equations (2.2) and (2.8) and we obtain:

$$\bar{\nabla} \times \left(\bar{\nabla} \times \left(\frac{1}{\mu} \bar{B} \right) \right) = -\sigma \frac{\partial}{\partial t} \bar{B} + \bar{\nabla} \times (\bar{q} \times \bar{B}). \quad (2.17)$$

Using the identities for the $\bar{\nabla}$ operator and two random vectors \bar{X}, \bar{Y} [28] we can calculate:

$$\bar{\nabla} \times (\bar{q} \times \bar{B}) = (\bar{B} \cdot \bar{\nabla}) \bar{q} - (\bar{q} \cdot \bar{\nabla}) \bar{B} \quad (2.18)$$

and

$$\bar{\nabla} \times (\bar{\nabla} \times \bar{B}) = -\bar{\nabla}^2 \bar{B}. \quad (2.19)$$

Substitute to Equation (2.17) and we get:

$$\frac{\partial}{\partial t} \bar{B} + (\bar{q} \cdot \bar{\nabla}) \bar{B} = \frac{1}{\mu\sigma} \bar{\nabla}^2 \bar{B} + (\bar{B} \cdot \bar{\nabla}) \bar{q}. \quad (2.20)$$

Equation (2.20) is called the **Induction Equation**.

This equation describes the temporal evolution of the magnetic field, $\partial \bar{B} / \partial t$ due to advection $(\bar{q} \cdot \bar{\nabla}) \bar{B}$, although in this study we will examine steady state problems, therefore the parameters will be time independent. The term $\bar{\nabla}^2 \bar{B}$ describes diffusion and the term $(\bar{B} \cdot \bar{\nabla}) \bar{q}$ describes field intensity sources generated by mechanical stretching of the field lines by the velocity field.

In some cases, it is easier to study the fluid mechanic equations in the dimensionless form. In this form, the depended and independent variables are normalized and dimensionless quantities are introduced. With this change dimensionless parameters are applied, with whom the Fluid Mechanics problem can be classified [22].

We now introduce the non-dimensional parameters as:

$$\bar{q}' = \frac{\bar{q}}{u_0}, \quad \bar{\nabla}' = L \bar{\nabla}, \quad \bar{B}' = \frac{\bar{B}}{B_0}, \quad (2.21)$$

where u_0 is the characteristic velocity, L is the characteristic length of the flow and B_0 is the magnitude of the magnetic field. Applying these parameters in the Induction equation we have:

$$\begin{aligned} \frac{B_0 u_0}{L} (\bar{q}' \cdot \bar{\nabla}') \bar{B}' &= \frac{1}{\mu \sigma} \frac{B_0}{L^2} \bar{\nabla}'^2 \bar{B}' + \frac{B_0 u_0}{L} (\bar{B}' \cdot \bar{\nabla}') \bar{q} \Rightarrow \\ (\bar{q}' \cdot \bar{\nabla}') \bar{B}' &= \frac{1}{\mu \sigma} \frac{1}{L u_0} \bar{\nabla}'^2 \bar{B}' + (\bar{B}' \cdot \bar{\nabla}') \bar{q}' \Rightarrow \\ (\bar{q}' \cdot \bar{\nabla}') \bar{B}' &= \frac{1}{Re_m} \bar{\nabla}'^2 \bar{B}' + (\bar{B}' \cdot \bar{\nabla}') \bar{q}' \end{aligned} \quad (2.22)$$

Definition. $Re_m = \mu \sigma L u_0$ is called the **Magnetic Reynolds Number**.

2.2 The Conservation of Mass and Navier-Stokes equations

The equations that describe, the steady state flow of an incompressible fluid that is disturbed by a magnetic field are:

The Conservation of Mass:

$$\bar{\nabla} \cdot \bar{q} = 0. \quad (2.23)$$

The Navier-Stokes Equations with the Lorentz forces:

$$\rho (\bar{q} \cdot \bar{\nabla}) \bar{q} = -\bar{\nabla} p + \mu \bar{\nabla}^2 \bar{q} + \bar{J} \times \bar{B}. \quad (2.24)$$

In order to write the non-dimensional form of the equations we introduce the non-dimensional parameters:

$$\bar{q}' = \frac{\bar{q}}{u_0}, \quad \bar{\nabla}' = L \bar{\nabla}, \quad p' = \frac{p}{\rho u_0^2}, \quad \bar{J}' = \frac{\bar{J}}{\sigma u_0 B_0}, \quad \bar{B}' = \frac{\bar{B}}{B_0}. \quad (2.25)$$

Applying the dimensionless parameters we have for the Conservation of Mass:

$$L u_0 \bar{\nabla}' \cdot \bar{q}' = 0 \Rightarrow \bar{\nabla}' \cdot \bar{q}' = 0, \quad (2.26)$$

where we can see that retains the same form and for the Navier-Stokes Equations:

$$\begin{aligned} \rho \frac{u_0^2}{L} (\bar{q}' \cdot \bar{\nabla}') \bar{q}' &= -\rho \frac{u_0^2}{L} \bar{\nabla}' p' + \mu \frac{u_0}{L^2} (\bar{\nabla}'^2 \bar{q}') + \sigma u_0 B_0 (\bar{J}' \times \bar{B}') \Rightarrow \\ (\bar{q}' \cdot \bar{\nabla}') \bar{q}' &= -\bar{\nabla}' p' + \frac{\mu}{\rho U L} \bar{\nabla}'^2 \bar{q}' + \frac{\sigma L B_0^2}{\rho u_0} (\bar{J}' \times \bar{B}') \Rightarrow \\ (\bar{q}' \cdot \bar{\nabla}') \bar{q}' &= -\bar{\nabla}' p' + \frac{1}{Re} \bar{\nabla}'^2 \bar{q}' + N (\bar{J}' \times \bar{B}'), \end{aligned} \quad (2.27)$$

Definition. $Re = (\rho u_0 L) / \mu$ is called the **Reynolds Number** and it represents the ratio of the internal forces to the viscous forces.

Definition. $N = (\sigma L B_0^2) / (\rho u_0)$ is called the **Stuart Number** and it represents the ratio of the electromagnetic forces to the internal forces.

The product, NRe can also be found as $NRe = Ha^2$, where Ha is called **Hartmann Number**.

2.3 The Energy equation

The equation that describes the temperature of the fluid with the attributes we mentioned above is the Energy equation with the Joule dissipation:

$$\rho c_p (\bar{q} \cdot \bar{\nabla}) T = k \bar{\nabla}^2 T + \frac{1}{\sigma} \bar{J}^2 + \mu \Phi. \quad (2.28)$$

The main interest lies in the steady state problem therefore the temperature is time independent. In order to write the dimensionless Energy equation we introduce the dimensionless parameters as in (2.21) and (2.25) along with the dimensionless dissipation function. We have that:

$$\bar{q}' = \frac{\bar{q}}{u_0}, \quad \bar{\nabla}' = L \bar{\nabla}, \quad T' = \frac{T}{T_\infty}, \quad \bar{J}' = \frac{\bar{J}}{\sigma u_0 B_0}, \quad \Phi' = \Phi \frac{\mu L}{\rho c_p u_0 T_\infty}, \quad (2.29)$$

where T_∞ is the characteristic temperature of the fluid. Applying these parameters in the Energy equations we have:

$$\begin{aligned} \rho c_p \frac{u_0}{L T_\infty} (\bar{q}' \cdot \bar{\nabla}') T' &= k \frac{T_\infty}{L^2} \bar{\nabla}'^2 T' + \frac{1}{\sigma} (\sigma^2 u_0^2 B_0^2) \bar{J}'^2 + \mu \Phi \Rightarrow \\ (\bar{q}' \cdot \bar{\nabla}') T' &= \frac{k}{\rho L u_0 c_p} \bar{\nabla}'^2 T' + \frac{\sigma L B_0^2}{\rho c_p T_\infty} \bar{J}'^2 + \Phi' \Rightarrow \\ (\bar{q}' \cdot \bar{\nabla}') T' &= \frac{1}{Re Pr} \bar{\nabla}'^2 T' + NE_c \bar{J}'^2 + \Phi' \end{aligned} \quad (2.30)$$

Definition. $Pr = (c_p \mu) / k$ is called the **Prandtl Number** and it represents the ratio of the momentum diffusivity with the thermal diffusivity.

Definition. $E_c = u_0^2 / (c_p T_\infty)$ is called the **Eckert Number** and it represents the ratio of kinetic energy to the accumulated enthalpy.

The product, $Re Pr$ can also be found as Pe which is a dimensionless number called **Peclet Number**. N is **Stuart Number** which we introduced earlier. The product, NE_c describes the ratio of energy source due to Joule dissipation to the accumulated enthalpy [12].

CHAPTER 3

THE FINITE VOLUME METHOD, NEWTON'S METHOD AND THE TRUST REGION METHOD

3.1 The Finite Volume Method

The Finite Volume Method (FVM) is a method that transforms the partial differential equations representing conservation laws over differential volumes into discrete algebraic equations over finite volumes or control volumes. Similarly to other discretization methods such as the finite difference or finite element method, the first step in the solution process is the discretization of the geometric domain, which in FVM, is discretized into finite volumes as it can be seen in Figure 3.2. The partial differential equations are then discretized (transformed) into many algebraic equations by integrating them over each discrete element (volume, where a visual aspect of it can be seen in Figure 3.3). In the FVM the term *cell*, usually, replace the term *element* which mostly used in the finite elements method. The system of the algebraic equations is then solved to compute the values of the dependent variable for each of the elements.

In the FVM, the terms in the conservation equation represent the face fluxes and evaluated at the finite volume faces. Because the flux entering a given volume is similar to that leaving the adjacent volume, the FVM is conservative or divergence free, $\bar{\nabla} \cdot \bar{q} = 0$. Finally in the FVM, it is quite easy to implement a variety of boundary conditions in a non-invasive manner, since the unknown variable are evaluated at the centroids of the volume elements, not at the boundary faces [11].

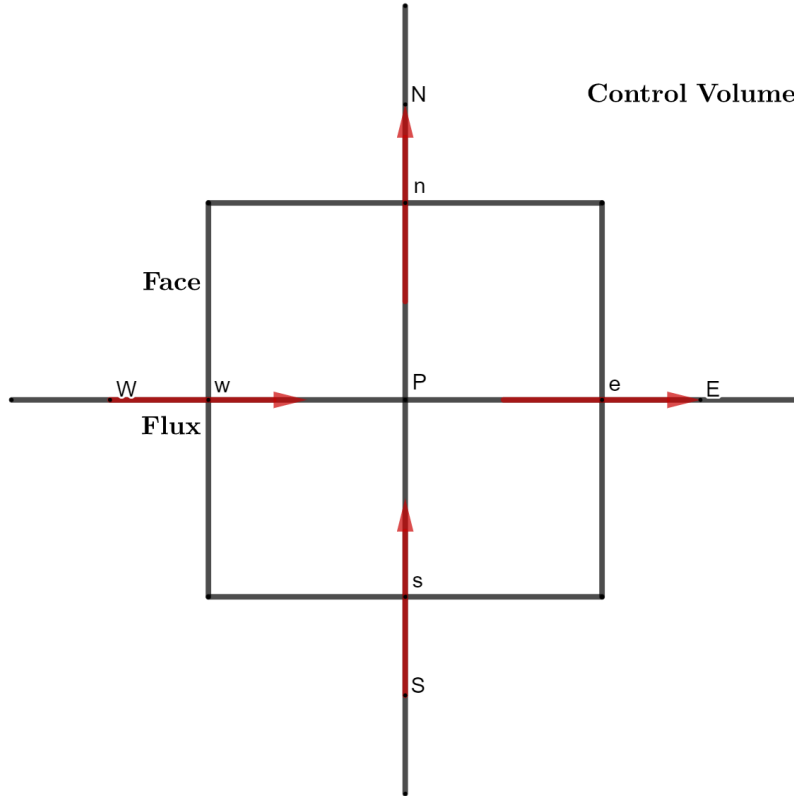


Figure 3.1: The control volume (CV) or Finite Volume with the faces w, e, n, s along with the flux through them.

After the discretization of the domain Ω into subdomains $CV_i \subseteq \Omega$, $i = 1, \dots, N$, we integrate the governing differential equations over each control volume. The result is that the discretization equations, contain the values of the unknown parameters of the problem, for example the velocity, the pressure, the temperature and the magnetic field, for a group of grid points.

The most attractive feature of this method is that the resulting solution would imply that the integral conservation of quantities such as mass (Conservation of Mass equation), momentum (Navier-Stokes equations) and energy (Energy equation) are satisfied over any group of control volumes and as a result over the whole domain. This characteristic exists for any number of nodes, not limited by the need of large number of them, meaning that even if do not

create a fine grid the conservation still exists, resulting in the exact integral balance of the solution even on a small grid.

When the discretized equations are solved, we obtain the values of the unknown parameters of the problem under consideration, on the grid points. In the Finite Volume Method these values all together construct the numerical solution, resulting in a more practical and easy to implement method [15].

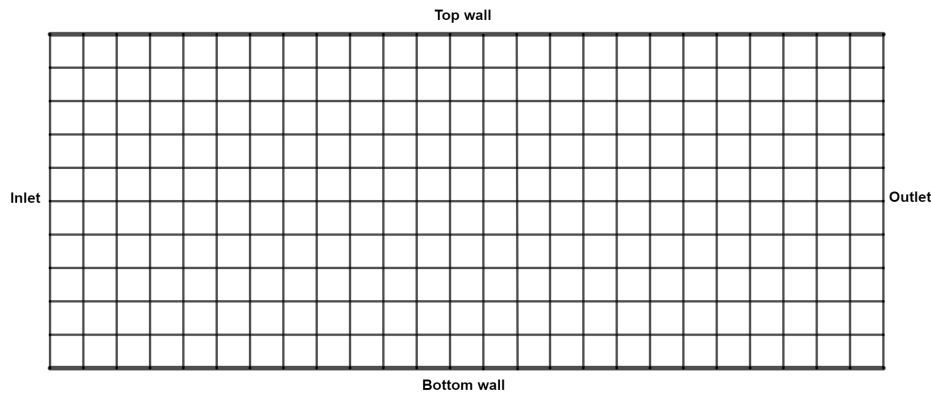


Figure 3.2: The discretized domain (channel) with the FVM. This is a simplified case where we have used square cells, meaning that: $\Delta x = \Delta y$. The domain can be discretized by other shapes as well, for example rectangles e.g. $\Delta x > \Delta y$ or $\Delta x < \Delta y$. Note that the smaller the values of Δx and Δy the finer the computational grid.

The FVM accentuate the satisfaction of the physical laws of the governing PDEs on finite sized control volumes. Imagine, we discretizing the large single control volume into a set of smaller control volumes, and the same conservation laws applied to all the smaller control volumes. The end result is a set of coupled algebraic equations that may be solved conveniently on a computer or by hand.

Since the smaller control volume is still of finite size and not infinitesimally small, gives the method its finite character. The FVM originates from the fluid dynamics analysis. The earliest example of using the FVM can be traced around nineteen-sixties in the work of [6] as well as in the work of [15]. More recent studies and textbooks on the FVM can be found in [20] and [23].

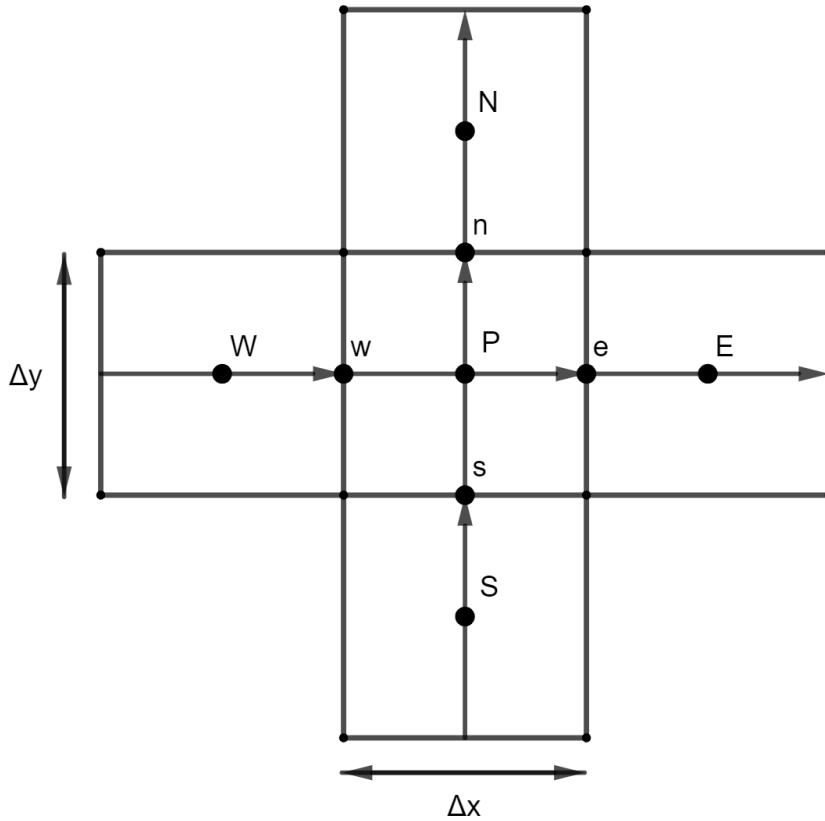


Figure 3.3: Visualization of the control volume along with the neighbours in a Cartesian Coordinates configuration [27].

With the growing realization that conservation of basic physical quantities, that we mentioned above can be found in various cases on our planet, the FVM became the method of choice for analysis of problems that involve fluid flow and other transport phenomena, for example heat, radiation or chemical agent transport. The conservation laws are easily understood by scientists and engineers and since the FVM is capable to preserve these laws, the method is easy to be implemented in a numerical code [9].

3.2 Newton's Method (advantages of the method)

3.2.1 Newton's Method

The non linear system of algebraic equations came from the discretization of the governing equations using the FVM. Assume a system of n non linear equations and n unknowns:

$$\bar{f}(\bar{x}) = \bar{0} \quad (3.1)$$

where $\bar{f} = (f_1, \dots, f_n)^\top$, $\bar{x} = (x_1, \dots, x_n)^\top$ and $\bar{0} = (0, \dots, 0)^\top$. In order to start the algorithm an initial guess is needed, $\bar{x}^{(0)}$ which satisfies: $\bar{f}(\bar{x}^{(0)}) \neq 0$. We seek $\Delta\bar{x}^{(0)}$ so that: $\bar{f}(\bar{x}^{(0)} + \Delta\bar{x}^{(0)}) = 0$ [2]. The first order Taylor series, around $\bar{x}^{(0)}$ gives:

$$\bar{f}(\bar{x}^{(0)} + \Delta\bar{x}^{(0)}) = \bar{f}(\bar{x}^{(0)}) + \mathbf{Jac}^{(0)} \Delta\bar{x}^{(0)}, \quad (3.2)$$

where \mathbf{Jac} is the $n \times n$ Jacobian matrix:

$$\mathbf{Jac}^{(0)} = \left(\bar{\nabla} f_1(\bar{x}^{(0)}), \dots, \bar{\nabla} f_n(\bar{x}^{(0)}) \right)^\top. \quad (3.3)$$

Because of the relation $\bar{f}(\bar{x}^{(0)} + \Delta\bar{x}^{(0)}) = 0$, we need the $\Delta\bar{x}^{(0)}$ to satisfy and the first order Taylor approximation we get: $\Delta\bar{x}^{(0)} \approx \left(\mathbf{Jac}^{(0)} \right)^{-1} \bar{f}(\bar{x}^{(0)})$. or in general:

$$\Delta\bar{x}^{(\nu)} \approx \left(\mathbf{Jac}^{(\nu)} \right)^{-1} \bar{f}(\bar{x}^{(\nu)}). \quad (3.4)$$

Update the vector \bar{x} as $\bar{x}^{(1)} = \bar{x}^{(0)} + \Delta\bar{x}^{(0)}$ or in general:

$$\bar{x}^{(\nu+1)} = \bar{x}^{(\nu)} + \Delta\bar{x}^{(\nu)} = \bar{x}^{(\nu)} + \left(\mathbf{Jac}^{(\nu)} \right)^{-1} \bar{f}(\bar{x}^{(\nu)}), \quad (3.5)$$

where ν is the Newton iteration [2]. The steps that the algorithm follows are:

1. Provide an initial value for the vector \bar{x} : $\bar{x}^{(0)}$.
2. Compute the Jacobian using equation (3.3).
3. Compute the new vector (updated) at the next iteration from equation (3.5).
4. Check that the absolute difference of two consecutive iterations is less than the specified tolerance ε : $\|\bar{x}^{(\nu+1)} - \bar{x}^{(\nu)}\| < \varepsilon$. If this holds true, the algorithm has found the solution and is the updated vector $\bar{x}^{(\nu+1)}$. If not, increase the Newton iteration by one and repeat the process.

The convergence however is not guaranteed in all cases which makes the Newton's method a locally convergent method. The cause is that the Jacobian matrix may be singular at any iteration.

Definition. *A matrix M is singular if and only if: $\det(M) = 0$.*

From this definition we conclude that when the matrix M is singular the inverse Jacobian matrix, $(\mathbf{Jac})^{-1}$, does not exist. In order to solve this problem we use trust region methods which are introduced in the next section.

3.2.2 The trust-region method

A trust region method generates steps with the help of a quadratic model of the objective function. These methods create a region around the current iteration within they trust the model to be a suitable approximation of the objective function, and then choose the step to be the approximate minimizer of the model in this region. A non acceptable step results in the reduce of the region and a search for a new minimizer is now applied. An alteration of the size of the trust region, changes the direction of the step.

The effectiveness of the step is affected by the size of the trust region. If the region is too small the algorithm might not take a substantial step that will move it to a better minimizer of the objective function. If the region is too large the minimizer may be too far, forcing to reduce the region and apply the algorithm again [13].

In practical algorithms the size of the region is chosen based on the performance of the algorithm during the previous iterations. A consistently reliable model, means that produces good steps and predicts the behaviour of the objective function during these steps, with accuracy, the size of the trust region may be increased allowing to take longer steps to find a better minimizer. Should the step fail is an indication that the model does not have the same behaviour as the objective function, over the current trust region. After such a step, we reduce the size of the region and try again.

Let's assume that the model function: m_k , that is used at each iteration k , is quadratic and based in the Taylor series expansion of the objective function, f around the point x_k , meaning:

$$f(x_k + p) = f(x_k) + \bar{\nabla}^T f(x_k) p + \frac{1}{2} p^T \bar{\nabla}^2 f(x_k + tp) p, \quad (3.6)$$

where $t \in (0, 1)$. By using an approximation B_k for the Hessian in the second-order term, the model function m_k is defined by:

$$m_k(p) = f(x_k) + \bar{\nabla}^T f(x_k) p + \frac{1}{2} p^T B_k p, \quad (3.7)$$

where B_k is a symmetric matrix. The difference between the model and the objective function is of order $\mathcal{O}(\|p\|^2)$, which is very small when $\|p\|$ is very small, giving a very small error. A special case is when B_k is equal to the true Hessian $\bar{\nabla}^2 f(x_k)$, then the error is smaller because it is of order $\mathcal{O}(\|p\|^3)$, providing even smaller errors for small $\|p\|$ resulting in a more accurate model function. This special case leads to the trust-region Newton method [13].

To obtain each step, we seek a solution to the subproblem:

$$\min_p m_k(p) = \min_p \left(f(x_k) + \bar{\nabla}^T f(x_k) p + \frac{1}{2} p^T B_k p \right), \quad (3.8)$$

so that: $\|p\| \leq \Delta_k$, where Δ_k is the radius of the trust-region. Finding the minimum of the objective function achieves the global unconstrained minimization [14]. We define the magnitude to be expressed through the Euclidean norm, so that the solution p_k^* of equation (3.8) is the minimizer of m_k , in the ball of radius Δ_k . The trust-region approach requires to solve a sequence of sub problems (3.8) in which the objective function and constrain are both quadratic.

Proposition. *If the matrix B_k is positive defined and $\|B_k^{-1} \bar{\nabla} f(x_k)\| \leq \Delta_k$ the solution of the sub problem (3.8) is $p_k^* = -B_k^{-1} \bar{\nabla} f(x_k)$. This step is called full step.*

Proof. The suggested solution satisfies: $\|B_k^{-1} \bar{\nabla} f(x_k)\| \leq \Delta_k$. We only need to show that $\min_p m_k(p_k^*) < \min_p m_k(p)$.

By definition we have:

$$B_k \text{ positive defined} \Leftrightarrow x^T B_k x > 0 \Leftrightarrow (B_k^T x)^T x > 0, \forall x \in R^n - \{0\} \quad (3.9)$$

and the same holds true for the inverse matrix B_k^{-1} . Using transpose matrix properties we have:

$$m_k(p_k^*) = f(x_k) - \bar{\nabla}^T f(x_k) B_k^{-1} \bar{\nabla} f(x_k) - \frac{1}{2} (B_k^{-1})^T \bar{\nabla}^T f(x_k) \bar{\nabla} f(x_k) \quad (3.10)$$

and because of the definition (3.9) we have that: $m_k(p_k^*) < f(x_k)$ and $m_k(p) > f(x_k)$, concluding that: $m_k(p_k^*) < m_k(p)$ or the point p_k^* is a minimizer of the model function or a solution to the sub problem (3.8). \square

A strategy for an efficient trust-region radius, Δ_k is necessary. The choice is based on the agreement between the model function m_k and the objective function f at previous iterations. Given a step p_k we define the ratio:

$$\rho_k = \frac{f(x_k) - f(x_k + p_k)}{m_k(0) - m_k(p_k)}, \quad (3.11)$$

where the numerator is called the actual reduction, and the denominator the predicted reduction, meaning the reduction in objective predicted by the model function. Since the step p_k is obtained by minimizing the model function m_k over a region that includes $p = 0$, we have that: $m_k(0) > m_k(p_k)$ or $m_k - m_k(p_k) > 0$.

Remark: For the different values of the ratio ρ_k we have that:

- If $\rho_k < 0$, for the difference of the new objective value $f(x_k + p_k)$, with the current value $f(x_k)$ we have that: $f(x_k + p_k) > f(x_k)$ which implies that the step must be rejected.
- If $\rho_k \approx 1$, then there is good agreement between the model and the objective function, over this step, $f(x_k) \approx f(x_k + p_k)$, implying that it is safe to expand the trust region for the next iteration.
- If $0 < \rho_k \ll 1$, then we have, $f(x_k + p_k) < f(x_k)$, we do not alter the trust region, but if it is close to zero, we shrink the trust region by reducing the radius, at the next iteration.

An algorithm can be found explaining the process in [13].

3.2.3 The dogleg method

Our main concern in order to apply the method is the minimization of equation (3.8). We seek numerical solutions, which achieve at least as much reduction in m_k as the reduction achieved by the so called Cauchy point. This point is the minimizer of the model function along the steepest descent direction: $-\bar{\nabla}f(x_k)$. The approximate solutions can be found by the dogleg method, which is suitable when the model Hessian B_k is positive definite (equation (3.9)). The dogleg method calculate an approximate solution by replacing the curved trajectory for the solution of the sub problem with radius Δ_k , with a path consisting of two line segments. The first segment runs from the origin to the minimizer of the model function along the steepest descent direction, while the second runs from the minimizer to the (unconstrained) minimizer of the model function which is found when the matrix B_k is positive defined.

3.2.4 Quadratic Convergence of Newton's Method

Despite the convergence of the solution, for the obtained results to be consistent we must examine the way the norm of the numerical solutions drop as the grid becomes finer. Of course if it increases then the solution divergences.

Proposition. *Quadratic Convergence of Newton's Method:*

Assume $\bar{f} : \mathbf{R}^n \rightarrow \mathbf{R}^n$, a function in \mathcal{C}^1 in a convex open set D of \mathbf{R}^n that contains the exact solution of the problem $\bar{f}(\bar{x}) = \bar{0}$ which we assume is \bar{x} . Suppose that the matrix $\mathbf{Jac}^{-1}(\bar{x}) = \mathbf{Jac}^{-1}$ exists and that there exist positive constants R, C and L such that:

$$\|\mathbf{Jac}^{-1}\| \leq C \quad (3.12)$$

and

$$\|\mathbf{Jac}(\bar{x}) - \mathbf{Jac}(\bar{y})\| \leq L \|\bar{x} - \bar{y}\|, \forall \bar{x}, \bar{y} \in B(\bar{x}, R). \quad (3.13)$$

Then there exists $r > 0$ such that, for any $\bar{x}^{(0)} \in B(\bar{x}, r)$, the sequence which is given by equations (3.4) and (3.5), is uniquely defined and converges to the solution \bar{x} with the following ratio:

$$\|\bar{x}^{(\nu+1)} - \bar{x}\| \leq CL \|\bar{x}^{(\nu)} - \bar{x}\|^2. \quad (3.14)$$

Proof. In order to calculate the correction $\bar{x}^{(1)}$, we need to calculate $\Delta\bar{x}^{(0)}$, which as can be seen from equation (3.4), the $\mathbf{Jac}^{-1}(\bar{x}^{(0)}) = (\mathbf{Jac}^{(0)})^{-1}$ needs to be known. In the general case we need to know the value of $\mathbf{Jac}(\bar{x}^{(\nu)}) = (\mathbf{Jac}^{(\nu)})^{-1}$ so that the calculation of $\bar{x}^{(\nu+1)}$ is feasible. We proceed with induction over the ν Newton iteration. First we prove that for any initial guess $\bar{x}^{(0)}$, close to the exact solution \bar{x} , meaning that $\bar{x}^{(0)} \in B(\bar{x}, r)$, the inverse matrix $(\bar{\mathbf{J}}^{(0)})^{-1}$ exists.

$$\begin{aligned} \|\mathbf{Jac}^{-1}(\mathbf{Jac}^{(0)} - \mathbf{Jac})\| &= \|\mathbf{Jac}^{-1}\| \|\mathbf{Jac}^{(0)} - \mathbf{Jac}\| \Rightarrow \\ \|\mathbf{Jac}^{-1}(\mathbf{Jac}^{(0)} - \mathbf{Jac})\| &\leq CL \|\bar{x}^{(0)} - \bar{x}\| \leq CLr \leq \frac{1}{2}, \end{aligned} \quad (3.15)$$

or

$$\|I - \mathbf{Jac}^{-1}\mathbf{Jac}^{(0)}\| \leq \frac{1}{2} \quad (3.16)$$

Using a theorem that can be found in [16], along with the proof of it, we have that the matrix $\mathbf{Jac}^{-1}\mathbf{Jac}^{(0)}$ is invertible for $\bar{x}^{(0)} \in B(\bar{x}, r)$. Assume that the

matrix $(\mathbf{Jac}^{(0)})^{-1}$ exist, which is a true statement as shown below:

$$\left\| (\mathbf{Jac}^{(0)})^{-1} \mathbf{Jac} \right\| \leq \frac{1}{1 - \left\| \mathbf{Jac}^{-1} (\mathbf{Jac}^{(0)} - \mathbf{Jac}) \right\|} \leq \frac{1}{1 - \frac{1}{2}} \leq 2 \quad (3.17)$$

which is a result from the theorem in [16]. From equation (3.17) we can conclude that:

$$\left\| (\mathbf{Jac}^{(0)})^{-1} \right\| \leq 2 \left\| \mathbf{Jac}^{-1} \right\| \leq 2C < +\infty \quad (3.18)$$

implying that the inverse matrix at the initial iteration exists. Subtracting the exact solution, \bar{x} in each side of equation (3.5) gives:

$$\begin{aligned} \bar{x}^{(1)} - \bar{x} &= \bar{x}^{(0)} - \bar{x} + (\mathbf{Jac}^{(0)})^{-1} \bar{f}(\bar{x}^{(0)}) \Rightarrow \\ \left\| \bar{x}^{(1)} - \bar{x} \right\| &= \left\| \bar{x}^{(0)} - \bar{x} + (\mathbf{Jac}^{(0)})^{-1} \bar{f}(\bar{x}^{(0)}) \right\| = \\ & \left\| (\mathbf{Jac}^{(0)})^{-1} \right\| \left\| \mathbf{Jac}^{(0)} (\bar{x}^{(0)} - \bar{x}) + \bar{f}(\bar{x}^{(0)}) \right\| \end{aligned} \quad (3.19)$$

From the second order Taylor expansion of \bar{f} around the initial guess we get:

$$\begin{aligned} \bar{0} = \bar{f}(\bar{x}) &= \bar{f}(\bar{x}^{(0)}) + \mathbf{Jac}^{(0)} (\bar{x} - \bar{x}^{(0)}) + \mathcal{O} \left(\left\| \bar{x} - \bar{x}^{(0)} \right\|^2 \right) \Rightarrow \\ \bar{f}(\bar{x}^{(0)}) + \mathbf{Jac}^{(0)} (\bar{x} - \bar{x}^{(0)}) &= \mathcal{O} \left(\left\| \bar{x} - \bar{x}^{(0)} \right\|^2 \right) = \frac{L}{2} \left\| \bar{x} - \bar{x}^{(0)} \right\|^2. \end{aligned} \quad (3.20)$$

Substituting the results of equation (3.20) into equation (3.19) results in:

$$\left\| \bar{x}^{(1)} - \bar{x} \right\| \leq 2C \frac{L}{2} \left\| \bar{x}^{(0)} - \bar{x} \right\|^2 \Rightarrow \left\| \bar{x}^{(1)} - \bar{x} \right\| \leq CL \left\| \bar{x}^{(0)} - \bar{x} \right\|^2 \quad (3.21)$$

which proves the case if $\nu = 0$. Since $\bar{x}^{(0)} \in B(\bar{x}, r)$ we have that:

$$\left\| \bar{x}^{(1)} - \bar{x} \right\| \leq CL \left\| \bar{x}^{(0)} - \bar{x} \right\|^2 \leq CL \frac{1}{2CL} \left\| \bar{x}^{(0)} - \bar{x} \right\| = \frac{1}{2} \left\| \bar{x}^{(0)} - \bar{x} \right\| \quad (3.22)$$

or

$$\left\| \bar{x}^{(1)} - \bar{x} \right\| \leq \frac{1}{2} \left\| \bar{x}^{(0)} - \bar{x} \right\| \leq \frac{1}{2} r < r \quad (3.23)$$

meaning that $\bar{x}^{(1)} \in B(\bar{x}, \frac{1}{2}r) \subseteq B(\bar{x}, r)$.

Similar proof can be used for the induction over the ν Newton iteration. Assume that the equation (3.14) holds true, then the same inequality as in equation (3.21) would be true for the $\nu + 1$ Newton iteration. \square

Remark: The Newton method convergences quadratically if

- The initial guess $\bar{x}^{(0)}$ is sufficiently close to the exact solution \bar{x} .
- The Jacobian matrix, **Jac** is non-singular.

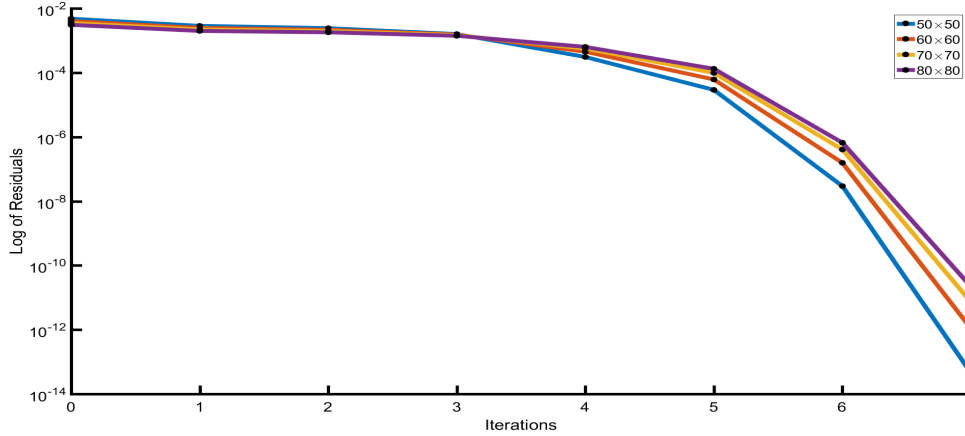


Figure 3.4: Quadratic drop of the residuals using Newton's method for the Poiseuille flow (Chapter 4), as the grid gets finer. The solver stops at the seventh iteration where it concludes that the residual is close to zero.

The main objective in the CFD algorithm developed in this study, is the minimization of the functions that formulate the problems studied in Chapters 4, 5, 6 and 7 below. In table 3.1 we introduce the values of the function at each iteration for the Poiseuille flow. At the final iteration the function is close enough for the solver to stop the process as it has succeed in the minimization, or in other words the solver was converged.

Iterations	50 × 50	60 × 60	70 × 70	80 × 80
0	$4.7619 \cdot 10^{-3}$	$4.0073 \cdot 10^{-3}$	$3.4770 \cdot 10^{-3}$	$3.0678 \cdot 10^{-3}$
1	$2.8483 \cdot 10^{-3}$	$2.4568 \cdot 10^{-3}$	$2.1919 \cdot 10^{-3}$	$1.9833 \cdot 10^{-3}$
2	$2.4158 \cdot 10^{-3}$	$2.1551 \cdot 10^{-3}$	$1.9612 \cdot 10^{-3}$	$1.7989 \cdot 10^{-3}$
3	$1.5848 \cdot 10^{-3}$	$1.5291 \cdot 10^{-3}$	$1.4699 \cdot 10^{-3}$	$1.4016 \cdot 10^{-3}$
4	$3.0687 \cdot 10^{-4}$	$4.4706 \cdot 10^{-4}$	$5.5925 \cdot 10^{-4}$	$6.3306 \cdot 10^{-4}$
5	$2.9034 \cdot 10^{-5}$	$6.1307 \cdot 10^{-5}$	$9.7961 \cdot 10^{-5}$	$1.3142 \cdot 10^{-4}$
6	$2.9389 \cdot 10^{-8}$	$1.5591 \cdot 10^{-7}$	$4.0529 \cdot 10^{-7}$	$6.5905 \cdot 10^{-7}$
7	$4.4927 \cdot 10^{-14}$	$1.0838 \cdot 10^{-12}$	$7.2205 \cdot 10^{-12}$	$2.1865 \cdot 10^{-11}$

Table 3.1: Residuals for the Poiseuille flow for various grid sizes.

3.3 Root Mean Square

As we will discuss in the Chapters 4 and 5, an analytical solution can be obtained, therefore it is reasonable to compare it with the numerical one we find from the algorithm. A close approximations to the analytical solution, lay more robust foundation, for the FVM, which is applied in more complex problems with no analytical one. RMS measures the difference of the numerical and analytical results, in pairs, giving an average error. An RMS close to zero indicates a good approximation.

$$RMS = \sqrt{\frac{1}{N} \sum_{i=1}^N |\bar{x}_i - x_i|^2}, \quad (3.24)$$

where \bar{x}_i is the numerical solution and x_i is the analytical solution at i . N is the size of the data, in this case, the nodes of the partition.

3.4 Grid Independence

In CFD codes it is necessary to find an optimal grid size so that the algorithm convergences to a solution that matches the theory behind the problem. Creating a very fine grid increases the computational cost and the results might not change drastically compared to a less finer grid. In the figure below we present the results from the various grid sizes compared to the grid we believe generates acceptable results for the velocity, pressure and temperature for the Poiseuille flow on the next chapter.

Grid Size	Velocity	Pressure	Temperature
20×20	$9.9775 \cdot 10^{-1}$	$2.5397 \cdot 10^{-1}$	$9.9988 \cdot 10^{-1}$
30×30	$9.9897 \cdot 10^{-1}$	$2.5809 \cdot 10^{-1}$	$9.9995 \cdot 10^{-1}$
40×40	$9.9942 \cdot 10^{-1}$	$2.6017 \cdot 10^{-1}$	$9.9997 \cdot 10^{-1}$
50×50	$9.9963 \cdot 10^{-1}$	$2.6145 \cdot 10^{-1}$	$9.9998 \cdot 10^{-1}$
60×60	$9.9957 \cdot 10^{-1}$	$2.6231 \cdot 10^{-1}$	$9.9999 \cdot 10^{-1}$

Table 3.2: The infinity norm of each parameter changes as the grid becomes finer. For the cases 40×40 to 60×60 we observe slight differences, less than 5%, which verifies the grid independence of the 40×40 grid.

Remark: The Poiseuille numerical solution is also compared with the analytical solution (see Chapter 4).

CHAPTER 4

POISEUILLE FLOW

4.1 Introduction to the Poiseuille Flow

On this section we will study the two dimensional, steady and laminar flow of a viscous, Newtonian and incompressible fluid between two parallel plates at a height $2h$. Using the Conservation of Mass and the Navier-Stokes Equations we will calculate numerically the velocity and the pressure of the fluid using the Finite Volumes Method. Using the, known, velocity field we will calculate the temperature of the fluid using the Energy Equation.

A validation for the results is the conservation of the velocity and temperature profiles at the channel outlet (fully developed flow).

Boundary Conditions: We provide a parabolic profile for the velocity in the inlet of the channel and using Newmann boundary conditions at the channel outlet. We assume no slip condition at both channel walls. For the pressure we apply Newmann boundary condition at the channel inlet and we assume the pressure to be equal to zero, at the channel outlet. For both channel walls, we apply Newmann boundary conditions. Finally, for the fluid temperature, we apply the higher order parabolic profile at the channel inlet and we assume the temperature at the channel walls to be equal to zero.

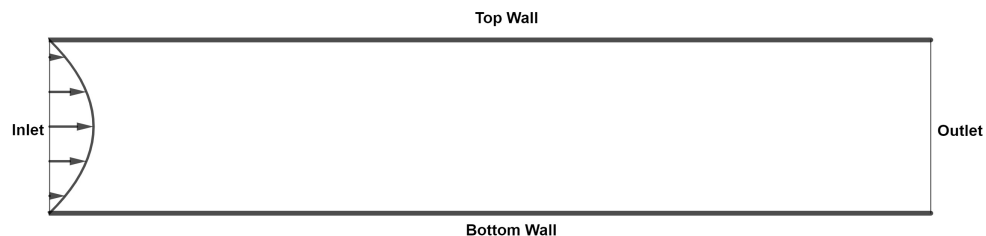


Figure 4.1: The channel and the parabolic profile of the velocity.

4.1.1 Analytical Solution of the Poiseuille Flow

The non-dimensional Poiseuille Flow is a simplified case of the general non-dimensional Conservation of Mass, Navier-Stokes and Energy equations in the two dimensional case. We assume that the fluid is incompressible and the flow is steady (time independent) and laminar. The boundary conditions that formulate the Poiseuille flow are:

$$\begin{aligned} u = 0 \quad \text{and} \quad T = T_w = \text{constant}, \quad \text{at} \quad y = \pm h, \\ \frac{\partial u}{\partial y} = 0, \quad \text{at} \quad y = 0, \quad \text{and} \quad v = 0, \quad \forall (x, y) \in \Omega. \end{aligned} \quad (4.1)$$

The $u = 0$ implies the non-slip condition at the wall of the channel and the constant temperature at the walls implies that the temperature is constant along the horizontal axis, meaning $T = T(y)$. The $v = 0$ condition, at any point in the domain, implies that there is no vertical component for the velocity. We apply these boundary conditions at the non-dimensional Conservation of Mass, Navier-Stokes and Energy equations which results in:

Conservation of Mass

$$\frac{\partial u}{\partial x} + \frac{\partial v}{\partial y} = 0 \Rightarrow \frac{\partial u}{\partial x} = 0, \quad (4.2)$$

x-momentum

$$u \frac{\partial u}{\partial x} + v \frac{\partial u}{\partial y} = -\frac{\partial p}{\partial x} + \frac{1}{Re} \left(\frac{\partial^2 u}{\partial x^2} + \frac{\partial^2 u}{\partial y^2} \right) \Rightarrow 0 = -\frac{\partial p}{\partial x} + \frac{1}{Re} \frac{\partial^2 u}{\partial y^2}, \quad (4.3)$$

y-momentum

$$u \frac{\partial v}{\partial x} + v \frac{\partial v}{\partial y} = -\frac{\partial p}{\partial y} + \frac{1}{Re} \left(\frac{\partial^2 v}{\partial x^2} + \frac{\partial^2 v}{\partial y^2} \right) \Rightarrow 0 = -\frac{\partial p}{\partial y}, \quad (4.4)$$

Energy

$$\begin{aligned} u \frac{\partial T}{\partial x} + v \frac{\partial T}{\partial y} &= \frac{1}{RePr} \left(\frac{\partial^2 T}{\partial x^2} + \frac{\partial^2 T}{\partial y^2} \right) + \Phi \Rightarrow \\ 0 &= \frac{1}{RePr} \frac{\partial^2 T}{\partial y^2} + \Phi, \end{aligned} \quad (4.5)$$

$$\text{where} \quad \Phi = 2 \left(\left(\frac{\partial u}{\partial x} \right)^2 + \left(\frac{\partial v}{\partial y} \right)^2 \right) + \left(\frac{\partial v}{\partial x} + \frac{\partial u}{\partial y} \right)^2 \Rightarrow \Phi = \left(\frac{\partial u}{\partial y} \right)^2$$

The analytical velocity profile of the Poiseuille flow is a parabola of second degree, the pressure drops linear and the analytical profile of the temperature is a parabola of fourth degree.

Proof. For the equations (4.2) and (4.4), we can conclude for the u -velocity and the pressure p that:

$$u = u(y) \quad \text{and} \quad p = p(x) \quad (4.6)$$

and from equation (4.3) we have that:

$$\frac{\partial p}{\partial x} = \frac{1}{Re} \frac{\partial^2 u}{\partial y^2}. \quad (4.7)$$

Since the relation (4.6) holds true, the equation (4.7) must be equal to constant, because the left part is a function of x and the right part is a function of y :

$$\frac{\partial p}{\partial x} = c_1 \quad \text{and} \quad \frac{1}{Re} \frac{\partial^2 u}{\partial y^2} = c_1, \quad (4.8)$$

from which we can see that:

$$\frac{\partial^2 u}{\partial y^2} = Re c_1 \Rightarrow \frac{\partial u}{\partial y} = Re c_1 y + c_2 \Rightarrow u = u(y) = Re c_1 \frac{y^2}{2} + c_2 y + c_3. \quad (4.9)$$

From the boundary conditions (4.1) for the u -velocity at $y = \pm h$ and $y = 0$ we have:

$$\left. \frac{\partial u}{\partial y} \right|_{y=0} = 0 = c_2 \Rightarrow c_2 = 0, \quad (4.10)$$

respectively and

$$u(\pm h) = 0 = Re c_1 \frac{(\pm h)^2}{2} + c_3 \Rightarrow c_3 = -Re c_1 \frac{h^2}{2}. \quad (4.11)$$

We substitute the values of c_2 and c_3 in equation (4.9) and we get:

$$u(y) = Re c_1 \frac{y^2}{2} - Re c_1 \frac{h^2}{2} = Re \frac{c_1}{2} (y^2 - h^2). \quad (4.12)$$

Since the u -velocity has no variation with respect of y and from the no-slip conditions at height $y = \pm h$, we can conclude that at height $y = 0$ has maximum value meaning that: $u(0) = u_{max}$.

From equation (4.12) to obtain for c_1 :

$$u(0) = u_{max} = -Re c_1 \frac{h^2}{2} \Rightarrow c_1 = -\frac{2u_{max}}{Re h^2}, \quad (4.13)$$

which we substitute in equation (4.12) giving the solution of u -velocity in the non-dimensional Poiseuille Flow:

$$u(y) = u_{max} \left(1 - \frac{y^2}{h^2}\right), \quad (4.14)$$

which is a second degree parabolic profile.

Despite the analytical solution for the u -velocity we have a very interesting result for the variation of pressure along the x -axis. Because of the relation (4.8) and the equation (4.13) we have:

$$\frac{\partial p}{\partial x} = c_1 = -\frac{2u_{max}}{Re h^2} \Rightarrow \frac{\partial p}{\partial x} < 0, \quad (4.15)$$

since: $Re > 0$, $u_{max} > 0$.

This means that the pressure drops as the fluid flows along the x -axis.

With the u -velocity known, we can calculate the temperature, T of the fluid using the Energy equation (4.5):

$$\frac{1}{RePr} \frac{\partial^2 T}{\partial y^2} = -\left(\frac{\partial u}{\partial y}\right)^2 = -4u_{max}^2 \frac{y^2}{h^4}, \quad (4.16)$$

from which we get:

$$\begin{aligned} \frac{\partial^2 T}{\partial y^2} &= -4 RePr u_{max}^2 \frac{y^2}{h^4} \Rightarrow \\ \frac{\partial T}{\partial y} &= -4 RePr u_{max}^2 \frac{1}{h^4} \frac{y^3}{3} + c_4 \Rightarrow \\ T = T(y) &= -RePr u_{max}^2 \frac{y^4}{3h^4} + c_4 y + c_5 \end{aligned} \quad (4.17)$$

and applying the boundary conditions for the temperature from (4.1) at height $y = \pm h$ we get:

$$\begin{aligned} T(h) = T_w &= -RePr u_{max}^2 \frac{h^4}{3h^4} + c_4 h + c_5 \Rightarrow \\ T_w &= -\frac{1}{3} RePr u_{max}^2 + c_4 h + c_5, \\ T(-h) = T_w &= -RePr u_{max}^2 \frac{(-h)^4}{3h^4} - c_4 h + c_5 \Rightarrow \\ T_w &= -\frac{1}{3} RePr u_{max}^2 - c_4 h + c_5, \end{aligned} \quad (4.18)$$

since the left part are equal, the constant c_4 must be equal to zero, meaning: $c_4 = 0$. We substitute in one of the equations (4.18) and we get for the constant c_5 :

$$T(h) = T_w = -\frac{1}{3}RePr u_{max}^2 + c_5 \Rightarrow c_5 = T_w + \frac{1}{3}RePr u_{max}^2. \quad (4.19)$$

We can now substitute the values of c_4 and c_5 in equation (4.17) resulting in:

$$\begin{aligned} T = T(y) &= -RePr u_{max}^2 \frac{y^4}{3h^4} + T_w + \frac{1}{3}RePr u_{max}^2 \Rightarrow \\ T = T(y) &= T_w + RePr u_{max}^2 \frac{1}{3} \left(1 - \frac{y^4}{h^4}\right), \end{aligned} \quad (4.20)$$

which is a fourth degree parabolic profile.

The maximum value of temperature is at height $y = 0$ and is equal to:

$$T(0) = T_{max} = T_w + \frac{1}{3}RePr u_{max}^2. \quad (4.21)$$

□

Remark: The calculations and the assumptions for the boundary conditions for the analytical solution are similar to that in [21].

4.2 The Finite Volume Method on the Poiseuille Flow

In order to discretize the differential equations we apply the Finite Volume method (FVM) in the Conservation of Mass, Navier-Stokes and Energy equations respectively, by integrating the equations over the control volume and we get:

$$\begin{aligned} \iint_{CV} \frac{\partial u}{\partial x} dx dy &= \int \frac{\partial u}{\partial x} dx \int 1 dy = u|_w^e \Delta y = \\ &\left(\frac{u_E + u_P}{2} - \frac{u_P + u_W}{2} \right) \Delta y = \frac{1}{2} (u_E - u_W) \Delta y \\ \iint_{CV} \frac{\partial v}{\partial y} dx dy &= \int \frac{\partial v}{\partial y} dy \int 1 dx = v|_s^n \Delta x = \\ &\left(\frac{v_N + v_P}{2} - \frac{v_P + v_S}{2} \right) \Delta x = \frac{1}{2} (v_N - v_S) \Delta x \end{aligned}$$

It is more convenient to apply the method in the closed form of the Navier-Stokes equations and Energy equation.

Remark: The closed form allows to “break” the double integral over the control volume into two integrals, independent from each other, where the functions inside are evaluated over the direction of the variation (flux).

For the **convection** terms for each equation, we have the following formulations, respectively:

x-momentum

$$\begin{aligned} \iint_{CV} \frac{\partial u^2}{\partial x} dx dy &= \int_w^e \frac{\partial u^2}{\partial x} dx \int_s^n 1 dy = u^2|_w^e \Delta y = \\ &\left(\frac{u_E^2 + u_P^2}{2} - \frac{u_P^2 + u_W^2}{2} \right) \Delta y = \frac{1}{2} (u_E^2 - u_W^2) \Delta y \\ \iint_{CV} \frac{\partial(uv)}{\partial y} dx dy &= \int_s^n \frac{\partial(uv)}{\partial y} dy \int_w^e 1 dx = (uv)|_s^n \Delta x = \\ &\left(\frac{(uv)_N + (uv)_P}{2} - \frac{(uv)_P + (uv)_S}{2} \right) \Delta x = \frac{1}{2} (u_N v_N - u_S v_S) \Delta x, \end{aligned}$$

y-momentum

$$\begin{aligned} \iint_{CV} \frac{\partial(uv)}{\partial x} dx dy &= \int_w^e \frac{\partial(uv)}{\partial x} dx \int_s^n 1 dy = (uv)|_w^e \Delta y = \\ &\left(\frac{(uv)_E + (uv)_P}{2} - \frac{(uv)_P + (uv)_W}{2} \right) \Delta y = \frac{1}{2} (u_E v_E - u_W v_W) \Delta y \\ \iint_{CV} \frac{\partial v^2}{\partial y} dx dy &= \int_s^n \frac{\partial v^2}{\partial y} dy \int_w^e 1 dx = v^2|_s^n \Delta x = \\ &\left(\frac{v_N^2 + v_P^2}{2} - \frac{v_P^2 + v_S^2}{2} \right) \Delta x = \frac{1}{2} (v_N^2 - v_S^2) \Delta x, \end{aligned}$$

Energy equation

$$\begin{aligned} \iint_{CV} \frac{\partial(uT)}{\partial x} dx dy &= \int_w^e \frac{\partial(uT)}{\partial x} dx \int_s^n 1 dy = uT|_w^e \Delta y = \\ &\left(\frac{(uT)_E + (uT)_P}{2} - \frac{(uT)_P + (uT)_W}{2} \right) \Delta y = \frac{1}{2} (u_E T_E - u_W T_W) \Delta y \\ \iint_{CV} \frac{\partial(vT)}{\partial y} dx dy &= \int_s^n \frac{\partial(vT)}{\partial y} dy \int_w^e 1 dx = vT|_s^n \Delta x = \\ &\left(\frac{(vT)_N + (vT)_P}{2} - \frac{(vT)_P + (vT)_S}{2} \right) \Delta x = \frac{1}{2} (v_N T_N - v_S T_S) \Delta x, \end{aligned}$$

For the **diffusion** terms for each equation, we have the following formulations, respectively:

x -momentum

$$\begin{aligned} \iint_{CV} \frac{\partial p}{\partial x} dx dy &= \int_w^e \frac{\partial p}{\partial x} dx \int_s^n 1 dy = p|_p^e \Delta y = (p_E - p_P) \Delta y \\ \iint_{CV} \frac{\partial^2 u}{\partial x^2} dx dy &= \int_w^e \frac{\partial^2 u}{\partial x^2} dx \int_s^n 1 dy = \frac{\partial u}{\partial x} \Big|_w^e \Delta y = \\ &\left(\frac{u_E - u_P}{\Delta x} - \frac{u_P - u_W}{\Delta x} \right) \Delta y = (u_E - 2u_P + u_W) \frac{\Delta y}{\Delta x} \\ \iint_{CV} \frac{\partial^2 u}{\partial y^2} dx dy &= \int_s^n \frac{\partial^2 u}{\partial y^2} dy \int_w^e 1 dx = \frac{\partial u}{\partial y} \Big|_s^n \Delta x = \\ &\left(\frac{u_N - u_P}{\Delta y} - \frac{u_P - u_S}{\Delta y} \right) \Delta x = (u_N - 2u_P + u_S) \frac{\Delta x}{\Delta y}, \end{aligned}$$

y -momentum

$$\begin{aligned} \iint_{CV} \frac{\partial p}{\partial y} dx dy &= \int_s^n \frac{\partial p}{\partial y} dy \int_w^e 1 dx = p|_p^n \Delta x = (p_N - p_P) \Delta x \\ \iint_{CV} \frac{\partial^2 v}{\partial x^2} dx dy &= \int_w^e \frac{\partial^2 v}{\partial x^2} dx \int_s^n 1 dy = \frac{\partial v}{\partial x} \Big|_w^e \Delta y = \\ &\left(\frac{v_E - v_P}{\Delta x} - \frac{v_P - v_W}{\Delta x} \right) \Delta y = (v_E - 2v_P + v_W) \frac{\Delta y}{\Delta x} \\ \iint_{CV} \frac{\partial^2 v}{\partial y^2} dx dy &= \int_s^n \frac{\partial^2 v}{\partial y^2} dy \int_w^e 1 dx = \frac{\partial v}{\partial y} \Big|_s^n \Delta x = \\ &\left(\frac{v_N - v_P}{\Delta y} - \frac{v_P - v_S}{\Delta y} \right) \Delta x = (v_N - 2v_P + v_S) \frac{\Delta x}{\Delta y}, \end{aligned}$$

Energy equation

$$\begin{aligned} \iint_{CV} \frac{\partial^2 T}{\partial x^2} dx dy &= \int_w^e \frac{\partial^2 T}{\partial x^2} dx \int_s^n 1 dy = \int_w^e \frac{\partial^2 T}{\partial x^2} dx \Delta y = \\ \frac{\partial T}{\partial x} \Big|_w^e \Delta y &= \left(\frac{T_E - T_P}{\Delta x} - \frac{T_P - T_W}{\Delta x} \right) \Delta y = (T_E - 2T_P + T_W) \frac{\Delta y}{\Delta x} \\ \iint_{CV} \frac{\partial^2 T}{\partial y^2} dx dy &= \int_s^n \frac{\partial^2 T}{\partial y^2} dy \int_w^e 1 dx = \int_s^n \frac{\partial^2 T}{\partial y^2} dy \Delta x = \\ \frac{\partial T}{\partial y} \Big|_s^n \Delta x &= \left(\frac{T_N - T_P}{\Delta y} - \frac{T_P - T_S}{\Delta y} \right) \Delta x = (T_N - 2T_P + T_S) \frac{\Delta x}{\Delta y}, \end{aligned}$$

The Dissipation function in the Energy equation is:

$$\Phi = 2 \left(\left(\frac{\partial u}{\partial x} \right)^2 + \left(\frac{\partial v}{\partial y} \right)^2 \right) + \left(\frac{\partial v}{\partial x} + \frac{\partial u}{\partial y} \right)^2 = -4 \left(\frac{\partial u}{\partial x} \frac{\partial v}{\partial y} \right) + \left(\frac{\partial v}{\partial x} + \frac{\partial u}{\partial y} \right)^2,$$

written as, due to the Conservation of Mass.

For the discretization of the Dissipation Function we have:

$$\begin{aligned} \iint_{CV} \frac{\partial u}{\partial x} \frac{\partial v}{\partial y} dx dy &= \int_w^e \frac{\partial u}{\partial x} dx \int_s^n \frac{\partial v}{\partial y} dy = u|_w^e v|_s^n = \\ &\left(\frac{u_E + u_P}{2} - \frac{u_P + u_W}{2} \right) \left(\frac{v_N + v_P}{2} - \frac{v_P + v_S}{2} \right) = \\ &\left(\frac{1}{2} (u_E - u_W) \right) \left(\frac{1}{2} (v_N - v_S) \right) = \frac{1}{4} (u_E - u_W) (v_N - v_S). \end{aligned}$$

For the quadratic terms in the Dissipation Function Φ , we apply a different approach:

$$\begin{aligned} \iint_{CV} \left(\frac{\partial v}{\partial x} + \frac{\partial u}{\partial y} \right)^2 \Delta x \Delta y &= \left(\frac{\partial v}{\partial x} + \frac{\partial u}{\partial y} \right)^2 \Big|_P \Delta x \Delta y = \\ &\left(\frac{\partial v}{\partial x} \Big|_P + \frac{\partial u}{\partial y} \Big|_P \right)^2 \Delta x \Delta y = \left(\frac{v_E - v_W}{2\Delta x} + \frac{u_N - u_S}{2\Delta y} \right)^2 \Delta x \Delta y. \end{aligned}$$

Remark: As discussed, the system of PDEs have turned into a system of non linear algebraic equations through the FVM. For the evaluation of the integrals on the control volume we mainly used central differences, except for the pressure flux, where we use forward differences. The reason is that if we use central differences we might come across small fluctuations of the numerical solution (spurious solution). This is a common approach, where the pressure is evaluated utilizing the collocated point, P and the upstream point, E (see figure 3.3), resulting in a forward differences scheme (staggered approach). For the quadratic terms of the dissipation function we approximate the quadratic term on the center of the control volume and we use central differences for the discretization.

4.2.1 Numerical results of the Poiseuille flow

In summary, the result of the Finite Volumes method (FVM) on the equations that formulate the Poiseuille flow are (discrete form - equations of differences):

Conservation of Mass

$$\frac{1}{2} (u_E - u_W) \Delta y + \frac{1}{2} (v_N - v_S) \Delta x = 0 \quad (4.22)$$

x-momentum

$$\begin{aligned} & \frac{1}{2} (u_E^2 - u_W^2) \Delta y + \frac{1}{2} (u_N v_N - u_S v_S) \Delta x = - (p_E - p_P) \Delta y + \\ & + \frac{1}{Re} \left((u_E - 2u_P + u_W) \frac{\Delta y}{\Delta x} + (u_N - 2u_P + u_S) \frac{\Delta x}{\Delta y} \right), \end{aligned} \quad (4.23)$$

y-momentum

$$\begin{aligned} & \frac{1}{2} (u_E v_E - u_W v_W) \Delta y + \frac{1}{2} (v_N^2 - v_S^2) \Delta x = - (p_N - p_P) \Delta x + \\ & + \frac{1}{Re} \left((v_E - 2v_P + v_W) \frac{\Delta y}{\Delta x} + (v_N - 2v_P + v_S) \frac{\Delta x}{\Delta y} \right), \end{aligned} \quad (4.24)$$

Energy Equation

$$\begin{aligned} & \frac{1}{2} \Delta y (u_E T_E - u_W T_W) + \frac{1}{2} \Delta x (v_N T_N - v_S T_S) = \\ & \frac{1}{RePr} \left(\frac{\Delta y}{\Delta x} (T_E - 2T_P + T_W) + \frac{\Delta x}{\Delta y} (T_N - 2T_P + T_S) \right) - \\ & - (u_E - u_W) (v_N - v_S) + \left(\frac{v_E - v_W}{2\Delta x} + \frac{u_N - u_S}{2\Delta y} \right)^2 \Delta x \Delta y. \end{aligned} \quad (4.25)$$

Equations (4.22)-(4.25) are called discrete residuals equations where we bring all terms to the left hand side resulting the right hand side to be equal to zero. To successfully obtain the solution of the system means that the solver successfully minimized the residual equations as close to zero as possible (minimization problem).

To validate the solution of the non linear, coupled algebraic system, we compare the numerical solution with the analytical one. In the table 4.1 we present the Root Mean Square of the difference between the numerical and the analytical solution as the grid becomes finer (see also Chapter 3).

The physical description of the solution must also be verified. We can observe from figure 4.2, the contour plot of the velocity where the velocity has maximum value in the channel core and it becomes zero at the channel walls. The figure 4.3 shows the linear pressure drop as the theoretical analysis of the problem has shown. Figure 4.4 shows the higher order parabolic profile of the temperature in the channel, where, the maximum value is at the center of the domain. Finally, figure 4.5 shows the velocity magnitude using vector plot.

Figures 4.6 and 4.7 depict the analytical and numerical profile of the velocity and the temperature, respectively, where can be observed good agreement. Increasing the number of nodes in each axis partition results in a finer grid. The RMS reduces as the grid becomes finer.

We compare the analytical profiles at the inlet and the numerical solution at the outlet of the channel. The Reynolds and Prandtl numbers are equal to $Re = 300$ and $Pr = 21$ respectively. These values correspond to blood flow according to [24].

Grid	Area	RMS Velocity	RMS Temperature
100×10	$9.0009 \cdot 10^{-3}$	$1.1658 \cdot 10^{-4}$	$6.3435 \cdot 10^{-4}$
100×20	$4.7147 \cdot 10^{-3}$	$1.1083 \cdot 10^{-4}$	$1.7758 \cdot 10^{-4}$
100×30	$3.1938 \cdot 10^{-3}$	$1.1055 \cdot 10^{-4}$	$8.4221 \cdot 10^{-5}$
100×40	$2.4148 \cdot 10^{-3}$	$1.1037 \cdot 10^{-4}$	$5.0700 \cdot 10^{-5}$
100×50	$1.9413 \cdot 10^{-3}$	$1.1026 \cdot 10^{-4}$	$3.5106 \cdot 10^{-5}$
100×60	$1.6231 \cdot 10^{-3}$	$1.1020 \cdot 10^{-4}$	$2.6710 \cdot 10^{-5}$
100×70	$1.3954 \cdot 10^{-3}$	$1.1013 \cdot 10^{-4}$	$2.1741 \cdot 10^{-5}$
100×80	$1.2223 \cdot 10^{-3}$	$1.1001 \cdot 10^{-4}$	$1.8020 \cdot 10^{-5}$
100×90	$1.0880 \cdot 10^{-3}$	$1.0971 \cdot 10^{-4}$	$1.5011 \cdot 10^{-5}$
100×100	$9.8029 \cdot 10^{-4}$	$1.0934 \cdot 10^{-4}$	$1.2542 \cdot 10^{-5}$

Table 4.1: Comparison of the analytical and numerical solution of the velocity and the temperature for $Re = 300$ and $Pr = 21$, for different number of grid sizes.

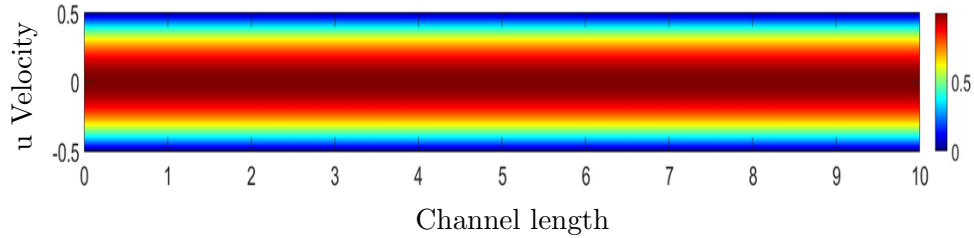


Figure 4.2: Contour plot of the numerical solution of the velocity.

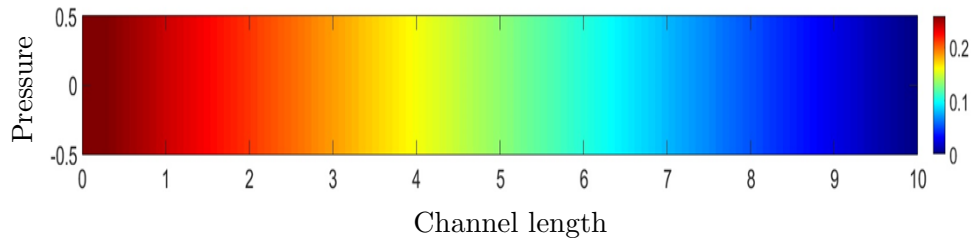


Figure 4.3: Contour plot of the numerical solution of the pressure.

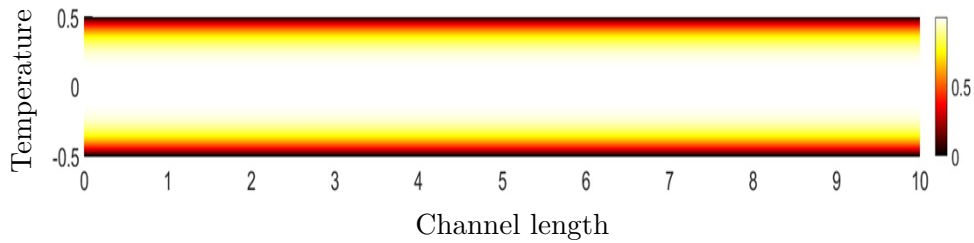


Figure 4.4: Contour plot of the numerical solution of the temperature.

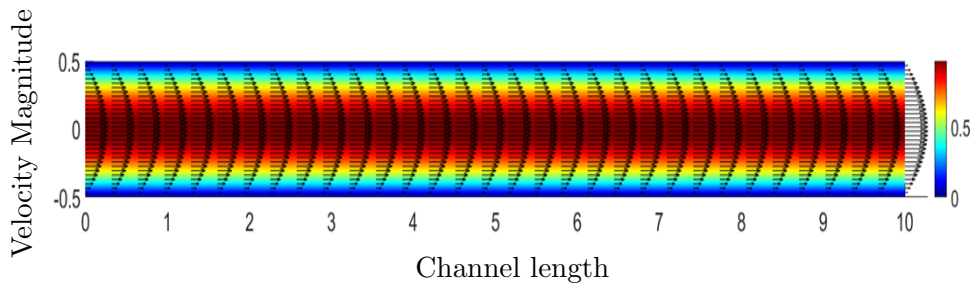


Figure 4.5: Contour and vector plot of the magnitude of the velocity.

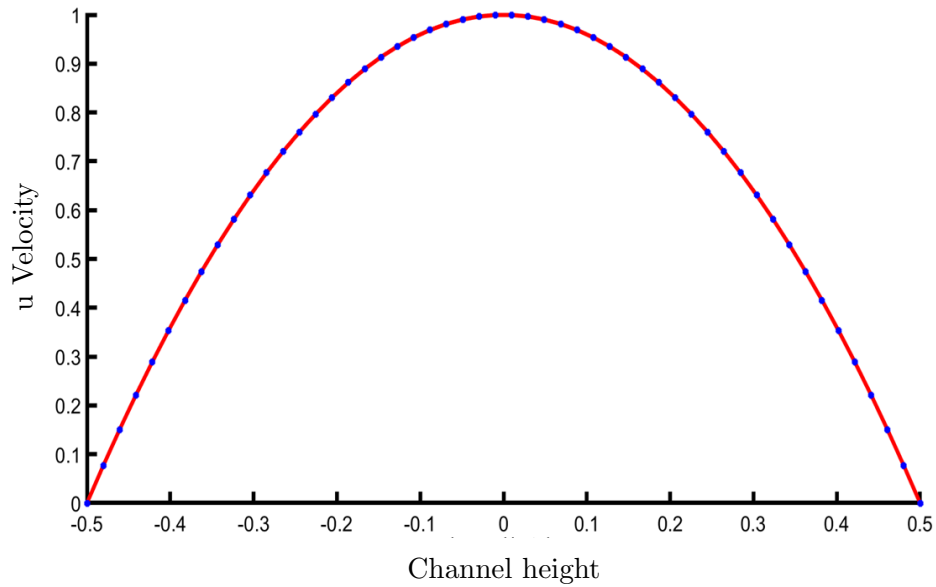


Figure 4.6: Second degree parabolic profile of the analytical (red) and the numerical (blue) velocity at the channel outlet.

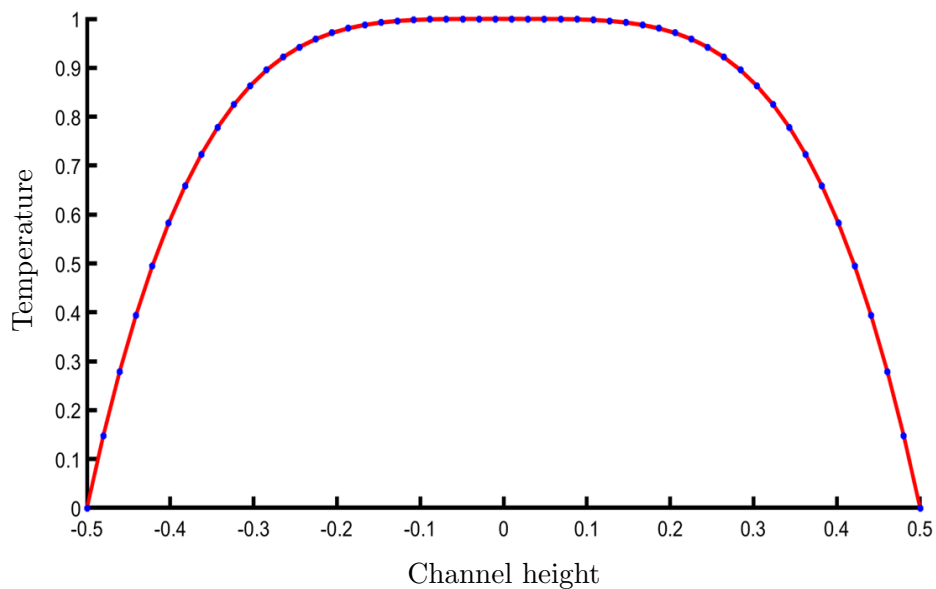


Figure 4.7: Fourth degree parabolic profile of the analytical (red) and the numerical (blue) temperature at the channel outlet.

HARTMANN FLOW

5.1 Lorentz Force influence on fluid flow

The Hartmann flow studies the flow of an electrically conducting fluid while a magnetic field is vertically applied to the bottom channel wall. It also studies the disturbance of the magnetic field due to the electrically conducting fluid. In order to study the influence of the magnetic field on the fluid flow, we must introduce the Lorentz force applied to the fluid. As we described in Chapter 2 the Lorentz force can be mathematically modelled by the term:

$$\bar{f}_L = \bar{J} \times \bar{B}, \quad (5.1)$$

along with the Hartmann number: Ha is a non-dimensional number defined as: $Ha = \sqrt{NRe}$.

In this study, we assume that the electric current density \bar{J} , is equal to $\bar{q} \times \bar{B}$ resulting in:

$$\bar{f}_L = (\bar{q} \times \bar{B}) \times \bar{B}, \quad (5.2)$$

which after the calculations of the outer products, we have for the general case of $\bar{q} = (u, v, w)$ and $\bar{B} = (B_x, B_y, B_z)$ for the Lorentz force \bar{f}_L :

$$\begin{aligned} & (-uB_z^2 + wB_xB_z - uB_y^2 + vB_xB_y) \bar{i} \\ & - (vB_z^2 - wB_yB_z - uB_yB_x + vB_x^2) \bar{j} \\ & + (vB_zB_y - wB_y^2 + uB_xB_z - wB_x^2) \bar{k} \end{aligned} \quad (5.3)$$

and since we study the two-dimensional case of the flow we have that: $w = B_z = 0$, resulting to:

$$\bar{f}_L = (-uB_y^2 + vB_xB_y) \bar{i} - (uB_yB_x + vB_x^2) \bar{j} + 0\bar{k}. \quad (5.4)$$

We also assume $v = 0$ as well as for the magnetic field $B_x = 0$ and $B_y = c$ giving for the Hartmann Flow:

$$\bar{f}_L = -uc^2\bar{i} + 0\bar{j} + 0\bar{k}, \quad (5.5)$$

in this formulation, we assume that the flow is laminar and the external magnetic field is constant in magnitude and vertical to the flow.

By calculating the norm of the Lorentz force, we obtain the effect of the force on the flow field,

$$\|\bar{f}_L\| = \sqrt{c^4u^2} = c^2u. \quad (5.6)$$

This implies that the relation of the Lorentz force and the fluid velocity is linear. Higher fluid velocity results in higher magnitude of the Lorentz force.

For the inducted magnetic field \bar{B} and Lorentz force \bar{f}_L we have that,

$$\bar{B} \perp \bar{f}_L. \quad (5.7)$$

The electric current I , does not contribute in the two dimensional case. Using the right hand rule (the electric current does not contribute in the two dimensional case) we conclude that the Lorentz force retards the fluid velocity.

Remark: Let's assume a parabolic profile in the inlet, no slip conditions on the walls and Neumann conditions at the channel outlet. In Poiseuille Flow we obtained zero velocity at the walls and maximum velocity at the center of the tube (core flow). The Lorentz force will create thin boundary layers which, in this case, are called *Hartmann Layers*, as well as decrease of the fluid velocity, as the magnitude of the magnetic field increases. This will also be proven by the analytical solution provided in the next section where the greater the value of the Hartmann Number is, the greater the drop of the velocity compared to the hydrodynamic flow occurs.

5.2 Introduction to the Hartmann Flow

We consider a straight channel where an external magnetic field \bar{B} is vertically applied, $\bar{B} = b\bar{j} = b(y)\bar{j}$. The flow is driven by a uniform pressure gradient and the fluid flows vertically to the magnetic field, \bar{q} that: $\bar{q} = u\bar{i} = u(y)\bar{i}$.

The magnetic field is composed by two factors: The external magnetic field and the magnetic field induced by the flow of the conducting fluid, resulting

to:

$$\bar{B} = 1\bar{j} + \frac{Re_m}{Ha}b\bar{i} = \left(\frac{Re_m}{Ha}b, 1 \right) = (B_x, B_y), \quad (5.8)$$

where we have scaled the induced part by the term: Re_m/Ha .

We substitute the results of equation (5.8) in the steady state Induction Equation, therefore time independent. We assume that we have a fully developed flow meaning: $(\bar{q} \cdot \bar{\nabla}) \cdot \bar{B} = \bar{0}$ resulting in the x -momentum of the Induction equation:

$$0 = \frac{1}{Re_m} \left(\frac{\partial^2 B_x}{\partial x^2} + \frac{\partial^2 B_x}{\partial y^2} \right) + \left(B_x \frac{\partial u}{\partial x} + B_y \frac{\partial u}{\partial y} \right) \quad (5.9)$$

and we substitute equation (5.8) in equation (5.9) giving:

$$\frac{1}{Ha} \frac{\partial^2 b}{\partial y^2} + \frac{\partial u}{\partial y} = 0 \Rightarrow \frac{\partial^2 b}{\partial y^2} + Ha \frac{\partial u}{\partial y} = 0. \quad (5.10)$$

For the electric current density \bar{J} we assume that:

$$\begin{aligned} \bar{J} &= \frac{1}{Ha} \left(\frac{\partial}{\partial x} \bar{i} + \frac{\partial}{\partial y} \bar{j} + \frac{\partial}{\partial z} \bar{k} \right) \times \left(\frac{Re_m}{Ha} b \bar{i} + 1\bar{j} + 0\bar{k} \right) = \\ &= \frac{1}{Ha} \left(0\bar{i} + \frac{\partial b}{\partial z} \bar{j} - \frac{\partial b}{\partial y} \bar{k} \right) = \frac{1}{Ha} \left(0, \frac{\partial b}{\partial z}, -\frac{\partial b}{\partial y} \right), \end{aligned} \quad (5.11)$$

resulting in the Lorentz force to be expressed with the inducted term b .

Using this assumption with equation (5.8) we have for the Lorentz force:

$$\bar{J} \times \bar{B} = \frac{1}{Ha} \left(\frac{\partial b}{\partial y}, -\frac{Re_m}{Ha} b \frac{\partial b}{\partial y}, \frac{Re_m}{Ha} b \frac{\partial b}{\partial z} \right). \quad (5.12)$$

We assume fully developed flow, $(\bar{q} \cdot \bar{\nabla}) \cdot \bar{q} = 0$, resulting in the x -momentum of the Navier-Stokes equation:

$$0 = -\frac{\partial p}{\partial x} + \frac{1}{Re} \left(\frac{\partial^2 u}{\partial x^2} + \frac{\partial^2 u}{\partial y^2} \right) + \frac{Ha^2}{Re} \left(\frac{1}{Ha} \frac{\partial b}{\partial y} \right), \quad (5.13)$$

where for convenience, we assume that: $\partial p / \partial x = (-\rho u_0 \mu) / (L^2 \rho)$ and from the non-dimensional pressure (which is shown in the non-dimensional Navier-Stokes) from (2.25) we have that:

$$\frac{\partial p'}{\partial x'} = \frac{L}{\rho u_0^2} \frac{\partial p}{\partial x} = \frac{L}{\rho u_0^2} \left(-\frac{\rho u_0 \mu}{L^2 \rho} \right) = -\frac{\mu}{u_0 L \rho} = -\frac{1}{Re}. \quad (5.14)$$

Substitution of equations (5.12) and (5.14) in equation (5.13) gives,

$$0 = \frac{1}{Re} + \frac{1}{Re} \frac{\partial^2 u}{\partial y^2} + \frac{Ha^2}{Re} \frac{1}{Ha} \frac{\partial b}{\partial y} \Rightarrow \frac{\partial^2 u}{\partial y^2} + Ha \frac{\partial b}{\partial y} = -1. \quad (5.15)$$

Equations (5.10) and (5.15) describe the two-dimensional Hartmann Flow which will be discussed and studied in the next section.

5.2.1 Boundary Conditions for the Hartmann flow

Similarly to the Poiseuille Flow, we assume that the fluid satisfies the no-slip condition at the walls of the channel,

$$\bar{q} = \bar{0} \Leftrightarrow (u, v) = (0, 0), \quad \text{at the bottom and top walls.} \quad (5.16)$$

According to [12] in engineering piping systems channel walls, as shown in figure 5.1, frequently consist of metallic substance with a finite electric conductivity σ_w . In most cases the walls thickness t_w is relative small in comparison to the distance between the two walls L , $t_w \ll L$. In [12] we can see a relation for the magnetic field for a surface with \bar{n} , the vector inward unit normal to the fluid wall interface, at the point P , as shown below:

$$\frac{1}{\mu\sigma} \frac{\partial b}{\partial \bar{n}} = \frac{1}{\mu_w\sigma_w} \frac{\partial b_w}{\partial \bar{n}}, \quad \text{at a point } P \text{ on the surface,} \quad (5.17)$$

where μ is the magnetic permeability. The directional derivative can be approximated by finite differences such as:

$$\frac{\partial b_w}{\partial \bar{n}} = \frac{b_P - b_{\tilde{P}}}{t_w}, \quad \text{at a point } P \text{ on the surface,} \quad (5.18)$$

where P is a point on the surface inside the channel and \tilde{P} is a point on the surface outside the channel. As there are no currents in the insulating domain outside the wall the, induced magnetic field is considered $b(\tilde{P}) = 0$. This results, for non-ferromagnetic materials ($\mu = \mu_w$) in:

$$\frac{\partial b}{\partial \bar{n}} = \frac{\sigma}{\sigma_w} \frac{1}{t_w} b, \quad \text{at point } P \text{ on the surface.} \quad (5.19)$$

We use the non-dimensional parameters: $y' = y/L$ and $b' = b/B_0$, we substitute to equation (5.19) giving:

$$\frac{\partial b}{\partial \bar{n}} - \frac{1}{c} b = 0, \quad \text{at point } P \text{ on the surface,} \quad (5.20)$$

where $c = (\sigma_w t_w) / (\sigma L)$ which is the wall conductance ratio. This parameter describes the ratio of the electrical conductance of the wall and the fluid material. The limit cases of $c \rightarrow 0$ or $c \rightarrow \infty$ mean that the walls are insulating or perfectly conducting, respectively. We will examine the case of insulating, parallel to the flow, walls or $c \rightarrow 0$.

In the case of the Hartmann flow, this vector can be written as: $\bar{n}_+ = (0, 1)$ and $\bar{n}_- = (0, -1)$ for the top and bottom wall respectively. The directional derivative at a point on the walls of the channel can be calculated by,

$$\frac{\partial b}{\partial \bar{n}} = \bar{\nabla} b \cdot \bar{n}. \quad (5.21)$$

Using equation (5.20) and (5.21) we get,

$$\frac{\partial b}{\partial \bar{n}_+} + \frac{1}{c} b = 0 \Rightarrow \bar{\nabla} b \cdot \bar{n}_+ + \frac{1}{c} b = 0 \Rightarrow \frac{\partial b}{\partial y} + \frac{1}{c} b = 0 \quad (5.22)$$

and

$$\frac{\partial b}{\partial \bar{n}_-} + \frac{1}{c} b = 0 \Rightarrow \bar{\nabla} b \cdot \bar{n}_- + \frac{1}{c} b = 0 \Rightarrow -\frac{\partial b}{\partial y} + \frac{1}{c} b = 0 \quad (5.23)$$

at $y = +1$ and $y = -1$, respectively.

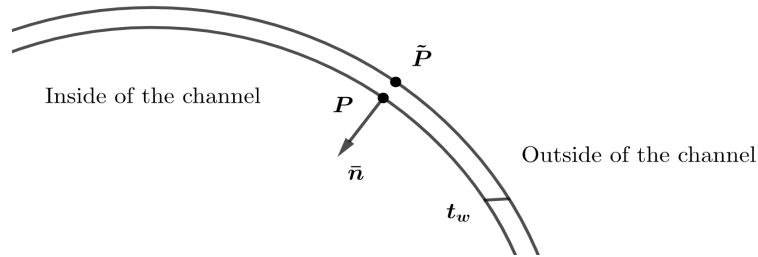


Figure 5.1: Part of the pipe with thickness t_w . The point P on the inside the channel and the point \tilde{P} is outside the channel.

5.3 The Hartmann Flow

The Hartmann flow can be considered as a special magnetohydrodynamic (MHD) case and an extension of Poiseuille flow, where, an electrical conducting fluid flows through a channel with conducting or non conducting walls at distance $2h$ and an inducted magnetic field on the channel walls, the Lorentz

forces causes the velocity to drop. Using higher values of the Hartmann number we are able to apply stronger Lorentz forces. Using a simplification of the Navier-Stokes and Induction equations we will calculate the velocity as well as the magnetic field inside the channel which changes because of the fluid, by discretizing the domain and the equations with the Finite Volume Method. We apply a parabolic velocity profile, at the inlet of the channel and Neumann boundary condition at the channel outlet. We assume zero magnetic field at the channel inlet and outlet. We apply no slip boundary conditions for the velocity and the boundary conditions we calculated above for the magnetic field.

5.3.1 Analytical solution of the Hartmann Flow

Similar to the Poiseuille flow examined in the previous sections, we will describe how the fluid flow changes by applying an external magnetic field. In this case we will assume that the magnetic field is applied vertically to the flow, meaning that the magnetic field b is a function of the variable y or $b = b(y)$. Similar assumption can be considered for the u -velocity, $u = u(y)$. Along with many applications of this flow, this is a test problem due to the fact that with the known analytical solution we can test the Finite Volume Method on different problems.

The system of PDEs that describe the Hartmann Flow is [12]:

$$Ha \frac{\partial b}{\partial y} + \frac{\partial^2 u}{\partial y^2} = -1, \text{ for } -1 < y < 1, \quad (5.24)$$

$$Ha \frac{\partial u}{\partial y} + \frac{\partial^2 b}{\partial y^2} = 0, \text{ for } -1 < y < 1, \quad (5.25)$$

with the boundary conditions:

$$u = 0, \text{ at } y = \pm 1, \quad \pm \frac{\partial b}{\partial y} + \frac{1}{c} b = 0, \text{ at } y = \pm 1, \quad (5.26)$$

which is a well defined second order, linear system with constant coefficients. Here $c \rightarrow 0$ implies that the walls are electrically insulated.

The analytical solution, of the system (5.24) and (5.25), that describes the Hartmann Flow, with the boundary conditions (5.26) for the velocity u and the magnetic field b are respectively:

$$u(y) = \bar{u} \left(1 - \frac{\cosh(Hay)}{\cosh(Ha)} \right), \quad b(y) = -\frac{y}{Ha} + \bar{u} \frac{\sinh(Hay)}{\cosh(Ha)} \quad (5.27)$$

where \bar{u} is the characteristic magnitude of velocity:

$$\bar{u} = \frac{1}{Ha} \left(\frac{c+1}{cHa + \tanh(Ha)} \right) \quad (5.28)$$

Proof. By differentiating equation (5.24) we get:

$$Ha \frac{\partial^2 b}{\partial y^2} + \frac{\partial^3 u}{\partial y^3} = 0 \Rightarrow \frac{\partial^2 b}{\partial y^2} = -\frac{1}{Ha} \frac{\partial^3 u}{\partial y^3}, \quad (5.29)$$

which we substitute in equation (5.25) resulting to:

$$Ha \frac{\partial u}{\partial y} - \frac{1}{Ha} \frac{\partial^3 u}{\partial y^3} = 0 \xrightarrow{u'=w} w'' - Ha^2 w = 0, \quad (5.30)$$

where the solution is:

$$w(y) = c_1 e^{Hay} + c_2 e^{-Hay} \Rightarrow u(y) = \frac{c_1}{Ha} e^{Hay} - \frac{c_2}{Ha} e^{-Hay} + \tilde{c}_1, \quad (5.31)$$

where \tilde{c}_1 is the integration constant. Applying the boundary conditions (5.26) for the velocity we have,

$$c_1 = -\frac{e^{Ha} \tilde{c}_1 Ha}{1 + e^{2Ha}}, \quad c_2 = \frac{e^{Ha} \tilde{c}_1 Ha}{1 + e^{2Ha}}. \quad (5.32)$$

We substitute in equation (5.31) and we simplify the exponential with the hyperbolic functions,

$$u(y) = \tilde{c}_1 \left(1 - \frac{\cosh(Hay)}{\cosh(Ha)} \right). \quad (5.33)$$

From equation (5.25), we can find the analytical solution of the magnetic field by integrating:

$$b(y) = -\frac{y}{Ha} + \tilde{c}_1 Ha \frac{\sinh(Hay)}{\cosh(Ha)} + \tilde{c}_2, \quad (5.34)$$

where \tilde{c}_2 is the integration constant. Differentiating and applying the boundary conditions (5.26) for the magnetic field we have:

$$\tilde{c}_1 = \frac{1}{Ha} \left(\frac{c+1}{cHa + \tanh(Ha)} \right), \quad \tilde{c}_2 = 0. \quad (5.35)$$

Finally, we substitute the values of the constants \tilde{c}_1 and \tilde{c}_2 in the analytical solutions of the velocity and the magnetic field. The constant \tilde{c}_1 is called the characteristic magnitude of the velocity \bar{u} [12]:

$$u(y) = \bar{u} \left(1 - \frac{\cosh(Hay)}{\cosh(Ha)} \right), \quad b(y) = -\frac{y}{Ha} + \bar{u} \frac{\sinh(Hay)}{\cosh(Ha)} \quad (5.36)$$

□

Since we know the analytical solution, we can examine the cases where the Hartmann Number approaches zero, $Ha \rightarrow 0$ and the Hartmann Number is way greater than 1, $Ha \gg 1$.

Lemma. *i) The velocity profile of the Hartmann flow approaches asymptotically, the parabolic profile of the Hydrodynamic case for small values of the Hartmann number. ii) High values of the Hartmann number create Hartmann Layers and decrease the fluid velocity.*

Proof. i) ($Ha \rightarrow 0$) In the general case the Taylor Expansion of the hyperbolic functions $\cosh(x)$ and $\tanh(x)$ as $x \rightarrow 0$ (x approaches zero) are:

$$\cosh(x) = 1 + \frac{1}{2}x^2 + \mathcal{O}(x^4), \quad \tanh(x) = x - \frac{1}{3}x^3 + \mathcal{O}(x^5). \quad (5.37)$$

We substitute the value of $\tanh(Ha)$ as $Ha \rightarrow 0$ in equation (5.28) and we get:

$$\bar{u} = -\frac{3(1+c)}{Ha^2(-3-3c+Ha^2)} \quad (5.38)$$

and the value of $\cosh(Ha)$ as $Ha \rightarrow 0$ in the analytical solution of velocity u resulting in:

$$u(y) = -\frac{3(1+c)(-1+y^2)}{(3+3c-Ha^2)(2+Ha^2)}. \quad (5.39)$$

Since we study the case of low Hartmann Number this implies that there is no induced magnetic field b therefore, $b = 0$.

By taking the limit:

$$\lim_{Ha \rightarrow 0} u(y) = \lim_{Ha \rightarrow 0} -\frac{3(1+c)(-1+y^2)}{(3+3c-Ha^2)(2+Ha^2)} = \frac{1}{2}(1-y^2), \quad (5.40)$$

we can see that the analytical solution of the velocity is similar to that of the Hydrodynamic case (parabolic profile) as well as:

$$\lim_{Ha \rightarrow 0} u(\pm 1) = \frac{1}{2}(1 - (\pm 1)^2) = 0, \quad (5.41)$$

meaning that it satisfies the boundary conditions (5.26).

ii) ($Ha \gg 1$) A very useful definition for the hyperbolic functions $\cosh(x)$ and $\tanh(x)$ is:

$$\cosh(x) = \frac{e^x + e^{-x}}{2}, \quad \sinh(x) = \frac{e^x - e^{-x}}{2}, \quad \tanh(x) = \frac{e^x + e^{-x}}{e^x - e^{-x}} \quad (5.42)$$

and for $x \gg 1$ we get asymptotically:

$$\cosh(x) \rightarrow \frac{1}{2}e^x, \quad \sinh(x) \rightarrow \frac{1}{2}e^x, \quad \tanh(x) \rightarrow 1. \quad (5.43)$$

We substitute the values of $\tanh(Ha)$ for $Ha \gg 1$ in equation (5.28) and we get:

$$\bar{u} \rightarrow \frac{1}{Ha} \frac{c+1}{cHa+1} \Rightarrow \bar{u} \xrightarrow{Ha \gg 1} 0 \quad (5.44)$$

and the value of $\cosh(Ha)$ and $\sinh(Ha)$ for $Ha \gg 1$ in the analytical solutions of velocity and magnetic field respectively resulting to:

$$u(y) = \bar{u} \left(1 - e^{Ha(y-1)}\right), \quad b(y) = -\frac{y}{Ha} + \bar{u} \left(e^{Ha(y-1)}\right), \quad |y| \leq 1. \quad (5.45)$$

Equations (5.45) must satisfy the boundary conditions (5.26), where for the u -velocity we have:

$$\begin{aligned} u(1) &= \bar{u} \left(1 - e^{Ha(1-1)}\right) = 0 \xrightarrow{Ha \gg 1} 0, \\ u(-1) &= \bar{u} \left(1 - e^{-2Ha}\right) \xrightarrow{Ha \gg 1} \bar{u} \xrightarrow{Ha \gg 1} 0. \end{aligned} \quad (5.46)$$

For the magnetic field, after some simplifications, we have:

$$\begin{aligned} +b'(1) + \frac{1}{c}b(1) &= 0 \xrightarrow{Ha \gg 1} 0, \\ -b'(-1) + \frac{1}{c}b(-1) &= 0 \xrightarrow{Ha \gg 1} 0 \end{aligned} \quad (5.47)$$

implying that the boundary conditions in (5.26) are satisfied for large Hartmann numbers.

From the asymptotic analytical solution of the velocity we can see exponentially decreased profile where it maximizes in the core flow of the channel at $y = 0$ and is equal to:

$$u_{max} = u(0) = \bar{u} \left(1 - e^{-Ha}\right) \xrightarrow{Ha \gg 1} \bar{u} \xrightarrow{Ha \gg 1} 0, \quad (5.48)$$

this exponentially velocity drop, according to [12], creates thin boundary layers close to the walls of the channel with an order of thickness: $\delta = \mathcal{O}(Ha^{-1})$. We will further verify this statement by comparing, the Hartmann layers in the numerical solution. \square

5.4 The Finite Volume Method for The Hartmann Flow

Similar FVM formulation will be followed for the Hartmann flow:

$$\begin{aligned}
\iint_{CV} \frac{\partial b}{\partial y} dx dy &= \int_s^n \frac{\partial b}{\partial y} dy \int_w^e 1 dx = b|_s^n \Delta x = (b|_n - b|_s) \Delta x = \\
&\left(\frac{b_N + b_P}{2} - \frac{b_P + b_S}{2} \right) \Delta x = \frac{1}{2} (b_N - b_S) \Delta x, \\
\iint_{CV} \frac{\partial^2 u}{\partial y^2} dx dy &= \int_s^n \frac{\partial^2 u}{\partial y^2} dy \int_w^e 1 dx = \frac{\partial u}{\partial y} \Big|_s^n \Delta x = \left(\frac{\partial u}{\partial y} \Big|_n - \frac{\partial u}{\partial y} \Big|_s \right) \Delta x = \\
&\left(\frac{u_N - u_P}{\Delta y} - \frac{u_P - u_S}{\Delta y} \right) \Delta x = (u_N - 2u_P + u_S) \frac{\Delta x}{\Delta y}, \\
\iint_{CV} \frac{\partial u}{\partial y} dx dy &= \int_s^n \frac{\partial u}{\partial y} dy \int_w^e 1 dx = u|_s^n \Delta x = (u|_n - u|_s) \Delta x = \\
&\left(\frac{u_N + u_P}{2} - \frac{u_P + u_S}{2} \right) \Delta x = \frac{1}{2} (u_N - u_S) \Delta x, \\
\iint_{CV} \frac{\partial^2 b}{\partial y^2} dx dy &= \int_s^n \frac{\partial^2 b}{\partial y^2} dy \int_w^e 1 dx = \frac{\partial b}{\partial y} \Big|_s^n \Delta x = \left(\frac{\partial b}{\partial y} \Big|_n - \frac{\partial b}{\partial y} \Big|_s \right) \Delta x = \\
&\left(\frac{b_N - b_P}{\Delta y} - \frac{b_P - b_S}{\Delta y} \right) \Delta x = (b_N - 2b_P + b_S) \frac{\Delta x}{\Delta y}, \\
\iint_{CV} -dx dy &= - \int_w^e dx \int_s^n dy = -\Delta x \Delta y.
\end{aligned}$$

5.4.1 Residual equations and numerical results of the discretization for the Hartmann Flow

x-momentum

$$\frac{1}{2} Ha (b_N - b_S) \Delta x + (u_N - 2u_P + u_S) \frac{\Delta x}{\Delta y} + \Delta x \Delta y = 0, \quad (5.49)$$

Induction x-momentum

$$\frac{1}{2} Ha (u_N - u_S) \Delta x + (b_N - 2b_P + b_S) \frac{\Delta x}{\Delta y} = 0. \quad (5.50)$$

Remark: These equations, (5.49) and (5.50) are the equations of difference for the Hartmann problem. These equations hold for each computational point in the domain and compose a linear algebraic system of equations.

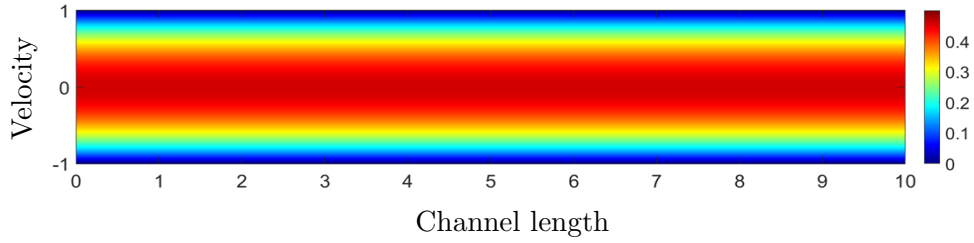
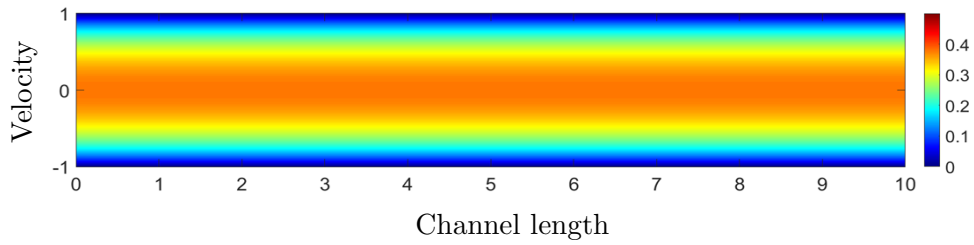
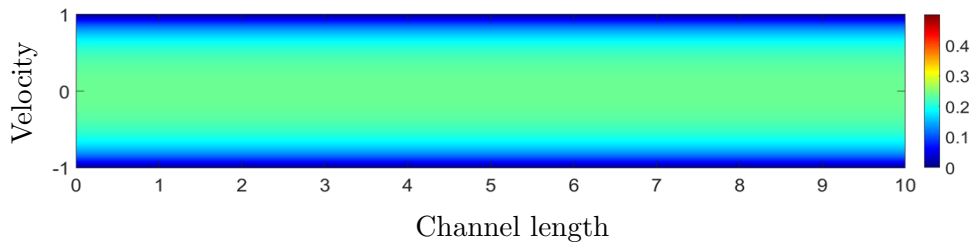
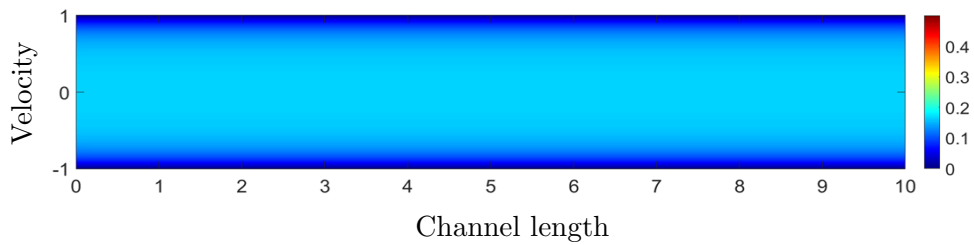
We validate the solution of the algebraic system of the Hartmann flow. In the table 5.1 below observe, using as a golden standard the analytical solutions in the inlet, the results by comparing the analytical to the numerical solution at the channel outlet.

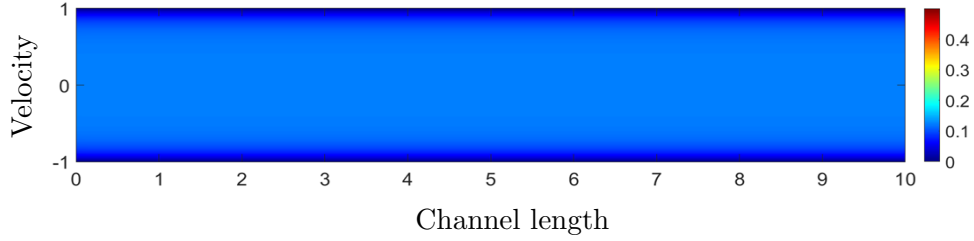
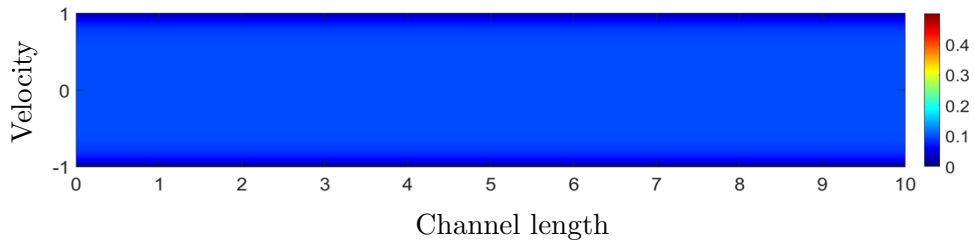
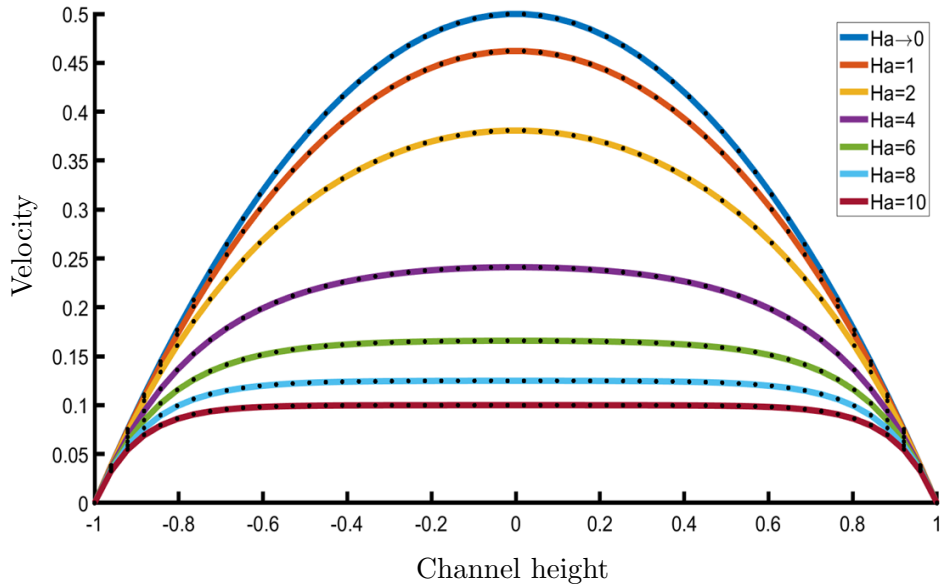
In figures 5.2 to 5.7, we observe the reduction of the velocity profile inside the channel as we increase the Hartmann number, implying stronger magnetic field. In the hydrodynamic case we observe that the maximum velocity is $u_{max} = 0.5$. Due to the Lorentz forces the maximum value drops and we have: $u_{max} \approx 0.48, 0.37, 0.25, 0.17, 0.12$ and 0.1 for $Ha = 1, 2, 4, 6, 8$ and 10 , respectively. The Hartmann layers are more and more visible as the magnitude of the magnetic field increases as shown in figure 5.8.

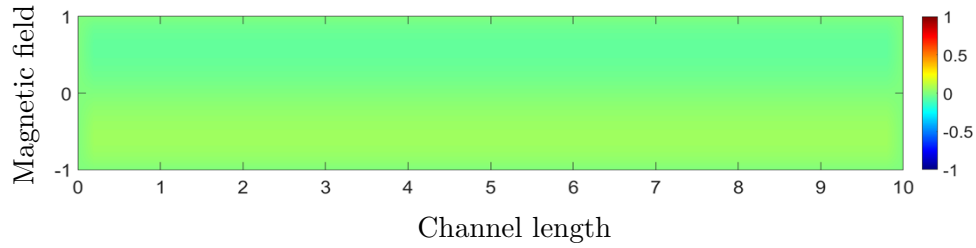
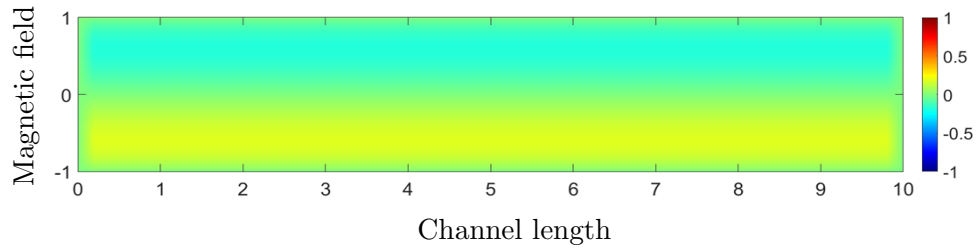
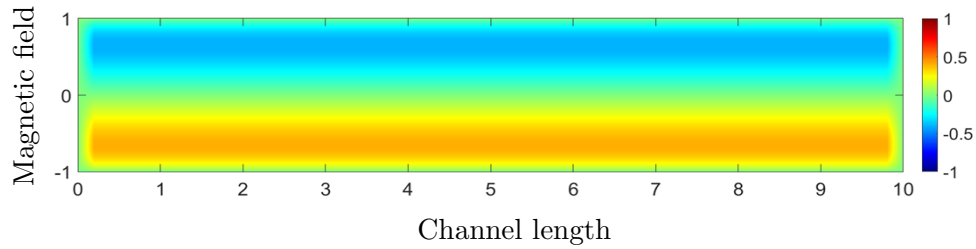
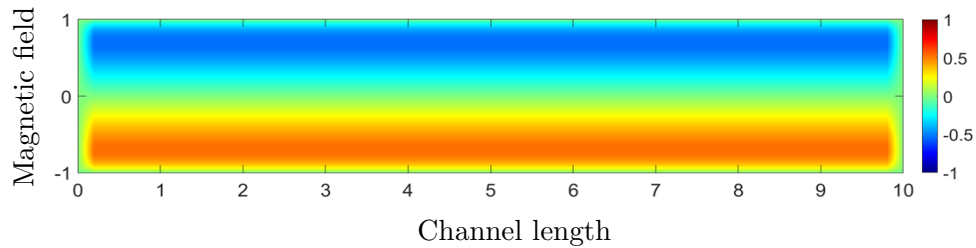
The magnetic field inside the channel, due to the insulating walls and the conducting fluid, has a periodic form which can be seen in figures 5.9 to 5.14. The increase of the Hartmann number creates a steeper profile of the magnetic field as shown in figure 5.15.

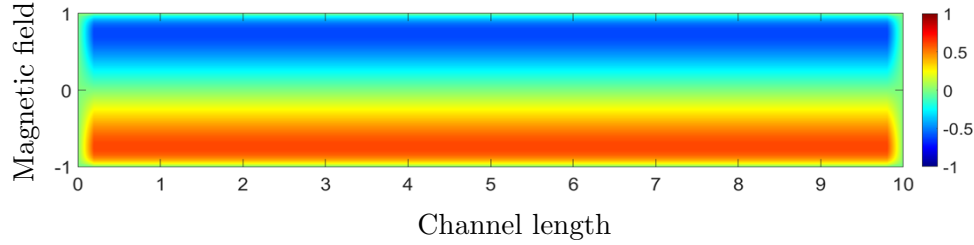
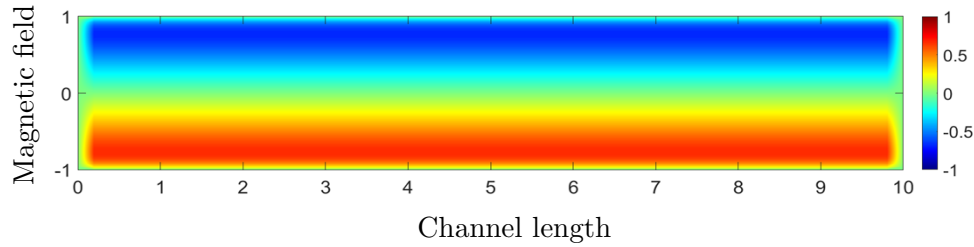
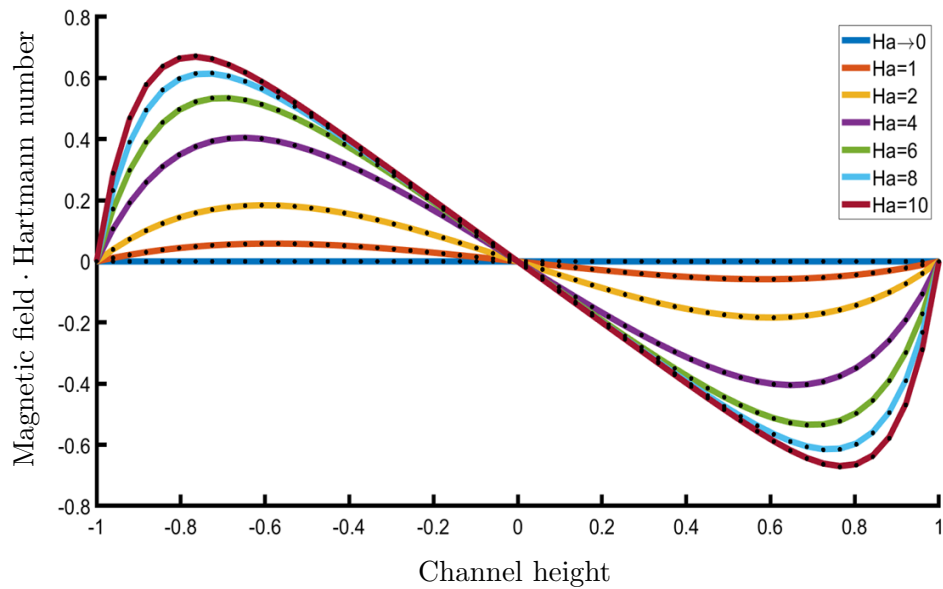
Area	RMS Velocity		RMS Magnetic field	
	$Ha = 1$	$Ha = 2$	$Ha = 1$	$Ha = 2$
$1.6529 \cdot 10^{-2}$	$8.6524 \cdot 10^{-4}$	$2.1329 \cdot 10^{-3}$	$2.2090 \cdot 10^{-4}$	$1.1121 \cdot 10^{-3}$
$4.5351 \cdot 10^{-2}$	$2.3122 \cdot 10^{-4}$	$5.6631 \cdot 10^{-4}$	$5.9014 \cdot 10^{-5}$	$2.9440 \cdot 10^{-4}$
$2.0812 \cdot 10^{-2}$	$1.0519 \cdot 10^{-4}$	$2.5792 \cdot 10^{-4}$	$2.6844 \cdot 10^{-5}$	$1.3365 \cdot 10^{-4}$
$1.1898 \cdot 10^{-2}$	$5.9878 \cdot 10^{-5}$	$1.4639 \cdot 10^{-4}$	$1.5279 \cdot 10^{-5}$	$7.6020 \cdot 10^{-5}$
$7.6894 \cdot 10^{-3}$	$3.8600 \cdot 10^{-5}$	$9.4345 \cdot 10^{-5}$	$9.8494 \cdot 10^{-6}$	$4.8987 \cdot 10^{-5}$
Area	$Ha = 4$	$Ha = 6$	$Ha = 4$	$Ha = 6$
$1.6529 \cdot 10^{-2}$	$3.1142 \cdot 10^{-3}$	$3.8286 \cdot 10^{-3}$	$2.8555 \cdot 10^{-3}$	$3.8122 \cdot 10^{-3}$
$4.5351 \cdot 10^{-2}$	$8.1345 \cdot 10^{-4}$	$9.7631 \cdot 10^{-4}$	$7.4144 \cdot 10^{-4}$	$9.7069 \cdot 10^{-4}$
$2.0812 \cdot 10^{-2}$	$3.6810 \cdot 10^{-4}$	$4.3855 \cdot 10^{-4}$	$3.3505 \cdot 10^{-4}$	$4.3587 \cdot 10^{-4}$
$1.1898 \cdot 10^{-2}$	$2.0911 \cdot 10^{-4}$	$2.4841 \cdot 10^{-4}$	$1.9024 \cdot 10^{-4}$	$2.4685 \cdot 10^{-4}$
$7.6894 \cdot 10^{-3}$	$1.3467 \cdot 10^{-4}$	$1.5975 \cdot 10^{-4}$	$1.2249 \cdot 10^{-4}$	$1.5874 \cdot 10^{-4}$
Area	$Ha = 8$	$Ha = 10$	$Ha = 8$	$Ha = 10$
$1.6529 \cdot 10^{-2}$	$4.5678 \cdot 10^{-3}$	$5.2448 \cdot 10^{-3}$	$4.5674 \cdot 10^{-3}$	$5.2448 \cdot 10^{-3}$
$4.5351 \cdot 10^{-2}$	$1.1441 \cdot 10^{-3}$	$1.3037 \cdot 10^{-3}$	$1.1438 \cdot 10^{-3}$	$1.3037 \cdot 10^{-3}$
$2.0812 \cdot 10^{-2}$	$5.0962 \cdot 10^{-4}$	$5.7592 \cdot 10^{-4}$	$5.0949 \cdot 10^{-4}$	$5.7591 \cdot 10^{-4}$
$1.1898 \cdot 10^{-2}$	$2.8760 \cdot 10^{-4}$	$3.2367 \cdot 10^{-4}$	$2.8752 \cdot 10^{-4}$	$3.2367 \cdot 10^{-4}$
$7.6894 \cdot 10^{-3}$	$1.8461 \cdot 10^{-4}$	$2.0730 \cdot 10^{-4}$	$1.8465 \cdot 10^{-4}$	$2.0730 \cdot 10^{-4}$

Table 5.1: Root mean square of the velocity and the magnetic field as the grid becomes finer for $Ha = 1, 2, 4, 6, 8$ and 10 .

Figure 5.2: Contour plot of the velocity for $Ha = 1$.Figure 5.3: Contour plot of the velocity for $Ha = 2$.Figure 5.4: Contour plot of the velocity for $Ha = 4$.Figure 5.5: Contour plot of the velocity for $Ha = 6$.

Figure 5.6: Contour plot of the velocity for $Ha = 8$.Figure 5.7: Contour plot of the velocity for $Ha = 10$.Figure 5.8: The velocity profiles of the Hartmann flow for different values of the Hartmann number. The x -axis represents the diameter of the channel, L .

Figure 5.9: Contour plot of the magnetic field for $Ha = 1$.Figure 5.10: Contour plot of the magnetic field for $Ha = 2$.Figure 5.11: Contour plot of the magnetic field for $Ha = 4$.Figure 5.12: Contour plot of the magnetic field for $Ha = 6$.

Figure 5.13: Contour plot of the magnetic field for $Ha = 8$.Figure 5.14: Contour plot of the magnetic field for $Ha = 10$.Figure 5.15: The magnetic field profiles of the Hartmann flow for different values of the Hartmann number, multiplied with the respected Hartmann number (bHa). The x -axis represents the diameter of the channel, L .

What we know is a drop, what
we don't know is an ocean.

Isaac Newton

CHAPTER 6

MAGNETOHYDRODYNAMICS

6.1 Introduction to the MHD Flow

Magnetohydrodynamics (MHD), is the study where an electrically conducting fluid flows with a velocity \bar{q} under the influence of a magnetic field \bar{B} [10]. This flow is usually described by an extended Navier-Stokes as well as Energy model.

The additional terms in the Navier-Stokes and Energy equations are the Lorentz force and Joule heating terms, respectively. The walls of the channel are considered perfect insulators, such that any magnetically induced electric currents in the fluid remain inside the flow [7].

In this chapter, the main focus lies in the flow of a electrically conducting fluid, in the two-dimensional channel, while we apply a uniform, constant in magnitude, magnetic field B_0 , for different angles, ϕ with respect to the horizontal axis which can be depicted in figure 6.1.

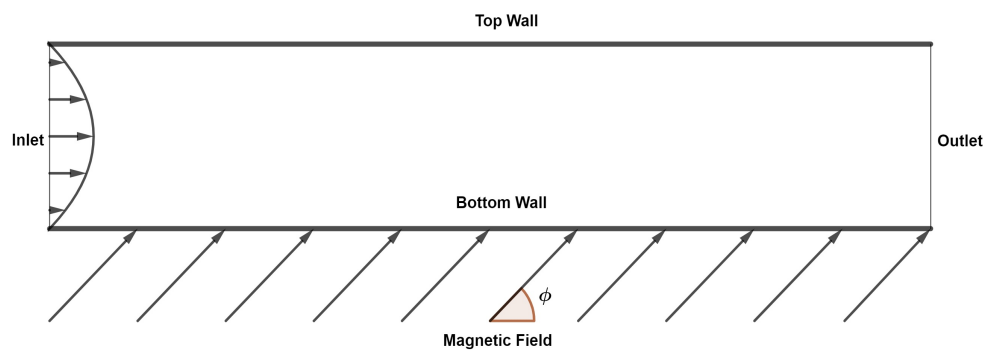


Figure 6.1: The channel of the Magnetohydrodynamic case where the magnetic field is constant in magnitude and applied with an angle, $0 \leq \phi \leq \pi/2$

The MHD terms that formulate the system of equations are the Lorentz force, $\bar{J} \times \bar{B}$, for the momentum equations and the Joule heating, \bar{J}^2 , for the Energy equation. The induced electric current and the Lorentz forces tend to oppose the mechanisms which create them (fluid flow with the velocity field). As a result, the Lorentz forces decreases the fluid flow [10].

It is convenient to simplify the system of equations and eliminate the electric current density, \bar{J} . We assume for the density of the electric current that $\bar{J} = \bar{q} \times \bar{B}$ and therefore the Lorentz force and the Joule heating terms can be, respectively, written as [17]:

$$\bar{J} \times \bar{B} = (\bar{q} \times \bar{B}) \times \bar{B}, \quad \bar{J}^2 = \bar{J} \cdot \bar{J} = (\bar{q} \times \bar{B}) \cdot (\bar{q} \times \bar{B}), \quad (6.1)$$

where $\bar{q} = (u, v, 0)$, and $\bar{B} = (B_x, B_y, 0)$. We substitute and we get:

$$\bar{J} \times \bar{B} = (-uB_y^2 + vB_xB_y, -vB_x^2 + uB_xB_y, 0), \quad \bar{J}^2 = (uB_y - vB_x)^2 \quad (6.2)$$

As we mentioned above, we apply the magnetic field with an angle ϕ . Using the definitions of the trigonometric functions we have for the magnetic field components, $B_x = B_0 \cos \phi$ and $B_y = B_0 \sin \phi$. Substituting the components of the inducted magnetic field provides: $\bar{B} = B_0 (\cos(\phi), \sin(\phi), 0)$.

Since the magnetic field is independent from the spatial variables the Induction equation reduces to the Conservation of Mass. The Navier-Stokes equations, in closed form, for each momentum are:

$$\frac{\partial(u^2)}{\partial x} + \frac{\partial(uv)}{\partial y} = -\frac{\partial p}{\partial x} + \frac{1}{Re} \left(\frac{\partial^2 u}{\partial x^2} + \frac{\partial^2 u}{\partial y^2} \right) - N(\sin^2(\phi)u - \sin(\phi)\cos(\phi)v), \quad (6.3)$$

and

$$\frac{\partial(uv)}{\partial x} + \frac{\partial(v^2)}{\partial y} = -\frac{\partial p}{\partial y} + \frac{1}{Re} \left(\frac{\partial^2 v}{\partial x^2} + \frac{\partial^2 v}{\partial y^2} \right) - N(\cos^2(\phi)v - \sin(\phi)\cos(\phi)u) \quad (6.4)$$

and the Energy equation is:

$$\frac{\partial(uT)}{\partial x} + \frac{\partial(vT)}{\partial y} = \frac{1}{Re Pr} \left(\frac{\partial^2 T}{\partial x^2} + \frac{\partial^2 T}{\partial y^2} \right) + E_c N (u \sin \phi - v \cos \phi)^2 + \Phi, \quad (6.5)$$

where the dissipation function is,

$$\Phi = 4 \left(\frac{\partial u}{\partial x} \frac{\partial v}{\partial y} \right) + \left(\frac{\partial v}{\partial x} + \frac{\partial u}{\partial y} \right)^2. \quad (6.6)$$

6.2 The Finite Volume Method on the MHD Flow

The formulation for the conservative and diffusive terms remains the same as introduced in Chapter 4. We present the formulation for the Lorentz force and Joule heating in momentum and energy equations.

x momentum

$$\begin{aligned}\iint_{CV} \sin^2 \phi u \, dx dy &= \sin^2 \phi u_P \Delta x \Delta y, \\ \iint_{CV} \sin \phi \cos \phi v \, dx dy &= \cos \phi \sin \phi v_P \Delta x \Delta y,\end{aligned}$$

y momentum

$$\begin{aligned}\iint_{CV} \cos^2 \phi v \, dx dy &= \cos^2 \phi v_P \Delta x \Delta y, \\ \iint_{CV} \sin \phi \cos \phi u \, dx dy &= \cos \phi \sin \phi u_P \Delta x \Delta y,\end{aligned}$$

Energy equation

$$\iint_{CV} (u \sin \phi - v \cos \phi)^2 \, dx dy = (u_P \sin \phi - v_P \cos \phi)^2 \Delta x \Delta y.$$

6.2.1 Residual equations, numerical results of the discretization for the MHD Flow

In summary, the residual equations discretized with the Finite Volumes Method on the equations formulating the MHD Flow are:

Conservation of Mass

$$\frac{1}{2} (u_E - u_W) \Delta y + \frac{1}{2} (v_N - v_S) \Delta x = 0, \quad (6.7)$$

x momentum

$$\begin{aligned}\frac{1}{2} (u_E^2 - u_W^2) \Delta y + \frac{1}{2} (u_N v_N - u_S v_S) \Delta x &= -(p_E - p_P) \Delta y + \\ + \frac{1}{Re} \left((u_E - 2u_P + u_W) \frac{\Delta y}{\Delta x} + (u_N - 2u_P + u_S) \frac{\Delta x}{\Delta y} \right) - \\ - N (\sin^2 \phi u_P - \sin \phi \cos \phi v_P) \Delta x \Delta y,\end{aligned} \quad (6.8)$$

y momentum

$$\begin{aligned}
& \frac{1}{2} (u_E v_E - u_W v_W) \Delta y + \frac{1}{2} (v_N^2 - v_S^2) \Delta x = - (p_N - p_P) \Delta x + \\
& + \frac{1}{Re} \left((v_E - 2v_P + v_W) \frac{\Delta y}{\Delta x} + (v_N - 2v_P + v_S) \frac{\Delta x}{\Delta y} \right) - \\
& - N (\cos^2 \phi v_P - \sin \phi \cos \phi u_P) \Delta x \Delta y,
\end{aligned} \tag{6.9}$$

Energy Equation

$$\begin{aligned}
& \frac{1}{2} \Delta y (u_E T_E - u_W T_W) + \frac{1}{2} \Delta x (v_N T_N - v_S T_S) = \\
& \frac{1}{RePr} \left(\frac{\Delta y}{\Delta x} (T_E - 2T_P + T_W) + \frac{\Delta x}{\Delta y} (T_N - 2T_P + T_S) \right) - \\
& - E_c N (u_P \sin \phi - v_P \cos \phi)^2 \Delta x \Delta y - \\
& - (u_E - u_W) (v_N - v_S) + \left(\frac{v_E - v_W}{2\Delta x} + \frac{u_N - u_S}{2\Delta y} \right)^2 \Delta x \Delta y.
\end{aligned} \tag{6.10}$$

For the boundary conditions of the velocity, we applied parabolic profile at the channel inlet and Newmann boundary conditions at the channel outlet. For the boundary conditions of the pressure, we applied Newmann boundary conditions at the channel inlet and at the channel outlet we assume zero pressure. For the boundary conditions of the temperature, we applied the higher order parabolic profile obtained from the Poiseuille flow, at the inlet and Newmann boundary conditions at the outlet.

A main objective is, due to the lack of the analytical solution, the comparison of the effect that the magnetic field on the flow, for different angles, with already published research. In [17], the effects and the Lorentz force is examined on an aneurysmal geometry which is a different geometry from the straight channel. As we present below, the results are of similar order of magnitude, which can be explained by the difference in the geometric domain and numerical method. The area of the cell is equal to $6.8301 \cdot 10^{-4}$. The Stuart number, N is equal to, $6.7000 \cdot 10^{-3}$, $2.6800 \cdot 10^{-2}$, $6.0300 \cdot 10^{-2}$ and $1.0730 \cdot 10^{-1}$ for each magnetic field magnitude, respectively.

Table 6.1 presents the maximum percentages of the fluid acceleration and deceleration as well as the maximum percentages of fluid temperature variation (increased and decreased temperature), at the boundary layer and channel core, respectively. We can also observe the maximum percentage increase for the point with the higher and lower pressure at the channel entrance.

Table 6.2 depicts similarly the percentages as in table 6.1. The case of $\phi = \pi/3$ presents the maximum acceleration and heating effect on the fluid, whereas, the fluid decelerates the most at the case of $\phi = \pi/2$ and is cooled at the case of $\phi = \pi/6$. The maximum percentage increase for the point with the higher and lower pressure at the channel entrance is observed at the case of $\phi = \pi/2$.

In figure 6.2 we show the difference between the MHD and the Hydrodynamic velocity profile for various magnetic field intensities. The velocity decelerates at the core flow of the channel as expected also from the literature [17]. The velocity accelerates in the boundary layers formed close to the walls. The case of the most intense magnetic field (16T) effects the flow more than any other magnetic field magnitude, which is a predictable outcome due to the Lorentz forces.

Figure 6.3 shows the difference between the MHD and the Hydrodynamic velocity profile for various angles under constant magnetic field magnitude. The magnetic field applied with an angle creates similar acceleration in the boundary layer and deceleration in the core flow. In this case however, this behaviour does not appear to have a certain pattern due to the angle variation. The case of $\pi/3$ has the maximum fluid acceleration and the case of $\pi/2$ has the maximum fluid deceleration .

Figure 6.4 depicts the difference between the MHD and Hydrodynamic temperature profile for various magnetic field magnitudes. Due to the application of the magnetic field the temperature increases as expected, around the channel walls as the magnitude of the magnetic field rises. At the channel core the temperature remains almost the same as it happens for the hydrodynamic case.

The difference between the MHD and Hydrodynamic temperature profile for various angles under constant magnetic field magnitude is depicted at figure 6.5. The differences in this cases are very small. The case of $\pi/3$ has the maximum increase of the temperature close to the top channel wall, whereas, the case of $\pi/6$ appears to have the higher decrease of the temperature close to the bottom channel wall.

In figures 6.6 to 6.9 we can see the increase of the pressure at the channel and the almost linear drop of it. This increase is called MHD pressure increase documented in literature in many applications [19]. In figures 6.10 to 6.13 we can see the increase of the pressure at the channel as well as the change in the angle. The simultaneously increase and decrease of the velocity is explained

due to the fact that the fluid conserves mass.

	Acceleration	Maximum	Heating
Magnitude	Velocity	Pressure	Temperature
4T	$6.5047 \cdot 10^{-1}$	$18.7490 \cdot 10^{\pm 0}$	$3.8654 \cdot 10^{-1}$
8T	$2.5102 \cdot 10^{\pm 0}$	$75.0793 \cdot 10^{\pm 0}$	$1.4559 \cdot 10^{\pm 0}$
12T	$5.3359 \cdot 10^{\pm 0}$	$168.9040 \cdot 10^{\pm 0}$	$2.9951 \cdot 10^{\pm 0}$
16T	$8.7974 \cdot 10^{\pm 0}$	$300.1889 \cdot 10^{\pm 0}$	$4.7684 \cdot 10^{\pm 0}$
	Deceleration	Minimum	Cooling
Magnitude	Velocity	Pressure	Temperature
4T	$-8.0592 \cdot 10^{-1}$	$18.5507 \cdot 10^{\pm 0}$	$-1.0343 \cdot 10^{-2}$
8T	$-3.0744 \cdot 10^{\pm 0}$	$74.2218 \cdot 10^{\pm 0}$	$-3.4517 \cdot 10^{-2}$
12T	$-6.4166 \cdot 10^{\pm 0}$	$166.9528 \cdot 10^{\pm 0}$	$-6.1856 \cdot 10^{-2}$
16T	$-1.0333 \cdot 10^{-1}$	$296.6945 \cdot 10^{\pm 0}$	$-8.3059 \cdot 10^{-2}$

Table 6.1: Maximum percentage of acceleration and deceleration of the velocity, at the outlet, maximum percentage of the pressure increase at the inlet for the maximum and minimum values of it respectively and maximum percentage of heating and cooling of the fluid at the outlet, respectively, for various magnetic field magnitudes.

	Acceleration	Maximum	Heating
Angle	Velocity	Pressure	Temperature
$\pi/6 \text{ rad}$	$1.8387 \cdot 10^{\pm 0}$	$19.9168 \cdot 10^{\pm 0}$	$1.2357 \cdot 10^{\pm 0}$
$\pi/4 \text{ rad}$	$2.6323 \cdot 10^{\pm 0}$	$38.6923 \cdot 10^{\pm 0}$	$1.7024 \cdot 10^{\pm 0}$
$\pi/3 \text{ rad}$	$3.0535 \cdot 10^{\pm 0}$	$56.9992 \cdot 10^{\pm 0}$	$1.9087 \cdot 10^{\pm 0}$
$\pi/2 \text{ rad}$	$2.5102 \cdot 10^{\pm 0}$	$75.0793 \cdot 10^{\pm 0}$	$1.4559 \cdot 10^{\pm 0}$
	Deceleration	Minimum	Cooling
Angle	Velocity	Pressure	Temperature
$\pi/6 \text{ rad}$	$-1.0254 \cdot 10^{\pm 0}$	$17.0870 \cdot 10^{\pm 0}$	$-4.6408 \cdot 10^{-1}$
$\pi/4 \text{ rad}$	$-1.7255 \cdot 10^{\pm 0}$	$35.4184 \cdot 10^{\pm 0}$	$-2.9339 \cdot 10^{-1}$
$\pi/3 \text{ rad}$	$-2.4109 \cdot 10^{\pm 0}$	$54.2074 \cdot 10^{\pm 0}$	$-1.2739 \cdot 10^{-1}$
$\pi/2 \text{ rad}$	$-3.0744 \cdot 10^{\pm 0}$	$74.2218 \cdot 10^{\pm 0}$	$-3.4517 \cdot 10^{-2}$

Table 6.2: Maximum percentage of acceleration and deceleration of the velocity, at the outlet, maximum percentage of the pressure increase at the inlet for the maximum and minimum values of it respectively and maximum percentage of heating and cooling of the fluid at the outlet, respectively, for various magnetic field angles.

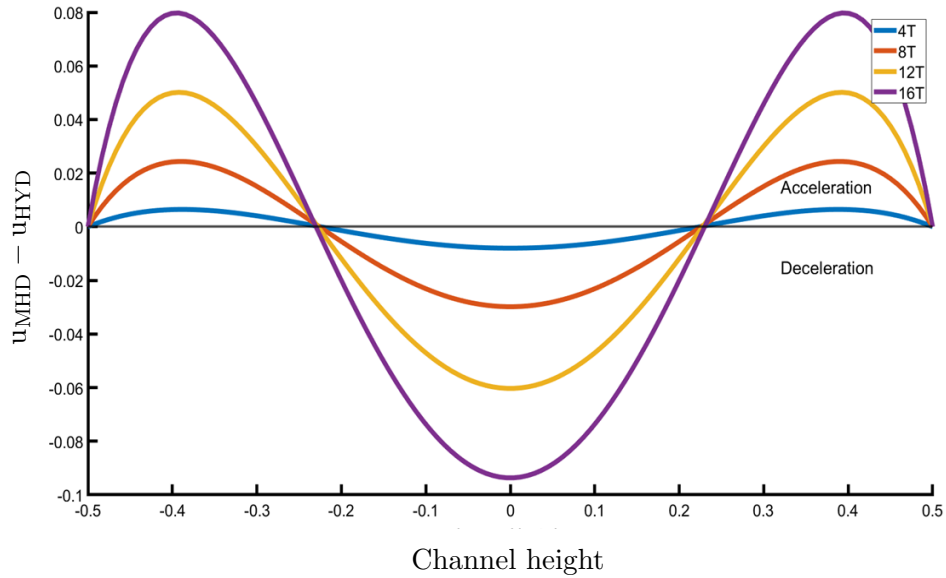


Figure 6.2: Profile of the u velocity, for various magnetic field magnitudes, compared with the hydrodynamic case. As the magnetic field magnitude rises the Hartmann layers become more visible.

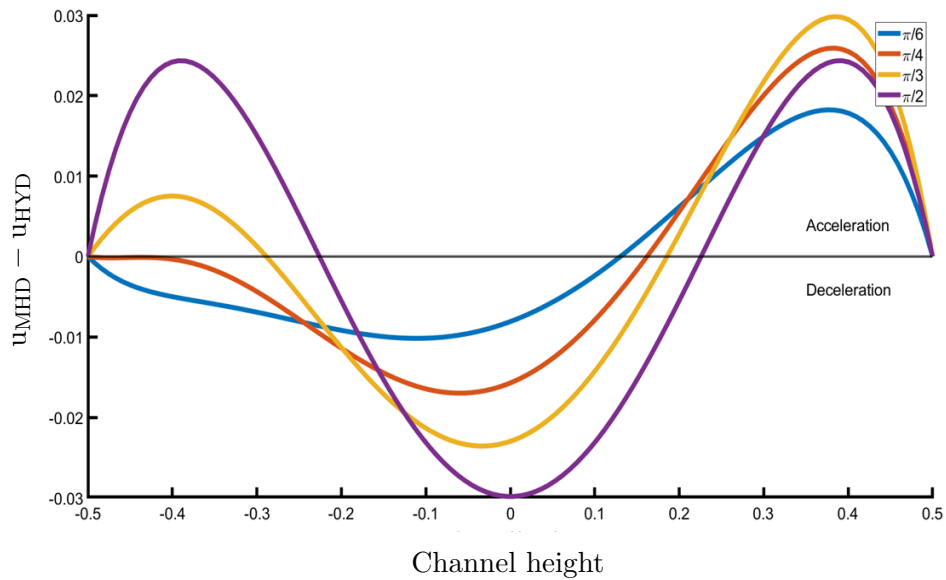


Figure 6.3: Profile of the u velocity, for various magnetic field angles, compared with the hydrodynamic case. As the magnetic field angle increases, the Hartmann layers become more visible.

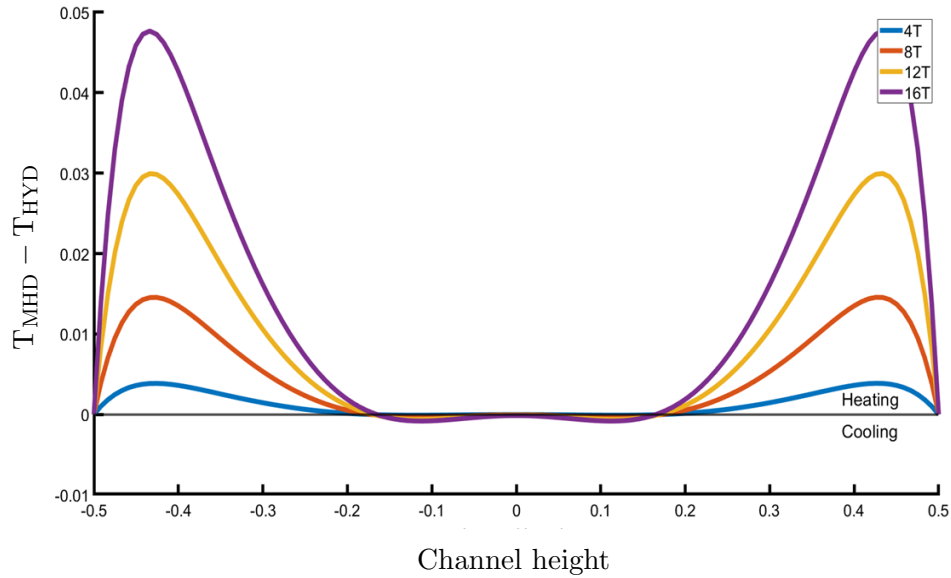


Figure 6.4: Profile of the temperature T , for various magnetic field magnitudes, compared with the hydrodynamic case. As the magnitude rises the Hartmann layers become more visible.

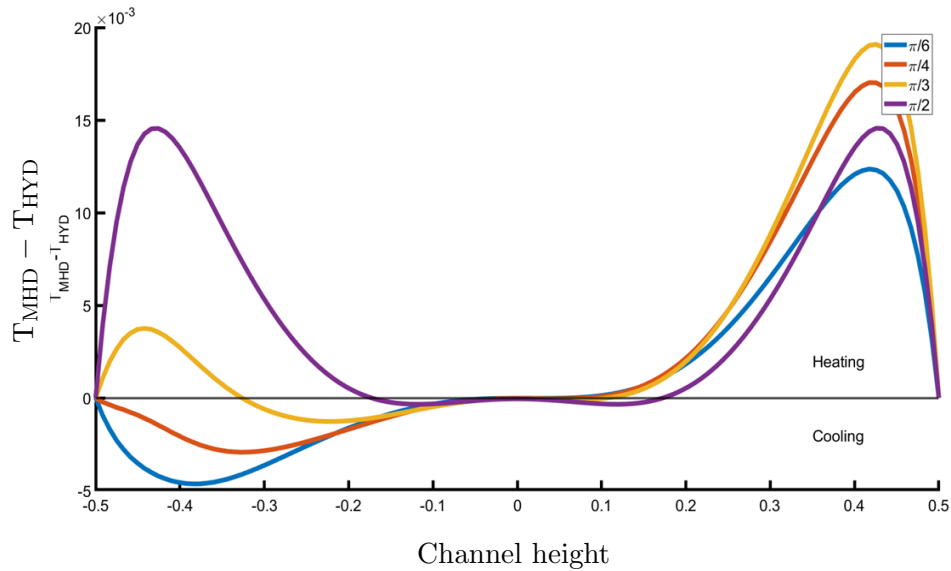
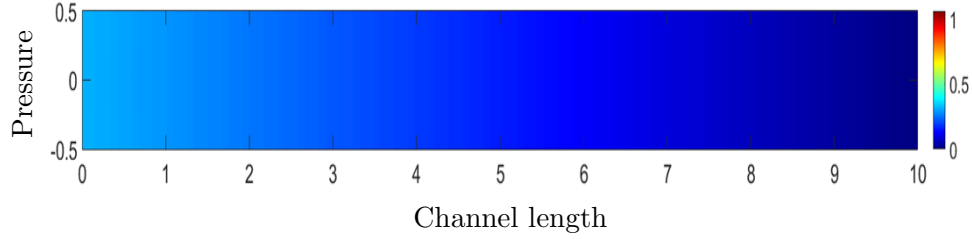
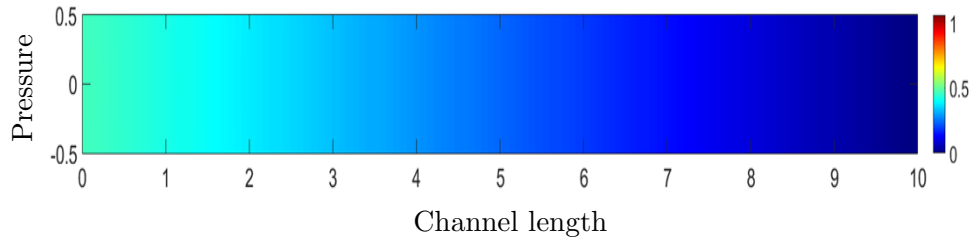
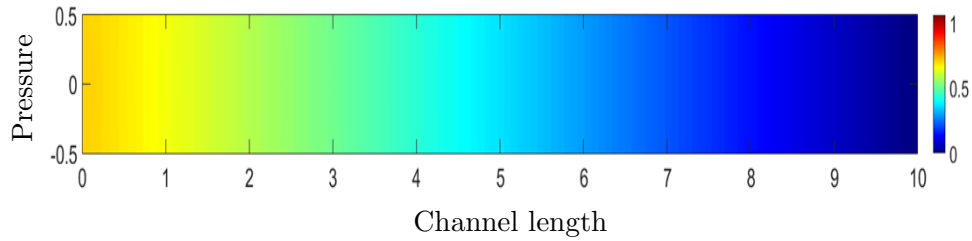
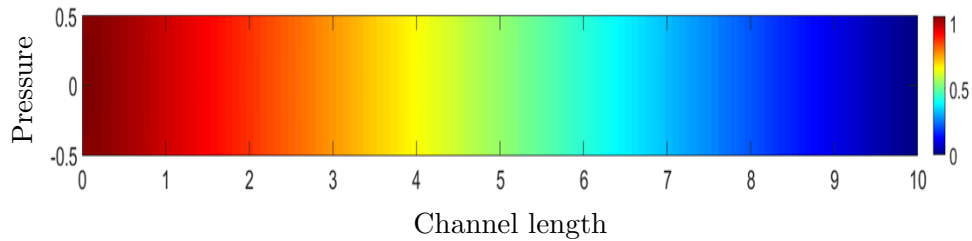
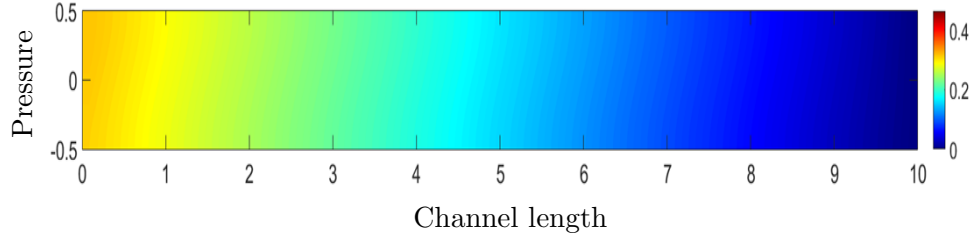
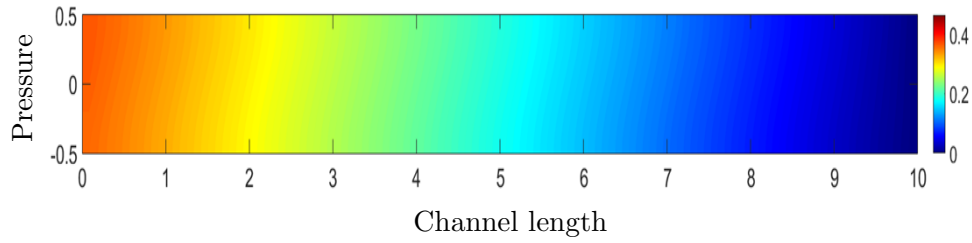
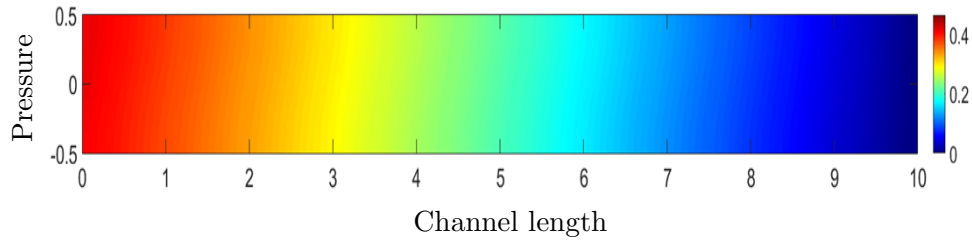
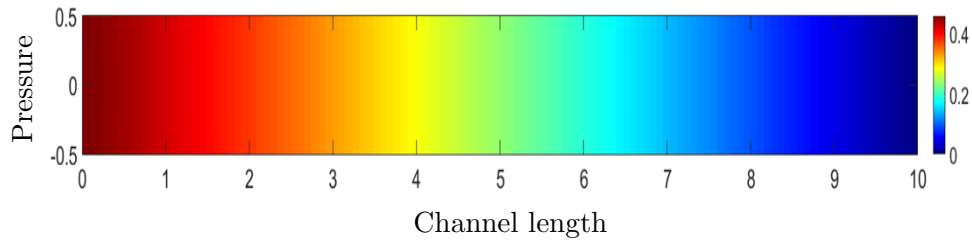


Figure 6.5: Profile of the temperature T , for various magnetic field angles, compared with the hydrodynamic case. As the magnetic field angles increases, the Hartmann layers become more visible.

Figure 6.6: Contour plot of the velocity for $B_0 = 4\text{T}$ and $\phi = \pi/2$.Figure 6.7: Contour plot of the velocity for $B_0 = 8\text{T}$ and $\phi = \pi/2$.Figure 6.8: Contour plot of the velocity for $B_0 = 12\text{T}$ and $\phi = \pi/2$.Figure 6.9: Contour plot of the velocity for $B_0 = 16\text{T}$ and $\phi = \pi/2$.

Figure 6.10: Contour plot of the pressure for $B_0 = 8T$ and $\phi = \pi/6$.Figure 6.11: Contour plot of the pressure for $B_0 = 8T$ and $\phi = \pi/4$.Figure 6.12: Contour plot of the pressure for $B_0 = 8T$ and $\phi = \pi/3$.Figure 6.13: Contour plot of the pressure for $B_0 = 8T$ and $\phi = \pi/2$.

CHAPTER 7

FERROHYDRODYNAMICS

7.1 Introduction to the FHD flow

In the previous chapters the main objective is to study the fluid flow in a channel under various circumstances, such as the application of non uniform, constant in magnitude, magnetic field, vertical to the flow. The FHD case is slightly different problem. In FHD the magnetic field is generated from a source (point) outside or inside the flow.

Let's assume a three-dimensional model of a channel geometry. We place a wire which is electrically conducting, at a distance, α , to the channel and at a distance, β , from the inlet of the channel. We apply an electric current at the wire which will create an axisymmetric magnetic field. In a two-dimensional model this implies that the wire, or in this case, the source has coordinates (α, β) as seen in figure 7.1 [4].

The distance where the source is placed at, as well as the magnitude of the magnetic field, will determine how much the parameters we study will change. The greater the distance of the source from the walls the greater the magnitude of the magnetic field must be, in order for the magnetic field to the change velocity and pressure profile [24].

As we mentioned in previous chapters, to study such problem we must first formulate it mathematically. Similar to the MHD case, we introduce a new term in the Navier-Stokes and Energy equations. Due to the formulation which we will present below, we will use a different approach to the system of equations for the FVM.

As in the Lorentz force and Joule heating in the MHD case, the non uniform magnetic field in the FHD case is formulated by new terms in the system of equations, $\mu_0 M \nabla H$ where M is a magnetization property, which describes

the behaviour of the fluid when it is exposed to a magnetic field [26]. A linear equation for isothermal case is: $M = \chi H$, where χ is a constant called magnetic susceptibility [25] and is given as,

$$H = H(x, y) = \sqrt{H_x^2 + H_y^2} = \frac{\gamma}{2\pi} \frac{1}{\sqrt{(x - \alpha)^2 + (y - \beta)^2}}, \quad (7.1)$$

where H , is the magnitude of the magnetic field generated by the electric current carrying wire, where γ , is the magnetic field strength at the current point.

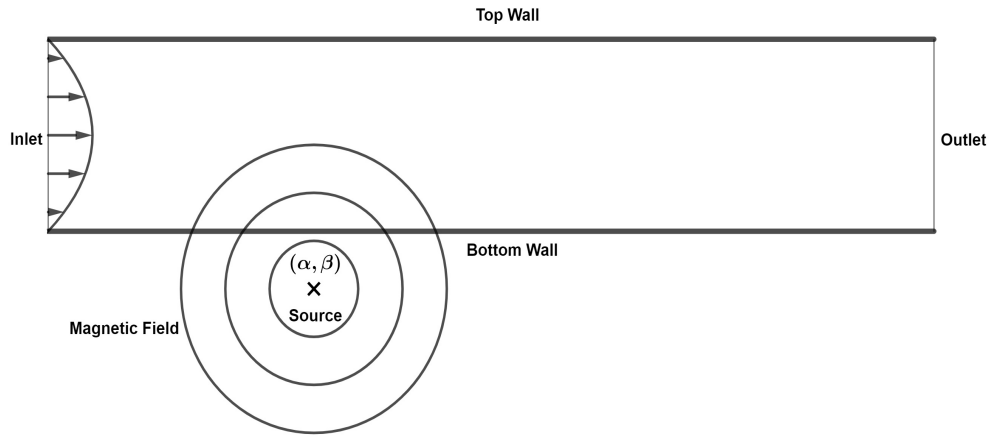


Figure 7.1: The source of the magnetic field (concentric circles with center (α, β)) and the parabolic profile of the velocity at the inlet of the channel.

The vector components of the magnetic field $\vec{H} = (H_x, H_y)$ are respectively:

$$\begin{aligned} H_x(x, y) &= -\frac{\gamma}{2\pi} \frac{x - \alpha}{(x - \alpha)^2 + (y - \beta)^2}, \\ H_y(x, y) &= \frac{\gamma}{2\pi} \frac{y - \beta}{(x - \alpha)^2 + (y - \beta)^2}. \end{aligned} \quad (7.2)$$

As usual we want to study the non dimensional equations from the governing system. We will introduce the same non dimensional parameters in (2.21) and for the new terms we will use the following formulation,

$$\vec{H}' = \frac{\vec{H}}{H_0} \Rightarrow H' = \frac{H}{H_0}, \quad (7.3)$$

where $H_0 = H(\alpha, 0)$, is the magnitude of the magnetic field at the bottom wall. The dimensionless magnitude of the magnetic field is as shown in figure 7.2:

$$H' = \frac{H}{H_0} = \frac{\beta}{\sqrt{(x - \alpha)^2 + (y - \beta)^2}}. \quad (7.4)$$

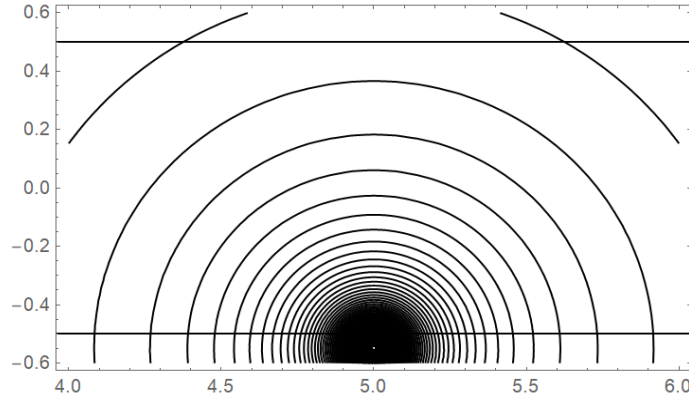


Figure 7.2: Contours of the dimensionless magnitude with the wire placed at: $(5, -0.55)$. The bottom wall is at: $y = -0.5$ and the top wall is at: $y = 0.5$.

The system of non dimensional equations that formulate the FHD flow is, along the Conservation of Mass which remains identically the same:

$$(\bar{q}' \cdot \bar{\nabla}') \bar{q}' = -\bar{\nabla}' p' + \frac{1}{Re} \bar{\nabla}'^2 \bar{q}' + Mn_F H' \bar{\nabla}' H', \quad (7.5)$$

Definition. $Mn_F = (\mu_0 \chi H_0^2) / (\rho u_0^2)$ is the magnetic number for the FHD flow.

We expand the vector form of the equation (7.5), into the equations in each momentum as follows: the Navier-Stokes equations for each momentum,

$$\begin{aligned} \frac{\partial (u^2)}{\partial x} + \frac{\partial (uv)}{\partial y} &= -\frac{\partial p}{\partial x} + \frac{1}{Re} \left(\frac{\partial^2 u}{\partial x^2} + \frac{\partial^2 u}{\partial y^2} \right) + Mn_F \frac{1}{2} \frac{\partial H^2}{\partial x}, \\ \frac{\partial (uv)}{\partial x} + \frac{\partial (v^2)}{\partial y} &= -\frac{\partial p}{\partial y} + \frac{1}{Re} \left(\frac{\partial^2 v}{\partial x^2} + \frac{\partial^2 v}{\partial y^2} \right) + Mn_F \frac{1}{2} \frac{\partial H^2}{\partial y}. \end{aligned} \quad (7.6)$$

7.2 The Finite Volume Method on FHD Flow

The new terms introduced in this flow are the ones that formulate the non uniform magnetic field generated by the source at (α, β) . We present the formulation for the FVM for these terms as the other remain the same.

x-momentum

$$\begin{aligned} \iint_{CV} \frac{\partial H^2}{\partial x} dx dy &= \int_w^e \frac{\partial H^2}{\partial x} \int_s^n 1 dy = (H_e^2 - H_w^2) \Delta y = \\ &\left(\frac{H_E^2 + H_P^2}{2} - \frac{H_P^2 + H_W^2}{2} \right) \Delta y = \frac{1}{2} (H_E^2 - H_W^2) \Delta y, \end{aligned}$$

y-momentum

$$\begin{aligned} \iint_{CV} \frac{\partial H^2}{\partial y} dx dy &= \int_s^e \frac{\partial H^2}{\partial y} \int_w^n 1 dx = (H_n^2 - H_s^2) \Delta x = \\ &\left(\frac{H_N^2 + H_P^2}{2} - \frac{H_P^2 + H_S^2}{2} \right) \Delta x = \frac{1}{2} (H_N^2 - H_S^2) \Delta x. \end{aligned}$$

7.2.1 Residual equations and numerical results of the discretization for the FHD Flow

Conservation of Mass

$$\frac{1}{2} (u_E - u_W) \Delta y + \frac{1}{2} (v_N - v_S) \Delta x = 0, \quad (7.7)$$

x-momentum

$$\begin{aligned} \frac{1}{2} (u_E^2 - u_W^2) \Delta y + \frac{1}{2} (u_N v_N - u_S v_S) \Delta x &= -(p_E - p_P) \Delta y + \\ + \frac{1}{Re} \left((u_E - 2u_P + u_W) \frac{\Delta y}{\Delta x} + (u_N - 2u_P + u_S) \frac{\Delta x}{\Delta y} \right) &+ \\ Mn_F \frac{1}{4} (H_E^2 - H_W^2) \Delta y, & \end{aligned} \quad (7.8)$$

y-momentum

$$\begin{aligned} \frac{1}{2} (u_E v_E - u_W v_W) \Delta y + \frac{1}{2} (v_N^2 - v_S^2) \Delta x &= -(p_N - p_P) \Delta x + \\ + \frac{1}{Re} \left((v_E - 2v_P + v_W) \frac{\Delta y}{\Delta x} + (v_N - 2v_P + v_S) \frac{\Delta x}{\Delta y} \right) &+ \\ Mn_F \frac{1}{4} (H_N^2 - H_S^2) \Delta x. & \end{aligned} \quad (7.9)$$

where for the formulation for the components of the magnetic field as well as the magnitude of it we use apply the formulation for these parameters into the spatial variables x and y as shown below for the point P . Similar formulation is followed for the rest of the points E, W, N and S .

$$H_P = -\frac{\beta}{\sqrt{(x_P - \alpha)^2 + (y_P - \beta)^2}}. \quad (7.10)$$

Remark: These equations of differences hold for all Finite Volume cells in the computational domain. For example if we have a 10×10 computational grid the equations of differences for this domain will be $100 \times 3 = 300$ algebraic equations.

From a numerical perspective, the magnetization terms that enter the governing equations due to the principles of FHD constitute a “source term”, which locally is of a greater order of magnitude than the other terms and gives rise to extended disturbances in the flow field, such as the formation of vortices. This could lead to a stiff numerical problem to solve. Thus, particularly for high values of the magnetic parameter combined with high gradient magnetic fields, the calculation of the numerical solution is not a trivial task [24].

For the boundary conditions of the velocity, we applied the parabolic profile at the channel inlet and Newmann boundary conditions at the channel outlet. For the boundary conditions of the pressure, we applied Newmann boundary conditions at the channel inlet and at the channel outlet we assume zero pressure.

In table 7.1 we depict the numerical results for the velocity and pressure. We apply various magnetic field magnitudes in the flow with a fixed position wire. Due to the creation of the vortices it is reasonable to examine the maximum and the minimum values of the parameters. The magnetic field source is placed at $(\alpha, \beta) = (2.5, -0.6)$. The non dimensional numbers are equal to: $Re = 300$, $Mn_F = -0.1563, -0.2251, -0.3064$ and -0.4002 , for each magnetic field magnitudes, 0.7, 0.85, 1.0 and 1.15, respectively.

In figures 7.3, we observe the local, steep, drop of pressure, which is at the position of the magnetic source. Higher magnitudes results in steeper drops. This can be explained by the flow recirculation (creation of vortices), implying that the fluid flows in the opposite direction. The creation of vortices can also be seen in [8], [22], [24], [25], and [26]. The maximum value at the channel inlet reduces as the magnitude rises, representing a local stenosis. In figures

7.4 to 7.7, we observe the effect of the magnetic field source at the fluid flow. The vortices are present even at the lower magnitude, due to the close distance of the wire. For magnitudes of 0.7, 0.85, 1.0 the maximum value of the flow remains the same as the hydrodynamic case whereas, for 1.15 we observe a slight increase of it. In all the case the flow at the channel outlet has become fully developed.

Maximum Values		
Magnitude	Velocity	Pressure
0.00T	$9.9961 \cdot 10^{-1}$	$2.6620 \cdot 10^{-1}$
0.70T	$9.9961 \cdot 10^{-1}$	$2.5408 \cdot 10^{-1}$
0.85T	$9.9961 \cdot 10^{-1}$	$2.4799 \cdot 10^{-1}$
1.00T	$9.9961 \cdot 10^{-1}$	$2.3993 \cdot 10^{-1}$
1.15T	$1.0062 \cdot 10^{\pm 0}$	$2.2915 \cdot 10^{-1}$
Minimum Values		
Magnitude	Velocity	Pressure
0.00T	$0.0000 \cdot 10^{\pm 0}$	$0.0000 \cdot 10^{\pm 0}$
0.70T	$-1.0072 \cdot 10^{-1}$	$-2.0222 \cdot 10^{\pm 0}$
0.85T	$-1.8304 \cdot 10^{-1}$	$-2.9890 \cdot 10^{\pm 0}$
1.00T	$-2.7724 \cdot 10^{-1}$	$-4.1293 \cdot 10^{\pm 0}$
1.15T	$-3.6600 \cdot 10^{-1}$	$-5.4322 \cdot 10^{\pm 0}$

Table 7.1: Maximum and minimum values of the velocity and the pressure for various magnetic field magnitudes. The cell area is equal to $3.9137 \cdot 10^{-4}$.

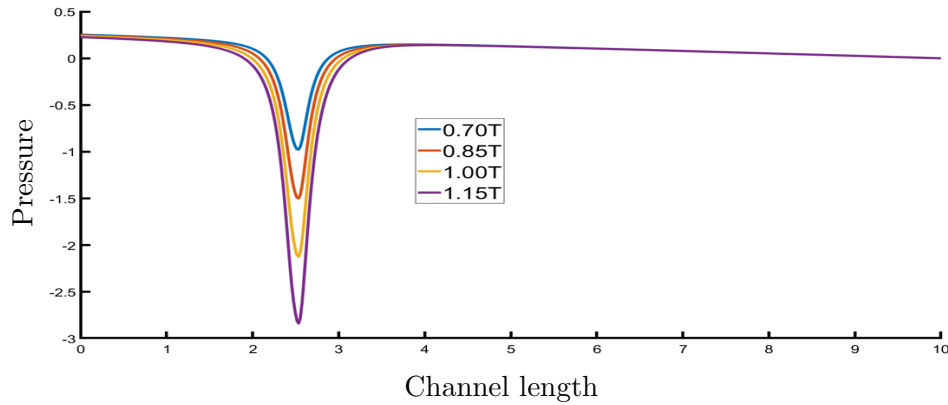
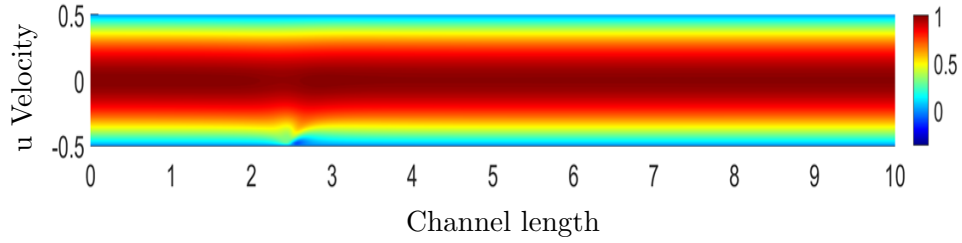
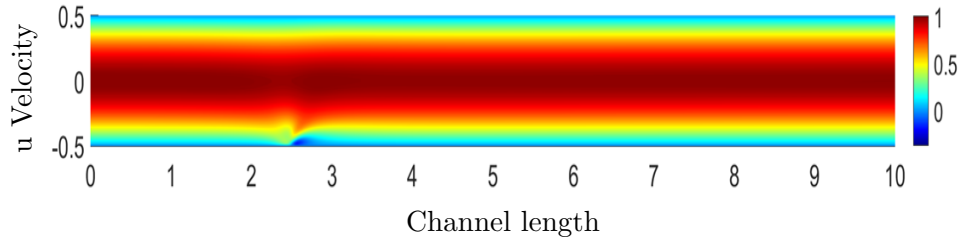
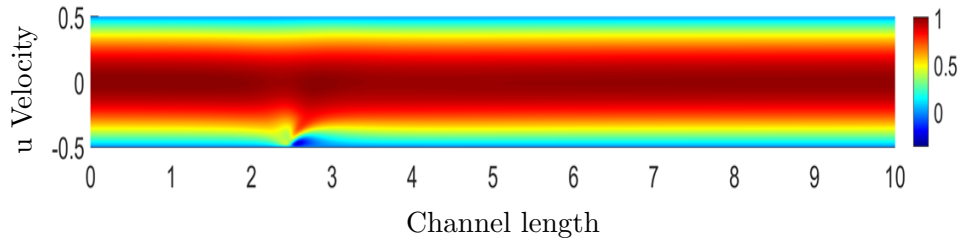
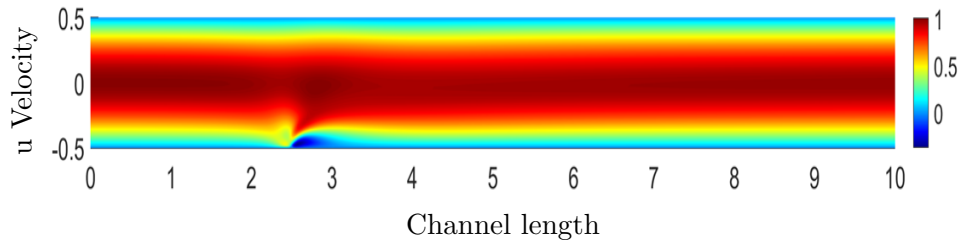


Figure 7.3: The profile of the pressure for fluid particle close to the bottom channel wall.

Figure 7.4: Contour plot of the velocity for $B_0 = 0.7\text{T}$.Figure 7.5: Contour plot of the velocity for $B_0 = 0.85\text{T}$.Figure 7.6: Contour plot of the velocity for $B_0 = 1.0\text{T}$.Figure 7.7: Contour plot of the velocity for $B_0 = 1.15\text{T}$.

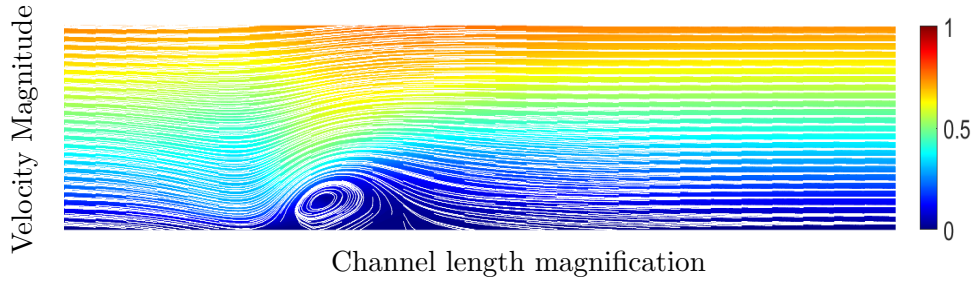


Figure 7.8: Vortex created at $B_0 = 0.7T$

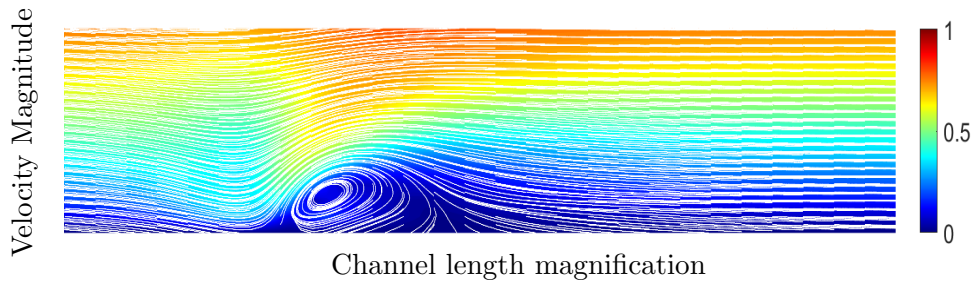


Figure 7.9: Vortex created at $B_0 = 0.85T$

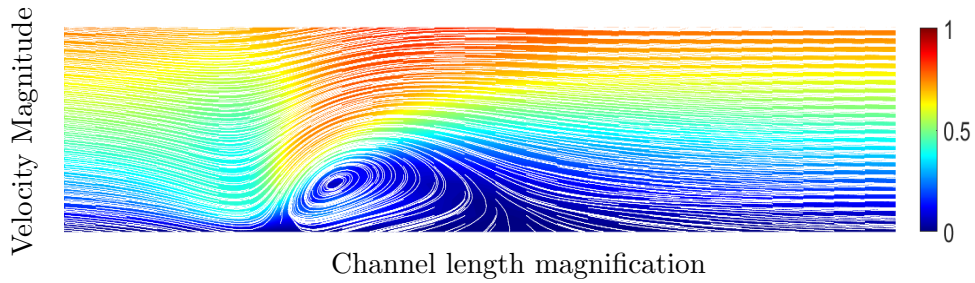


Figure 7.10: Vortex created at $B_0 = 1.0T$

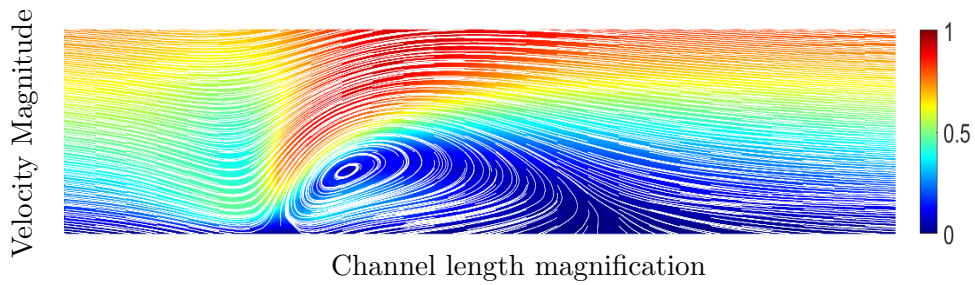


Figure 7.11: Vortex created at $B_0 = 1.15T$

CHAPTER 8

DISCUSSION AND CONCLUSION

In this thesis, the main objective was the numerical study of fluid flows under the effect of an externally inducted magnetic field, using the principles of MHD and FHD. The numerical solution was obtained by discretizing the governing fluid flow equations, resulting from a non linear PDEs system to a larger in size, non linear Algebraic one. The system is then solved using Newton's method, and trust region implementation.

Poiseuille flow: The first fluid flow problem studied in this thesis is the Poiseuille flow, which describes the flow of a fluid inside a two dimensional channel. An analytical solution can be found applying simplifications to the governing equations. The analytical solution implies that the fluid velocity has a second degree parabolic profile and the pressure drops linearly. The velocity is then substituted into the energy equation which results in the analytical solution of the fluid temperature, a fourth degree parabolic profile. The numerical solutions match very well the analytical ones, introducing a test problem for the validation of the numerical procedure.

Hartmann flow: The second fluid flow studied in this thesis is the Hartmann flow, which describes the flow of an electrically conducting fluid, between two parallel plates-walls, as an external induced magnetic field is vertically applied to the channel bottom wall. The application of the magnetic field results to increase of the fluid drag due to the Lorentz force opposing the fluid flow. The drop of velocity results in the creation of the Hartmann layers. The magnetic field in the channel is also studied, where due to the electrical conducting fluid, it is affected. Applying simplifications to the governing equations results to the analytical solution for the velocity as well as the magnetic field in the channel. The numerical solutions match very well the analytical ones, introducing another test problem for the validation of the numerical procedure.

In the following problems, there are no known analytical solutions, due to

the non-linearity of the problem, therefore the validation will be based on the matching results of the Poiseuille and Hartmann flow as well as already published research.

Classical MHD flow: The third fluid flow studied in this thesis is the fluid flow based on MHD principles which describes the flow of an electrically conducting fluid, while an external magnetic field is applied with an angle ϕ . Firstly, we study the case where the magnetic field is vertically applied while the magnitude changes. The application of the magnetic field results in areas where the fluid is accelerating and decelerating. Near the walls, symmetrical, boundary layers are created where the fluid accelerates, while near the channel core, the fluid decelerates due to the Lorentz force. The pressure is increased at the channel inlet and similar, to the velocity, results can be observed for the fluid temperature due to Joule heating, meaning that near the boundary layers the fluid is heated whereas, near the channel core is slightly cooled. Secondly, we study the case where a fixed in magnitude magnetic field is applied with an angle ϕ . This results in the creation of boundary layers where the same phenomena, as above, are observed, but due to the change of angle the results are not symmetrical as in the case of the vertically applied magnetic field. The results are the of same order of magnitude, of already published research [17].

FHD flow: The fourth and final fluid flow studied in this thesis is the fluid flow based in FHD principles, which describes the fluid flow with enhanced fluid conductivity so that it can be effected by an external magnetic field point source, constant in magnitude. The source is an electrically conducting wire placed close to the bottom wall. By applying an electrical current through the wire, a symmetrical magnetic field is created, affecting the fluid in the channel. The results are the creation of a main vortex near the magnetic field source, changing the direction of the fluid, by the recirculation of the flow close to the magnetic source. The pressure near the source is drastically decreased, explaining the creation of the vortex. These pressure changes are similar to the stenosis case of a channel. The results are the same with previously published studies [24].

In summary, this thesis is an introduction to Computational Fluid Dynamics where various problems, based on MHD and FHD principles, are formulated and solved using FV discretization and numerical methods. The numerical results are based on CFD code, developed in MATLAB (Release 2022a, The MathWorks, Inc., Natick, Massachusetts, United States). The complexity of the numerical solution is increased as the the equations given under consideration to solve are coupled all together. The user given nodes of the partition

Chapter 8

increases the number of equations to solve and the DOF (degrees of freedom), meaning the size of the system. This increases the computational cost of the method, but produces more consistent results, compared to analytical solutions where available.

The important thing is not to
stop questioning. Curiosity has
its own reason for existing.

Albert Einstein

CHAPTER 9

APPENDIX

9.1 Descritization in Matlab

In order to calculate the parameters of each problem we will assign these values when we need to calculate them

$$\text{East:}(i+1, j), \text{West:}(i-1, j), \text{Center:}(i, j), \text{North:}(i, j+1), \text{South:}(i, j-1) \quad (9.1)$$

along with:

$$\Delta x = dx, \quad \Delta y = dy. \quad (9.2)$$

We will use the general parameter f to describe the method for the general case, where we can substitute the unknown parameters of the dimensionless equations of each problem as shown for the edges E,W,N,S:

$$f_E = f(i+1, j), \quad f_W = f(i-1, j), \quad f_N = f(i, j+1), \quad f_S = f(i, j-1)$$

and for the center P:

$$f_P = f(i, j).$$

The parameters i and j obtain values from 1 to $K+2$ and 1 to $J+2$ respectively. The values at the points: $(1, 1)$, $(1, J+2)$, $(K+2, 1)$, $(K+2, J+2)$ shown the four corners of the tube, bottom left, top left, bottom right and top right respectively. The greater the values of K and J are the finer the grid is due to the fact that,

$$\begin{aligned} dx &= L/(K+1) \xrightarrow{K \rightarrow \infty} dx \rightarrow 0, \\ dy &= M/(J+1) \xrightarrow{J \rightarrow \infty} dy \rightarrow 0, \end{aligned} \quad (9.3)$$

where L is the length of the tube and M is the distance between the two walls (tube diameter). By bringing the wanted equations to the form of $g(i, j) = 0$

we can use the FSOLVE numerical routine in Matlab to minimize the left part of the equations close to zero giving a very good approximation. For the Boundary Conditions on the Matlab, on the walls can be described via the values of (i, j) . The bottom wall can be described by $i = 1, \dots, K + 2$ and by fixing the value $j = 1$. The top wall can be described by $i = 1, \dots, K + 2$ and by fixing the value of $j = J + 2$. The inlet can be described by fixing the value of $i = 1$ and by $j = 1, \dots, J + 2$. The outlet can be described by fixing the value of $i = K + 2$ and by $j = 1, \dots, J + 2$.

A Newmann Boundary Condition can be written in the following form in Matlab. For the general case we will use a general flux parameter f , where f is a scalar function,

$$\begin{aligned} \frac{\partial f}{\partial x} = 0, \text{ at bottom wall} &\Rightarrow \frac{f(i, 2) - f(i, 1)}{dx} = 0 \Rightarrow \\ &\Rightarrow f(i, 2) = f(i, 1), \quad \text{where } i = 1, \dots, K + 2, \end{aligned} \tag{9.4}$$

$$\begin{aligned} \frac{\partial f}{\partial x} = 0, \text{ at top wall} &\Rightarrow \frac{f(i, J + 2) - f(i, J + 1)}{dx} = 0 \Rightarrow \\ &\Rightarrow f(i, J + 2) = f(i, J + 1) = 0, \quad \text{where } i = 1, \dots, K + 2. \end{aligned}$$

Another example is the Neumann Boundary Conditions at the outlet of the tube for the u, v velocities of the Poiseille Flow,

$$\begin{aligned} \frac{\partial f}{\partial y} = 0, \text{ at the inlet} &\Rightarrow \frac{f(2, j) - f(1, j)}{dy} = 0 \Rightarrow \\ &\Rightarrow f(2, j) = f(1, j), \quad \text{where } j = 1, \dots, J + 2, \end{aligned} \tag{9.5}$$

$$\begin{aligned} \frac{\partial f}{\partial y} = 0, \text{ at the outlet} &\Rightarrow \frac{f(K + 2, j) - f(K + 1, j)}{dy} = 0 \Rightarrow \\ &\Rightarrow f(K + 2, j) = f(K + 1, j), \quad \text{where } j = 1, \dots, J + 2. \end{aligned}$$

The no-slip condition for the general parameter f , on the walls of the tube can be described as:

$$\begin{aligned} f(i, 1) &= 0, \text{ at the bottom wall,} \\ f(i, J + 2) &= 0, \text{ at the top wall.} \end{aligned} \tag{9.6}$$

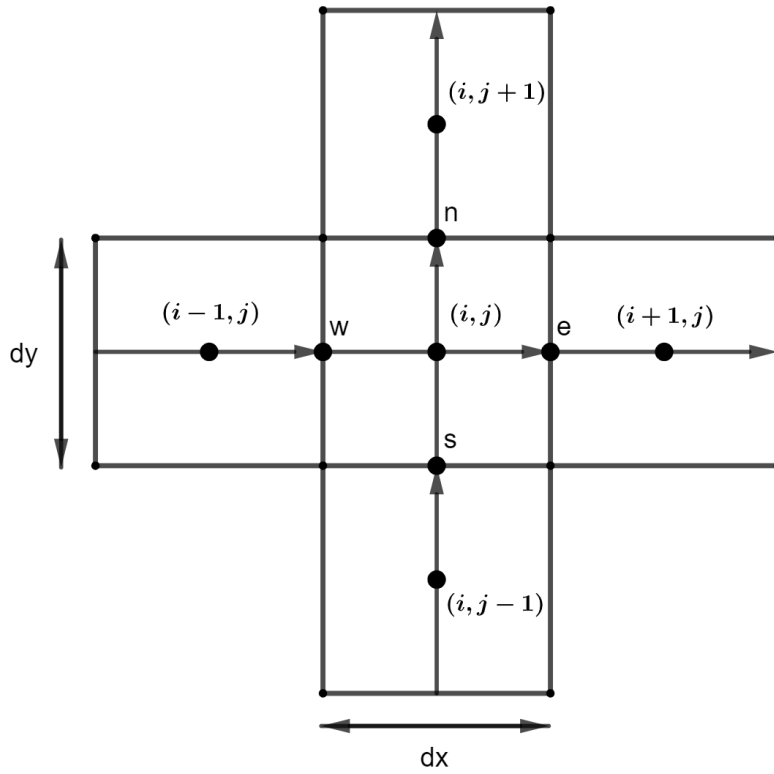


Figure 9.1: Schematic of the Finite Volume discretization in Cartesian Coordinates in Matlab

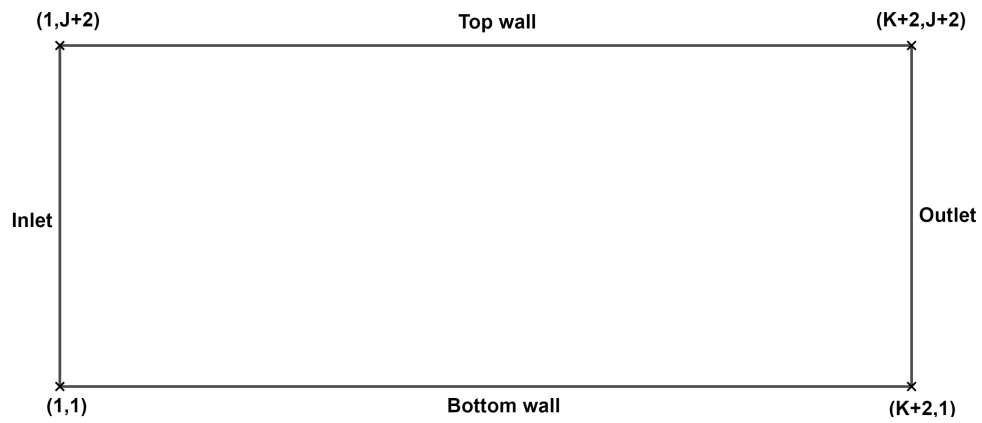


Figure 9.2: The coordinates of the four corners of the channel in Matlab

9.2 Structure and performance of the code

The structure of the code is based on different functions, which are called through a main one. In this function we input the fluid and geometry parameters such as the area of the grid, the length and the height of the channel, as well as the non-dimensional numbers and fluid properties.

We create a new function where we supply the algebraic system of equations which is called through the main function so that the solver minimizes the residuals. In this function another one is called which sets the coordinates for the channel-domain as well as the boundary conditions for the unknown parameters at the inlet, outlet, top and bottom wall respectively.

After the solver successfully minimizes the residuals we have obtained the numerical solution of the system, the main function displays the contour plots and the fluid variables such as velocity and pressure, as well as the errors of the method through a norm.

Building such a code helps the user to understand the implementation of the method as well as different procedures in already developed CFD algorithms. Another advantage of this structure is the convenient change of the algebraic system and the boundary conditions, meaning that we can solve multiple problems by changing these two functions. This is the basic structure of a CFD (Computational Fluid Dynamics) code developed in this thesis.

According to [11], we have a pre-processor which are the inputs of the parameters, the coordinates of the domain as well as the boundary conditions, a solver which is the function which solves the algebraic system of residual equations and finally the post-processor where the visualization of the problem is displayed through contour and vector plots. Our objective is to solve these algebraic equations over fine grids which means that the values of K and J are increased. This creates bigger loops, where more time is needed.

The appropriate options for the solver, in this case forward differences, the correct structure of the code as the loops grow in size, in our case preallocating, as well as the minimization of the numbers of the nested loops, when it is allowed, give relative low evaluation time as the grid gets finer. In figure 9.3 below we can see the evaluation time the computer needed to calculate the numerical solution as the grid becomes finer.

The time needed for a converged solution also depends on the nature of the differential equations that formulate each problem, meaning that if a system of equations is non linear, the algorithm needs more time for the convergence

of the solution comparing with a linear system of equations.

In conclusion, for a CFD code to work effectively, meaning that the algorithm can run in a relative small amount of time, a PC with good specifications can contribute in the process but it is also necessary the appropriate structure of the algorithm. The code developed in this study can achieve results that can hold very well against already developed codes in the CFD market, and results in a better understanding of these codes. More specifically the user can understand the background work that such code functions utilizing the FVM.

9.3 Non dimensional numbers calculations

For the problems studied in this thesis, we applied specific values for the non dimensional numbers. So, we introduce the following dimensionless parameters,

$$\begin{aligned} Re &= \frac{\rho u_0 L}{\mu}, & N &= \frac{\sigma L B_0}{\rho u_0}, & Mn_F &= \frac{\mu_0 \chi H_0^2}{\rho u_0^2} \\ Pr &= \frac{c_p \mu}{k}, & E_c &= \frac{u_0^2}{c_p T_{mean}}. \end{aligned} \quad (9.7)$$

In order to assign values to the dimensionless numbers above we will study a realistic case, which is the blood flow in a channel [8]. For this case we have: density $\rho = 1050 \text{ kg m}^{-3}$, dynamic viscosity $\mu = 3.2 \cdot 10^{-3} \text{ kg m}^{-1} \text{ s}^{-1}$, characteristic velocity $u_0 = 4.0 \cdot 10^{-2} \text{ m s}^{-1}$ and characteristic length of the channel: $L = 0.022 \text{ m}$. For the characteristic temperature we assumed that is equal to the integral of the temperature profile at the inlet divided by the number of nodes at y -axis ($J = 120$), or:

$$T_{mean} = \frac{1}{J} \int_{-\frac{1}{2}}^{\frac{1}{2}} T(y) dy = 14 \quad (9.8)$$

because we have a parabolic profile at the inlet. The electrical conductivity of blood is $\sigma = 0.8 \text{ S/m}$, the thermal conductivity is $k = 2.2 \cdot 10^{-3} \text{ J/(m s K)}$ and the heat capacity is $c_p = 14.64 \text{ J/kg K}$. The magnetic permeability of vacuum is $\mu_0 = 4\pi \cdot 10^{-7} \text{ N/A}^2$ and the magnetic susceptibility is $\chi = -6.6 \cdot 10^{-7}$.

Substitute the values to equations (9.7) gives: $Re \approx 300$, $Pr \approx 21$, $E_c = 7.8011 \cdot 10^{-6}$. For the values of the non dimensional numbers N and Mn_F we apply the values above and different magnetic field magnitudes depending on the problem under consideration.

9.4 Speed up and Residuals of the algorithm

As observed during the study, as the problems become more complicated, additional computational power was needed for the correct convergence of the numerical solution. This means that a finer grid creates a larger in size system of equations for the solver to minimize. This task in many cases can be very time consuming. For this cause, the usage of “parallel pool” is a helpful tool to decrease the time needed. The parallel pool assigns work load in each CPU the user allocates. Many last generation, or higher end CPUs have up to 12 physical cores or more, to be used for such problems. The work load of the algorithm was tested for a specific grid and specific parameters of the Poiseuille flow. In the table below, we present the results after various parallel evaluations. The evaluation time drops as the number of CPUs workers is increased. The results below correspond to a grid of 100×100 nodes for the x and y axis respectively, or 10000 FVs and area of $9.8030 \cdot 10^{-4}$ for $Re = 300$.

CPU(s) (cores)	Evaluation time		CPU(s) (cores)	Evaluation time	
1	1049.68s	0.00%	7	457.99s	56.37%
2	585.72s	42.20%	8	451.52s	56.98%
3	499.64s	52.40%	9	464.41s	55.76%
4	459.52s	56.22%	10	474.69s	54.78%
5	458.12s	56.36%	11	455.60s	56.60%
6	443.24s	57.77%	12	444.72s	57.63%

Table 9.1: CPUs used for the speed up test and the time evaluation. PC specifications: Intel(R) Xeon(R) CPU E5-2430 v2 @ 2.50GHz, 96GB RAM.

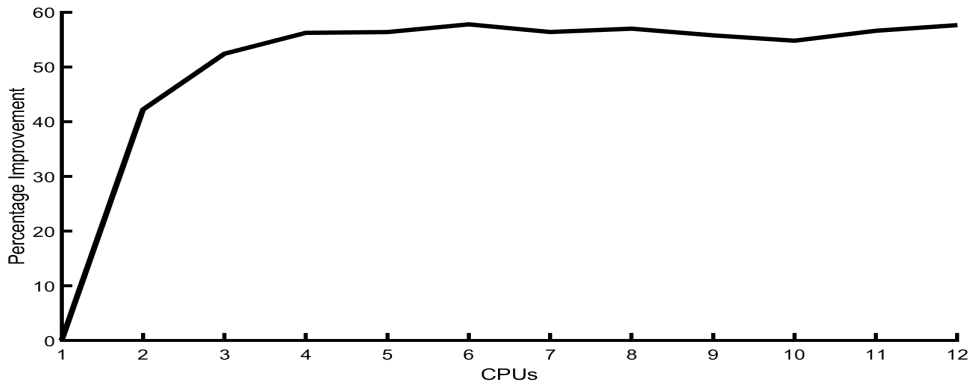


Figure 9.3: Percentage improvement for the parallel algorithm

The main objective in the CFD algorithm developed in this study, is the minimization of the functions that formulate the problems studied in Chapters 4, 5, 6 and 7. In table 9.2 we introduce the values of the function at each iteration. At the final iteration the function is close enough for the solver to stop the process as it has succeeded in the minimization or in other words the solver was converged.

Residuals for MHD flow				
Iterations	4T	8T	12T	16T
0	$2.1010 \cdot 10^{-3}$	$2.1010 \cdot 10^{-3}$	$2.1010 \cdot 10^{-3}$	$2.1010 \cdot 10^{-3}$
1	$1.4622 \cdot 10^{-3}$	$1.4622 \cdot 10^{-3}$	$1.4620 \cdot 10^{-3}$	$1.4618 \cdot 10^{-3}$
2	$1.3632 \cdot 10^{-3}$	$1.3653 \cdot 10^{-3}$	$1.3705 \cdot 10^{-3}$	$1.3789 \cdot 10^{-3}$
3	$1.1581 \cdot 10^{-3}$	$1.1652 \cdot 10^{-3}$	$1.1826 \cdot 10^{-3}$	$1.2113 \cdot 10^{-3}$
4	$7.3092 \cdot 10^{-4}$	$7.4642 \cdot 10^{-4}$	$7.8579 \cdot 10^{-4}$	$8.5353 \cdot 10^{-4}$
5	$9.8203 \cdot 10^{-5}$	$1.1117 \cdot 10^{-4}$	$1.4909 \cdot 10^{-4}$	$2.2985 \cdot 10^{-4}$
6	$5.5113 \cdot 10^{-6}$	$6.7946 \cdot 10^{-6}$	$1.1135 \cdot 10^{-5}$	$2.3244 \cdot 10^{-5}$
7	$7.4917 \cdot 10^{-10}$	$9.8746 \cdot 10^{-10}$	$2.0159 \cdot 10^{-9}$	$6.3107 \cdot 10^{-9}$
Iterations	$\pi/6 rad$	$\pi/4 rad$	$\pi/3 rad$	$\pi/2 rad$
0	$2.1010 \cdot 10^{-3}$	$2.1010 \cdot 10^{-3}$	$2.1010 \cdot 10^{-3}$	$2.1010 \cdot 10^{-3}$
1	$1.4622 \cdot 10^{-3}$	$1.4622 \cdot 10^{-3}$	$1.4622 \cdot 10^{-3}$	$1.4622 \cdot 10^{-3}$
2	$1.3632 \cdot 10^{-3}$	$1.3638 \cdot 10^{-3}$	$1.3645 \cdot 10^{-3}$	$1.3653 \cdot 10^{-3}$
3	$1.1581 \cdot 10^{-3}$	$1.1601 \cdot 10^{-3}$	$1.1625 \cdot 10^{-3}$	$1.1652 \cdot 10^{-3}$
4	$7.3073 \cdot 10^{-4}$	$7.3511 \cdot 10^{-4}$	$7.4036 \cdot 10^{-4}$	$7.4641 \cdot 10^{-4}$
5	$9.8095 \cdot 10^{-5}$	$1.0163 \cdot 10^{-4}$	$1.0599 \cdot 10^{-4}$	$1.1112 \cdot 10^{-4}$
6	$5.5075 \cdot 10^{-6}$	$5.8511 \cdot 10^{-6}$	$6.2788 \cdot 10^{-6}$	$6.7946 \cdot 10^{-6}$
7	$7.6566 \cdot 10^{-10}$	$8.3464 \cdot 10^{-10}$	$9.0963 \cdot 10^{-10}$	$9.8746 \cdot 10^{-10}$
Residuals for FHD flow				
Iterations	0.5T	0.6T	0.7T	0.8T
0	$8.9581 \cdot 10^{-3}$	$1.1701 \cdot 10^{-2}$	$1.6235 \cdot 10^{-2}$	$2.3182 \cdot 10^{-2}$
1	$5.9864 \cdot 10^{-3}$	$8.3925 \cdot 10^{-3}$	$1.2431 \cdot 10^{-2}$	$1.8719 \cdot 10^{-2}$
2	$3.6604 \cdot 10^{-3}$	$5.3106 \cdot 10^{-3}$	$8.1462 \cdot 10^{-3}$	$1.2762 \cdot 10^{-2}$
3	$2.6500 \cdot 10^{-3}$	$3.8785 \cdot 10^{-3}$	$6.0391 \cdot 10^{-3}$	$9.2200 \cdot 10^{-3}$
4	$1.7130 \cdot 10^{-3}$	$2.5151 \cdot 10^{-3}$	$3.9141 \cdot 10^{-3}$	$5.8834 \cdot 10^{-3}$
5	$5.2198 \cdot 10^{-4}$	$7.7775 \cdot 10^{-4}$	$1.2342 \cdot 10^{-3}$	$1.8911 \cdot 10^{-3}$
6	$4.0361 \cdot 10^{-5}$	$4.8754 \cdot 10^{-5}$	$7.3189 \cdot 10^{-5}$	$1.2037 \cdot 10^{-4}$
7	$1.2546 \cdot 10^{-9}$	$7.6934 \cdot 10^{-9}$	$7.5592 \cdot 10^{-8}$	$5.6223 \cdot 10^{-7}$

Table 9.2: Residuals reduction for the MHD and FHD flows respectively.

9.5 List of symbols

\bar{B} : Magnetic field induction (flux),
 B_0 : Magnetic field magnitude.
 M : Magnetization,
 \bar{H} : Magnetic field intensity,
 H : Magnetic field magnitude,
 χ : Magnetic susceptibility of the fluid,
 γ : Local magnetic field strength at point (α, β) ,
 σ : Electrical conductivity,
 μ_0 : Magnetic permeability of vacuum,
Jac : Jacobian matrix,
 \bar{J} : Electric current density,
 \bar{I} : Electric current,
 \bar{E} : Electric field.
 ρ : Density,
 c_p : Specific heat under constant pressure,
 k : Thermal conductivity
 T : Temperature,
 Φ : Dissipation Function,
 μ : Viscosity,
 \bar{q} : Velocity,
 ϕ : Magnetic field angle,
 p : Pressure,
 ν : kinematic viscosity,
 \bar{f}_L : Lorentz force,
 \bar{J}^2 : Joule heating,
 s : Seconds.

BIBLIOGRAPHY

- [1] BRAND, L. *Advanced calculus: An introduction to classical analysis*. Courier Corporation, 2006.
- [2] CONEJO, A. J., AND BARINGO, L. *Power system operations*, vol. 11. Springer, 2018.
- [3] CRAMER, K. R., AND PAI, S.-I. *Magnetofluid dynamics for engineers and applied physicists*. McGraw-Hill Book Company, 1973.
- [4] FARUK, M. H., FERDOWS, M., AND TZIRTZILAKIS, E. E. Hyperthermia temperature reduction in biomagnetic flow: Thermal transfer in Fe₃O₄-blood particle suspension with uniform and non-uniform effects. *Physics of Fluids* 35, 1 (2023), 011902.
- [5] HAIK, Y., PAI, V., AND CHEN, C.-J. Development of magnetic device for cell separation. *Journal of Magnetism and Magnetic Materials* 194, 1 (1999), 254–261.
- [6] HARLOW, F. H., AND AMSDEN, A. A. Numerical calculation of almost incompressible flow. *Journal of Computational Physics* 3, 1 (1968), 80–93.
- [7] HOSKING, R. J., AND DEWAR, R. L. *Fundamental fluid mechanics and magnetohydrodynamics*. Springer, 2016.
- [8] LOUKOPOULOS, V., AND TZIRTZILAKIS, E. Biomagnetic channel flow in spatially varying magnetic field. *International journal of engineering science* 42, 5-6 (2004), 571–590.

Bibliography

- [9] MAZUMDER, S. *Numerical methods for partial differential equations: finite difference and finite volume methods*. Academic Press, 2015.
- [10] MOREAU, R. J. *Magnetohydrodynamics*, vol. 3. Springer Science & Business Media, 1990.
- [11] MOUKALLED, F., MANGANI, L., AND DARWISH, M. *The Finite Volume Method in Computational Fluid Dynamics : An Advanced Introduction with OpenFOAM[®] and Matlab*, vol. 113 of *Fluid Mechanics and its Applications*. Springer, Cham, 2016.
- [12] MÜLLER, U., AND BÜHLER, L. *Magnetofluidynamics in Channels and Containers*. Springer Berlin Heidelberg, 2013.
- [13] NOCEDAL, J., AND WRIGHT, S. *Numerical Optimization*, 2 ed. Springer Series in Operations Research and Financial Engineering. Springer New York, 2006.
- [14] PARK, H. D., PAUL, M., HAMMOND, G. E., AND VALOCCHI, A. J. Newton trust-region methods with primary variable switching for simulating high temperature multiphase porous media flow. *Advances in Water Resources* 168 (2022), 104285.
- [15] PATANKAR, S. *Numerical Heat Transfer and Fluid Flow*. Electro Skills Series. Hemisphere Publishing Corporation, 1980.
- [16] QUARTERONI, A., SACCO, R., AND SALERI, F. *Numerical mathematics*, vol. 37. Springer Science & Business Media, 2010.
- [17] RAPTIS, A., XENOS, M., TZIRTZILAKIS, E., AND MATSAGKAS, M. Finite element analysis of magnetohydrodynamic effects on blood flow in an aneurysmal geometry. *Physics of Fluids* 26, 10 (2014), 101901.
- [18] ROBERTS, P. H. *An introduction to magnetohydrodynamics*, vol. 6. Longmans London, 1967.
- [19] SHARMA, A. Effect of applied pressure gradient on mhd flow between parallel plates under the influence of inclined magnetic field by differential transform method. *International Research Journal of Engineering and Technology (IRJET)* (2019).
- [20] SHYY, W., UDAYKUMAR, H., RAO, M. M., AND SMITH, R. W. *Computational fluid dynamics with moving boundaries*. Courier Corporation, 2012.

- [21] ΚΑΦΟΥΣΙΑΣ, Ν. *Ρευστομηχανική II*. Πανεπιστήμιο Πατρών, 1990.
- [22] ΞΕΝΟΣ, Μ. ΚΑΙ ΤΖΙΡΤΖΙΛΑΚΗΣ, Ε. *Μηχανική των Ρευστών με Εφαρμογές*. Gotsis, Πάτρα, 2008.
- [23] ΣΟΥΛΗΣ, Ι. *Υπολογιστική Μηχανική Ρευστών*. AIBAZI, 2008.
- [24] ΤΖΙΡΤΖΙΛΑΚΗΣ, Ε. Biomagnetic fluid flow in an aneurysm using ferrohydrodynamics principles. *Physics of Fluids* 27, 6 (2015), 061902.
- [25] ΤΖΙΡΤΖΙΛΑΚΗΣ, Ε., AND ΧΕΝΟΣ, Μ. Biomagnetic fluid flow in a driven cavity. *Meccanica* 48 (2013), 187–200.
- [26] ΤΖΙΡΤΖΙΛΑΚΗΣ, Ε. Ε. A mathematical model for blood flow in magnetic field. *Physics of Fluids* 17, 7 (July 2005), 077103–077103–15.
- [27] VERSTEEG, H. K., AND MALALASEKERA, W. *An introduction to computational fluid dynamics: the finite volume method*. Pearson education, 2007.
- [28] WREDE, R., AND SPIEGEL, M. *Schaum's Outline of Advanced Calculus, Third Edition*. Schaum's Outline Series. McGraw Hill LLC, 2010.
- [29] YUN, H. R., LEE, D. J., YOUN, J. R., AND SONG, Y. S. Ferrohydrodynamic energy harvesting based on air droplet movement. *Nano Energy* 11 (2015), 171–178.